GLACIO-ISOSTATIC ADJUSTMENT MODELLING OF IMPROVED RELATIVE SEA-LEVEL OBSERVATIONS IN SOUTHWESTERN BRITISH COLUMBIA, CANADA

by

Evan James Gowan
B.Sc., University of Manitoba, 2005

A Thesis Submitted in Partial Fulfillment of the Requirements for the Degree of

MASTERS OF SCIENCE

in the School of Earth and Ocean Sciences

GLACIO-ISOSTATIC ADJUSTMENT MODELLING OF IMPROVED RELATIVE SEA-LEVEL OBSERVATIONS IN SOUTHWESTERN BRITISH COLUMBIA, CANADA

by

Evan James Gowan
B.Sc., University of Manitoba, 2005

Supervisory Committee

Dr. Thomas S. James, Supervisor
(Geological Survey of Canada, School of Earth and Ocean Sciences)

Dr. George D. Spence, Supervior
(School of Earth and Ocean Sciences)

Dr. Kelin Wang, Departmental Member
(Geological Survey of Canada, School of Earth and Ocean Sciences)

Dr. Roy D. Hyndman, Departmental Member
(Geological Survey of Canada, School of Earth and Ocean Sciences)

Supervisory Committee

Dr. Thomas S. James, Supervisor
(Geological Survey of Canada, School of Earth and Ocean Sciences)

Dr. George D. Spence, Supervior
(School of Earth and Ocean Sciences)

Dr. Kelin Wang, Departmental Member
(Geological Survey of Canada, School of Earth and Ocean Sciences)

Dr. Roy D. Hyndman, Departmental Member
(Geological Survey of Canada, School of Earth and Ocean Sciences)

Abstract

In the late Pleistocene, most of British Columbia and northern Washington was covered by the Cordilleran ice sheet. The weight of the ice sheet caused up to several hundred metres of depression of the Earth's crust. This caused relative sea level to be higher in southwestern British Columbia despite lower global eustatic sea level. After deglaciation, postglacial rebound of the crust caused sea level to quickly drop to below present levels. The rate of sea-level fall is used here to determine the rheology of the mantle in southwestern British Columbia.

The first section of this study deals with determination of the postglacial sea-level history in the Victoria area. Constraints on sea-level position come from isolation basin cores collected in 2000 and 2001, as well as from previously published data from the past 45 years. The position of sea-level is well constrained at elevations greater than -4 m, and there are only loose constraints below that. The highstand position in the Victoria area is between 75-80 m. Sea level fell rapidly from the highstand position to below 0 m between 14.3 and 13.2 thousand calendar years before present (cal kyr BP). The magnitude of the lowstand position was between -11 and -40 m. Though there are few constraints on the lowstand position, analysis of the crustal response favours larger lowstand.

Well constrained sea-level histories from Victoria, central Strait of Georgia and northern Strait of Georgia are used to model the rheology of the mantle in southwestern British Columbia. A new ice sheet model for the southwestern Cordillera was developed as older models systematically underpredicted the magnitude of sea level in late glacial times. Radiocarbon dates are compiled to provide constraints on ice sheet advance and retreat. The Cordillera ice sheet reached maximum extent between 17 and 15.4 cal kyr BP. After 15.4 cal kyr, the ice sheet retreated, and by 13.7 cal kyr BP Puget Sound, Juan de Fuca Strait and Strait of Georgia were ice free. By 10.7 cal kyr BP, ice was restricted to mountain glaciers at levels similar to present. With the new ice model, and using an Earth model with a 60 km lithosphere, asthenosphere with variable viscosity and thickness, and transitional and lower mantle viscosity based on the VM2 Earth model, predicted sea level matches the observed sea level constraints in southwestern British Columbia. Nearly identical predicted sea-level curves are found using asthenosphere thicknesses between 140-380 km with viscosity values between 3×10^{18} and 4×10^{19} Pa s. Predicted sea level is almost completely insensitive to the mantle below the asthenosphere. Modeled present day postglacial uplift rates are less than 0.5 mm yr^{-1}. Despite the tight fit of the predicted sea level to observed late-glacial sea level observations, the modelling was not able to fit the early Holocene rise of sea level to present levels in the central and northern Strait of Georgia.

Table of Contents

List of Tables

List of Figures

Acknowledgements

I would like to thank my supervisor, Thomas James, for giving me the opportunity to work on this project. His patience and support through the past two years has led to an enjoyable and informative tenure at the University of Victoria.

I would like to thank the members of my supervisory committee: George Spence, Kelin Wang, and Roy Hyndman. I also thank the external reviewer, Dan Smith. Their advice and comments helped improve the quality of this thesis.

Ian Hutchinson helped me with issues concerning reservoir corrections and gave advice on interpreting sea level position.

The sediment cores used in this thesis for the Victoria sea level curve were collected in 2000 and 2001. The field work was led by Ian Hutchinson, John Clague and Thomas James. The geological interpretation of the cores was also done by these people. Other people who aided in collecting the cores include: Kim Conway, Bill Hill, Charlotte Bowman, Vaughn Barrie, Karen Simon, Jessica Jorna, Paul Ferguson, Michelle Watson and Mike Sanborn.

I would like to thank my fellow students in the School of Earth and Ocean Sciences. In particular discussions with Ikuko Wada, Sabine Hippchen, Yan Hu, Natalie Balfour, Lucinda Leonard, Ranjan Dash and Karen Simon helped with this work.

Thanks go out to the staff at the School of Earth and Ocean Sciences, in particular the graduate secretary, Sussi Arason, who helped with administrative issues.

The people at the Pacific Geoscience Center have made my experience in Victoria a great one. Discussions with many people provided useful feedback on my ideas.

Finally, I would like to thank my officemates Lisa Nykolaishen and Brian Schofield, as well as the rest of the geodynamics group at the Pacific Geoscience Center. Throughout my time here, they have allowed a casual work environment that probably aided in my timely completion of my thesis.

Chapter 1 - Introduction

1.1 Overview

During the late Pleistocene, continental ice sheets covered much of northern North America and Europe, reaching a maximum between 17,000 and 21,000 yr BP (Denton and Hughes, 1981; Fig. 1.1). The Cordilleran Ice Sheet covered most of southwestern British Columbia and parts of northwestern British Columbia, though it reached its maximum several thousand years after other northern hemisphere ice sheets (*e.g.* Clague 1981; Clague and James, 2002). The weight of the ice sheets caused tens to hundreds of metres of crustal depression along coastal areas in southwestern British Columbia (Clague *et al.*, 1982; James *et al.*, 2000). During this time, relative sea level was higher than present despite global sea level being over 100 m lower. As the ice sheet melted, the crust quickly rebounded and relative sea level fell.

Southwestern British Columbia is in an active subduction zone where the North American Plate overrides the Juan De Fuca Plate (Flück *et al.*, 1997; Fig. 1.2). In order to measure the amount of crustal motion due to tectonics, it is important to remove any residual signal due to postglacial rebound (James *et al.*, 2000). Relative sea-level change provides the best constraints on postglacial rebound as the rate of sea-level fall after deglaciation was fast enough that tectonic motion is unimportant. Using glacial lake tilts from the Puget Sound and previously collected relative sea-level data from the Strait of Georgia, James *et al*. (2000) made an initial estimate of upper mantle viscosity in southwestern British Columbia of 5×10^{18} - 5×10^{19} Pa s

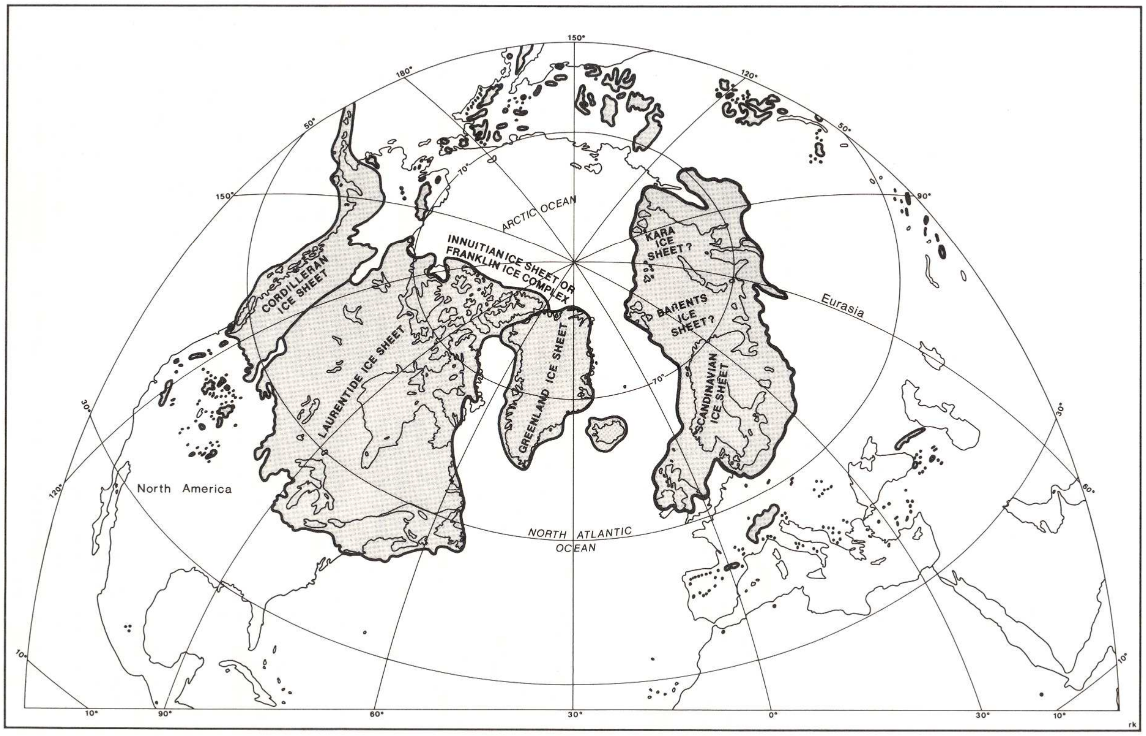

Figure 1.1. Maximum extent of northern hemisphere ice sheets during the last ice age (Denton and Hughes, 1981)

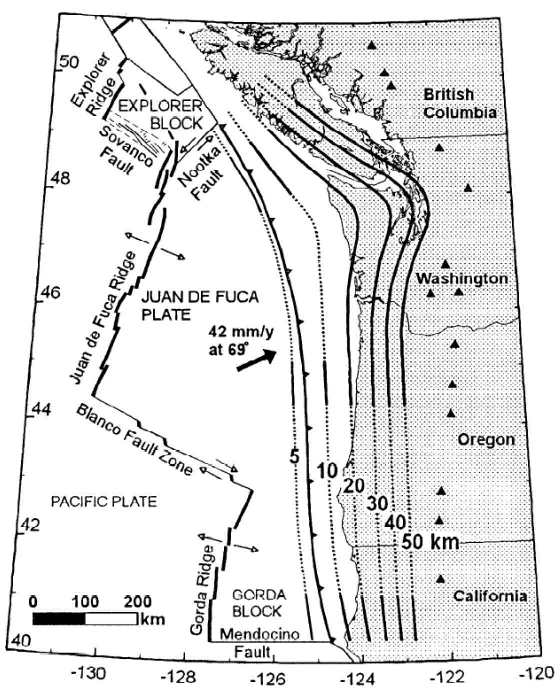

Figure 1.2. Configuration of the Cascadia subduction zone. Contours are the depth to the top of the Juan De Fuca plate as it subducts under the North American Plate. Triangles indicate arc volcanos. (Fluck *et al.*, 1997)

using a lithospheric thickness of 35 km. Using a mantle viscosity of 10^{20} Pa s, which is an intermediate value between the Cordilleran and cratonic North America mantle, the calculated present day uplift rates with their ice sheet model were less than 0.1 mm yr^{-1}. Clague and James (2002) used earth models with a thicker 60 km lithosphere, which is more consistent with heat flow and seismological values of lithospheric thickness, and an increased lower mantle viscosity. They found that a mantle viscosity of less than 10^{20} Pa s still produced the best fit to available data and that present day uplift rates were less than 1 mm yr^{-1}.

Due to sparse data in the literature to provide high precision relative sea-level histories in southwestern British Columbia, new data were collected in the Strait of Georgia (Hutchinson *et al.*, 2004a; James *et al.*, 2005, Fig. 1.3). The sea-level highstand position happened between 13.5 and 14 cal kyr BP. Data from the central Strait of Georgia indicate that sea level fell rapidly from a highstand position of about 150 m to below present sea level in 1500-2000 years (Hutchinson *et al.*, 2004a). After reaching an uncertain lowstand position, sea level returned to near present levels by 8000-9000 years ago. Sea level in the northern Strait of Georgia fell from a highstand position of about 175 m to present levels in about 2000-3000 years.

1.2 Objectives

The first objective in this study is to compile previously published data and describe recently collected cores to develop a relative sea-level curve for the Victoria area. Full descriptions and interpretations cores collected in 2000 and 2001 are given. Once constructed, this curve is compared with previously published sea-level curves for Victoria (Mathews *et al.*, 1970; Clague *et al.*, 1982; Linden and Schurer, 1988;

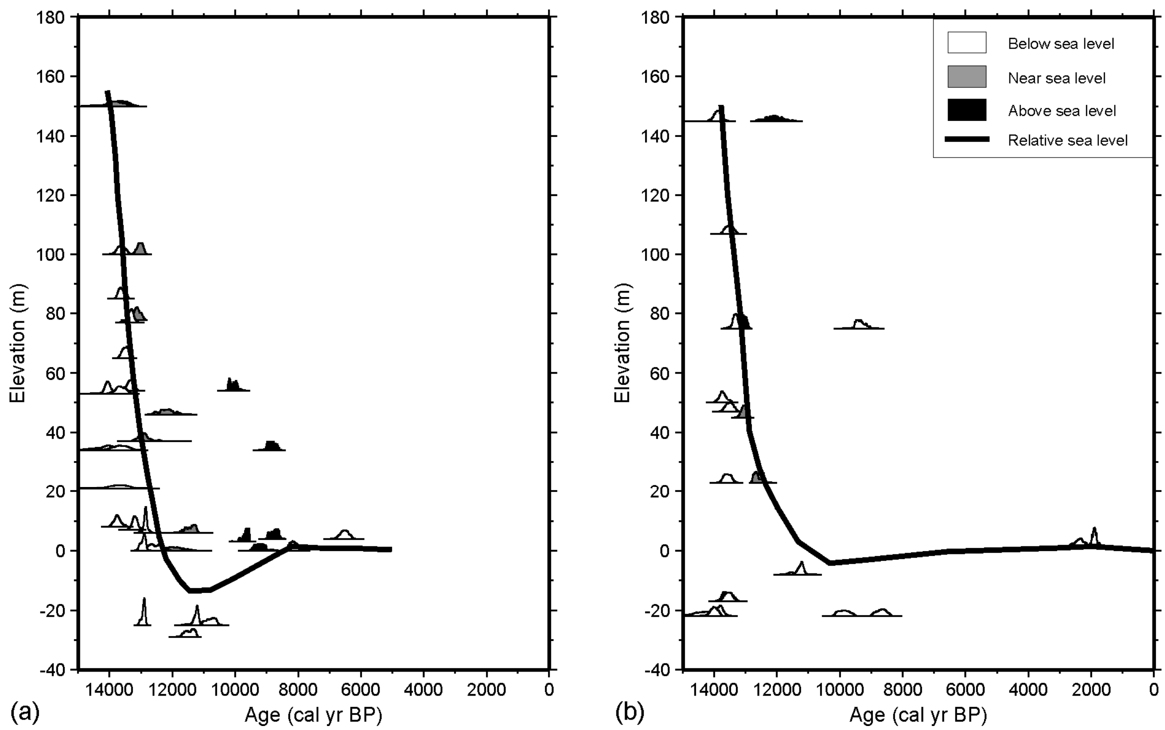

Figure 1.3. Relative sea-level constraints and interpreted sea-level curve for (a) the central Strait of Georgia (Hutchinson *et al.*, 2004a) and (b) northern Strait of Georgia (James *et al.*, 2005). The symbols correspond to the probability distribution of the sample age, scaled by a factor of 1000.

James *et al.*, 2002; Mosher and Hewitt, 2004) and with the relative sea- level curves for the central and northern Strait of Georgia (Hutchinson *et al.*, 2004a; James *et al.*, 2005).

The second objective of this study is to model postglacial rebound in southwestern British Columbia using the relative sea-level curves from Victoria and the central and northern Strait of Georgia. An improved ice sheet model is developed to fit the improved sea-level data. A range of earth models is investigated to find the optimal mantle viscosity to fit the sea-level data.

1.3 Thesis Outline

This thesis is split into four sections. Chapter 2 describes the sea-level history of southwestern British Columbia and the synthesis of a detailed sea-level curve for

Victoria. Chapter 3 describes the history of the Cordilleran ice sheet with constraints on the advance and retreat during the late Pleistocene. Chapter 4 describes the parameters used for postglacial rebound modelling and the tectonic setting of the study area. Chapter 5 shows the results of postglacial rebound modelling in southwestern British Columbia.

Most of the constraints on relative sea level and ice sheet history come from radiocarbon dates. All radiocarbon dates described in the text are corrected for reservoir effects (Hutchinson *et al.*, 2004b) and denoted as “yr BP”. Dates calibrated using the computer program Calib 5.0 (Stuiver and Reimer, 1993) are denoted as “cal yr BP”. Dates older than 50,000 years are denoted as “ka” (thousands of years ago) or “Ma” (millions of years ago).

Chapter 2 - Late Quaternary Sea Level Change in Victoria, British Columbia

2.1 Overview of sea level history in southwestern British Columbia and northwestern Washington

2.1.1 Introduction

Perched deltas and marine deposits above present sea level indicate that relative sea level was higher than present after deglaciation in coastal areas of British Columbia and Washington (Easterbrook, 1963; Mathews *et al.*, 1970; Clague *et al.*, 1982, Dethier, *et al.*, 1995; James *et al.*, 2000). Eustatic sea level, which is the average sea level associated with the total volume of water in the oceans, was significantly lower during the late Pleistocene and early Holocene (Fairbanks, 1989; Bassett *et al.*, 2005). Since sea level was higher than present during deglaciation in the study area, the Cordilleran ice sheet that covered most of British Columbia and parts of northern Washington State (Fig. 2.1) must have caused a significant amount of depression of the surface of the earth. The magnitude of the depression more than compensated the fall of eustatic level. The sea level highstand in southwestern British Columbia and northwestern Washington varied from more than 200 m in the eastern side of the Strait of Georgia to about 25 m on northwestern Vancouver Island (Clague *et al.*, 1982). Hutchinson *et al.* (2004a) and James *et al.* (2005) constructed relatively well-constrained postglacial sea-level curves in the central and northern Strait of Georgia, respectively. This chapter describes the observations and presents a detailed sea level history for the Victoria area (Fig. 2.1). First, a brief overview is given for postglacial sea-level observations in northwestern Washington State and southwestern British Columbia.

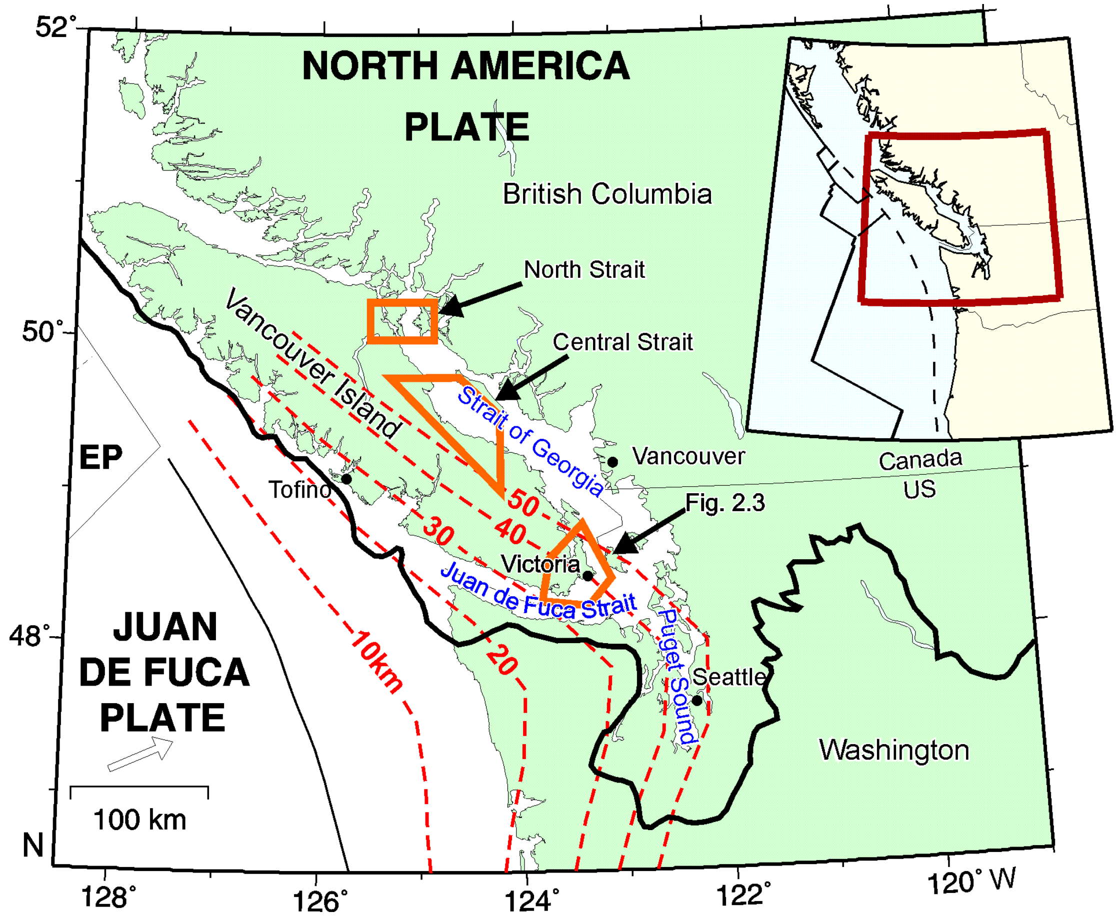

Figure 2.1. Location map showing the northern Cascadia subduction zone (after James *et al.*, 2005). The locations of previously constructed sea-level curves are from the central Strait of Georgia (Hutchinson *et al.*, 2004a), northern Strait of Georgia (James *et al.*, 2005) and Victoria (this study). Contour lines show the depth to the top of the subducting Juan de Fuca Plate (Fluck *et al.*, 1997). The thick line shows the maximum extent of the Cordilleran Ice Sheet (Clague, 1981).

2.1.2 Northwestern Washington State

Many studies document the sea level history of northwestern Washington (Easterbrook, 1963, 1969; Mathews *et al.*, 1970; Thorson, 1989; Anundsen *et al.*, 1994; Dethier *et al.*, 1995). Glaciomarine sediments are found throughout northern Puget Sound. The marine limit (maximum elevation of the sea-level highstand) varies from 30 m in central Puget Sound to over 125 m at the Canada-United States border (Dethier *et al.*, 1995). Valley outwash terraces indicate that sea level was at least 9 m higher than present on the northwestern Olympic Peninsula (Bretz, 1920).

2.1.3 Southwestern Vancouver Island

Few data exist to constrain the late glacial sea level history in southwestern Vancouver Island. Glaciomarine till is widespread in the Tofino area, indicating that sea level was higher than present after deglaciation (Valentine, 1971). Glaciomarine sediments indicate that sea level was at least 50 m above present after deglaciation (Bobrowski and Clague, 1992). Bamfield, 50 km southeast of Tofino, had postglacial sea level that was higher than 15 m above present (Blake, 1982). In Effingham Inlet, near Bamfield, freshwater sedimentation in a basin with a sill depth of -46 m indicates that sea-level fell to a lowstand position of over -46 m (Dallimore *et al.*, in press).

2.1.4 Eastern Georgia Strait

Marine deposits exist at elevations of up to 200 m along the eastern Georgia Strait (Mathews *et al.*, 1970; Clague, 1981; Clague *et al.*, 1982). For instance, in the Fraser Lowland, sea level was 200 m above present, and quickly subsided to below present sea level (Clague *et al.*, 1982). Data indicate that after 12 kyr BP, the rate of sea-level fall slowed, possibly due to a readvance of the Cordilleran ice sheet (James *et al.*, 2002). Sea level rose to near present during the mid-Holocene (Clague, 1981; Hutchinson, 1992).

2.1.5 Central Strait of Georgia

Hutchinson *et al.* (2004a) presented new radiocarbon dates and compiled old data pertaining to sea-level change in the central Strait of Georgia (Fig. 2.1). The data suggest that sea level dropped from a local highstand position of about 150 m to below present levels in 1500 to 2000 years after deglaciation of the region. It is uncertain exactly how much sea level fell during the late Pleistocene and early Holocene, though cores taken below -20 m do not show any evidence of subaerial exposure (Barrie and Conway, 2002). By the mid Holocene, sea level rose to about 2 m above present, then slowly dropped to present levels (Hutchinson *et al.*, 2004a).

2.1.6 Northern Strait of Georgia

James *et al.* (2005) used newly collected observations from isolation basins, archeological sites, natural exposures and marine samples to develop a sea-level curve for the northern Strait of Georgia. A large outwash delta indicates that the sea level highstand was about 175 m elevation in this area (McCammon, 1977). Sea level dropped rapidly, and less than 3000 years after deglaciation sea level dropped to the present level (James *et al.*, 2005). The lowstand position in the northern Strait of Georgia is uncertain. A core taken in a bay with a sill at 8 m depth shows no evidence of unconformities throughout the late Pleistocene and Holocene, suggesting that sea level did not drop below -8 m. The sea level history in the northern Strait of Georgia is similar to the central Strait of Georgia, though there was a slight delay in the timing of sea-level fall in the northern Strait. The rate of sea-level fall may have slowed in the northern Strait relative to the central Strait after 13 cal kyr BP, though this is not well constrained by radiocarbon dates.

2.1.7 Northern Vancouver Island

Howes (1981a) determined the maximum sea level in many areas in northern Vancouver Island. The sea level highstand position varied from 25 m to over 150 m.

The highstand was lowest on the northeastern part of the island, reflecting the further proximity from the center of the ice sheet. The west coast of northern Vancouver Island had much larger sea-level lowstand positions than the eastern coast, due to earlier deglaciation.

2.2 Radiocarbon dating

2.2.1 Introduction

Radiogenic carbon (^{14}C) forms by the interaction of atmospheric ^{14}N with cosmic rays (Libby, 1946). Organisms incorporate radiocarbon while they are alive and are dated by measuring the amount of radiocarbon remaining at present. Radiocarbon has a half-life of 5730 ± 40 yr, though an earlier measured value of 5568 yr is used when reporting the age of samples to remain consistent with samples dated before the determination of the more accurate half-life value (Godwin, 1962; Stuiver and Polach, 1977). Ages are stated in years before 1950 A.D. as a reference zero time. Radiocarbon dating is ideal for the dating of material that grew within the past 50,000 yr, because of its short half-life (*e.g.* Guilderson *et al.*, 2005).

2.2.2 Reservoir corrections

A lag between the incorporation of atmospheric carbon into the oceans and upwelling of water from the deep ocean causes samples in a marine or brackish environment to have artificially old ages (*e.g.* Bard, 1988; Hutchinson *et al.*, 2004b). The correction for these effects is found by dating paired terrestrial and marine samples in the same stratigraphic position. In southwestern British Columbia and northwestern Washington, marine samples older than 10 000 yr BP have an apparent age that is on average 950 ± 50 years older than contemporaneous terrestrial dates

(Hutchinson *et al.*, 2004b). This value may be a minimum, as factors such as the isolation from oceanic circulation due to seasonal ice variations and the influence of glacial meltwater make the correction as high as 1250 years in some areas (Kovanen and Easterbrook, 2002a; Hutchinson *et al.*, 2004b). For the purposes of determining the minimum ages of glacial retreat and late glacial sea level history, this study uses a reservoir age of 950 ± 50 yr. For dates younger than 10 000 yr BP, a smaller correction of 720 ± 90 yr is used (Hutchinson *et al.*, 2004b). The decreased reservoir correction during the early Holocene is likely due to lower amounts of oceanic mixing when sea level fell. The modern reservoir correction for western North America is 790 ± 35 yr (Southon *et al.*, 1990), which is used for samples younger than 3000 yr BP.

As sea level falls, organisms growing in recently isolated freshwater basins aquire a reservoir correction due to the incorporation of carbon from groundwater leeching of the recently deposited sediments (Hutchinson *et al.*, 2004b). This correction is generally needed only for a short period of time after deposition begins as the development of terrestrial plants and rapid loss of leechable carbon quickly removes any “old” carbon in the vicinity of the basin. The source for the carbon can be from outcrops of limestone, coal, and graphitic schists, decayed preglacial forest beds, or dissolved marine shells if the basin is in glaciomarine sediments. The average reservoir correction for basal limnic material such as gyttja and peat for southwestern British Columbia is 625 ± 60 yr (Hutchinson *et al.*, 2004b). This value is used in this study to correct all bulk basal freshwater radiocarbon dates. Caution is required for dates from basal bulk freshwater material, as the reservoir correction can be much greater than this value depending on the local conditions. For instance, paired terrestrial and basal freshwater sediments from lakes that formed after glacial retreat in northern Europe have reservoir corrections between 750 and 2000 yr (Pazdur *et al.*, 1994; Hedenström and Possner, 2001).

2.2.3 Calibration

The radiocarbon time scale is not one-to-one with the true age of organisms due to variations in the production rate of radiocarbon though time (Stuiver and Suess, 1966). After local reservoir corrections, all dates are calibrated to calendar age using the Calib 5.0 program (Stuiver and Reimer, 1993). Calibration of terrestrial samples utilizes the Intcal04 calibration dataset (Reimer *et al.*, 2004), while marine samples use the Marine04 dataset (Hughen *et al.*, 2004). Problems arise when dates fall in known plateaus on the calibration scale so that even dates with small errors may display a wide range of possible calendar ages (*e.g.* Guilderson *et al.*, 2005). Unless otherwise noted, all dates are in calibrated years before 1950 A.D.

Uncertainties in reservoir ages compound the problem with radiocarbon plateaus, as increasing a reservoir correction can move dates onto a calibration plateau. Figure 2.2 shows the calibration probability of a marine shell from the Juan de Fuca Strait with an uncorrected age of 13 690 ± 50 yr BP (CAMS-58696; Mosher and Hewitt, 2004). With a reservoir correction of 950 ± 50 yr, the sample has a tight probability distribution with a mean age of about 15.1 cal kyr BP. However, if the reservoir correction is increased to 1250 ± 50 yr, the date falls within a radiocarbon plateau, and the mean age is distributed between 14.2 and 14.6 cal kyr BP. Since the

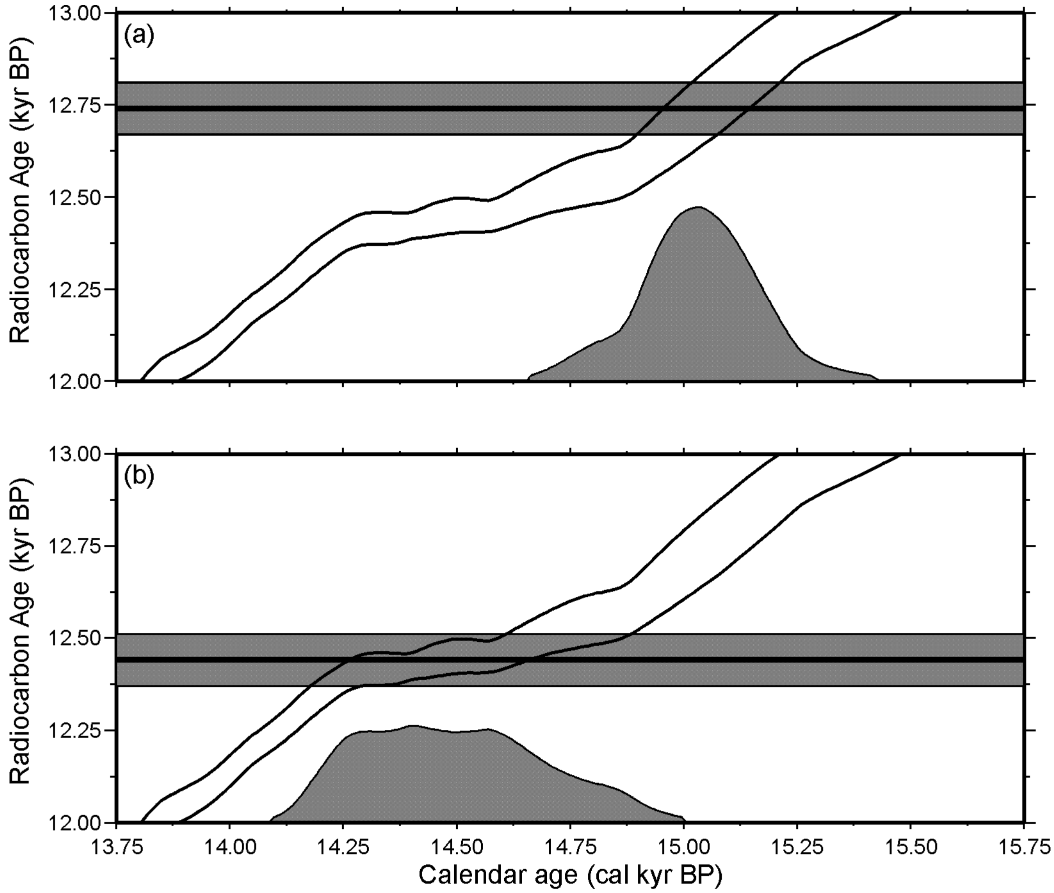

Figure 2.2. Calibrated age probability for CAMS-58696 using different reservoir corrections. (a) 950 ± 50 years, (b) 1250 ± 50 years. Bar shows the 1-sigma error range of the corrected radiocarbon age.

reservoir correction is uncertain, it should be noted that some calibrated dates may be significantly in error if the true reservoir correction for a sample is different from the one applied.

2.3 Constraints on sea level in Victoria

2.3.1 Introduction

A total of 47 radiocarbon dated samples were used to determine a sea level curve for the Victoria area. Of these, 23 samples were from isolation basin (basins that became isolated as sea level fell) cores collected in 2000 and 2001. Cores

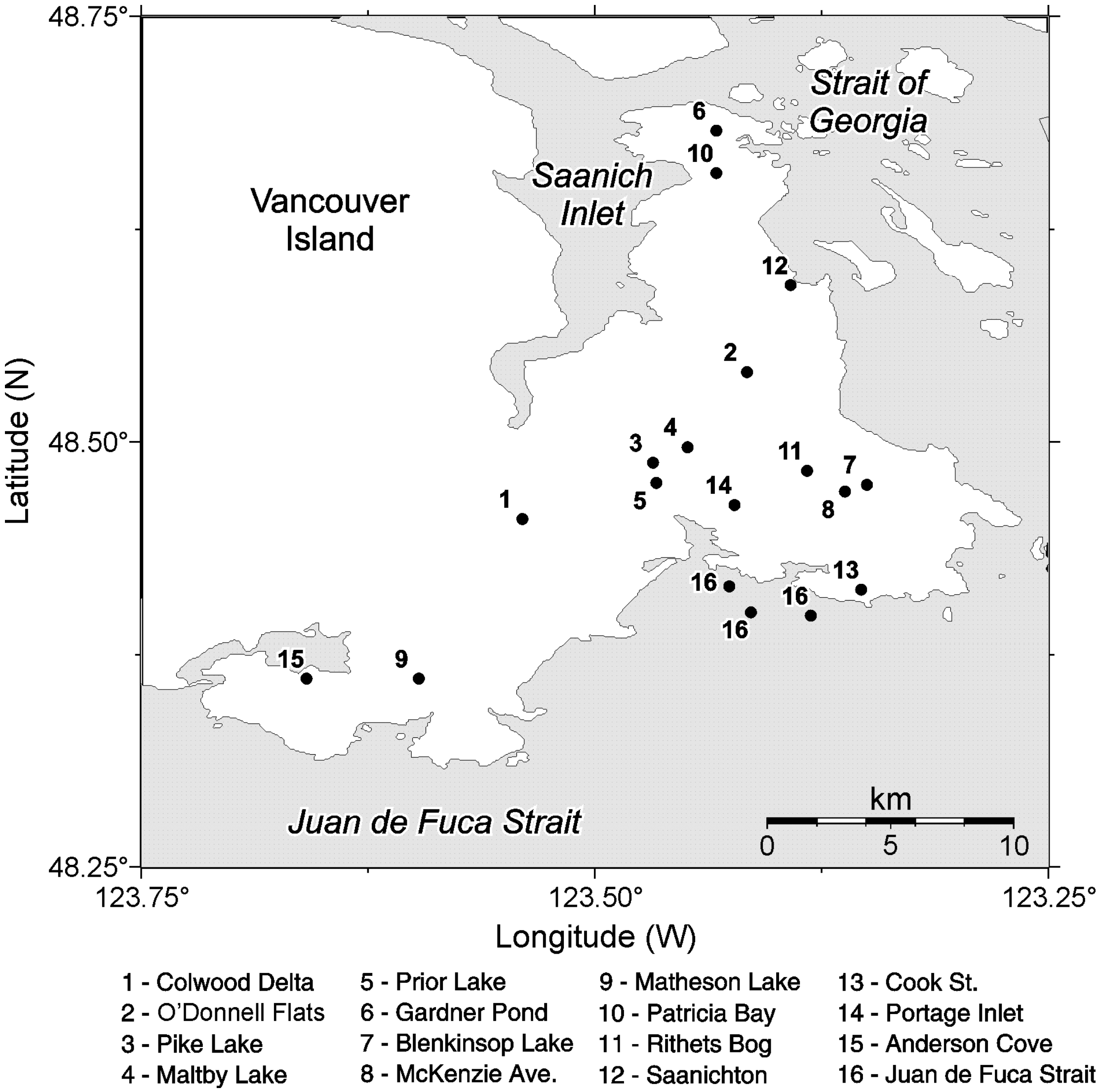

Figure 2.3. Map showing the location of samples used to constrain the Victoria sea-level curve.

collected in 2000 and 2001 utilized percussion coring and vibracoring. James *et al.* (2002) discussed the initial results for the samples collected in 2000. The other data were compiled from publications spanning the past 45 years. The sample locations range from Saanich Peninsula on the east to Anderson Cove on the west (Fig. 2.3). The sample elevations relative to present sea level range from 75 m to -62 m. All dates in the following sample descriptions are in corrected radiocarbon years before

Table 2.1. Radiocarbon ages of samples used for constraining postglacial sea level in the Victoria region

Location[a]	Site (Fig. 2.3)	Latitude (°N)	Longitude (°W)	Altitude (m)	Material Dated	Lab No.	Radiocarbon Age[b]	Corrected Age[c]	Calibrated Age (1 S.D.)	Sea level position
Colwood Delta[1]	1	48.455	123.540	75	Wood	B-109128	12360 ± 70	12360 ± 70	14128-14566	marginal
O'Donnell Flats	2	48.541	123.416	65	Plant detritus	TO-9193	11100 ± 80	11100 ± 80	12938-13083	below
O'Donnell Flats	2	48.541	123.416	65	Gyttja	TO-9194	12620 ± 90	11995 ± 108	13754-13970	marginal
O'Donnell Flats	2	48.541	123.416	65	Shell (Nuculana? fragments)	TO-9195	13170 ± 80	12220 ± 94	13941-14204	above
Pike Lake	3	48.488	123.468	60	Plant fragments	TO-9190	10890 ± 330	10890 ± 330	12397-13197	below
Pike Lake	3	48.488	123.468	60	Plant detritus	TO-9191	12280 ± 120	12280 ± 120	13982-14458	above
Pike Lake	3	48.488	123.468	60	Shell (Nuculana? valves)	TO-9192	13240 ± 80	12290 ± 94	14007-14392	above
Maltby Lake	4	48.497	123.449	53	Plant fragments	TO-9181	10600 ± 140	10600 ± 140	12395-12804	below
Maltby Lake	4	48.497	123.449	53	Organic mud	TO-9182	12620 ± 90	11995 ± 108	13754-13970	marginal
Maltby Lake	4	48.497	123.449	53	Shell fragments	TO-9183	13320 ± 90	12370 ± 103	14129-14596	above
Prior Lake	5	48.476	123.466	38	Twig	TO-9186	11540 ± 330	11540 ± 330	13118-13735	marginal
Prior Lake	5	48.476	123.466	38	Twig	TO-9187	12320 ± 100	12320 ± 100	14046-14489	marginal
Prior Lake	5	48.476	123.466	38	Shell (Nuculana? fragments)	TO-9189	13070 ± 90	12120 ± 103	13845-14073	above
Gardner Pond[2]	6	48.683	123.433	30	Bison skull	SFU-549	11750 ± 110	11750 ± 110	13472-13720	below
Blenkinsop Lake[3]	7	48.475	123.350	27	Shell	GSC-246	12660 ± 80	12110 ± 94	13844-14052	above
McKenzie Ave.[4]	8	48.471	123.362	26	Shell	GSC-763	12720 ± 80	12170 ± 94	13904-14133	above
Matheson Lake	9	48.361	123.597	23	Plant fragments	TO-9184	12210 ± 100	12210 ± 100	13925-14206	marginal
Matheson Lake	9	48.361	123.597	23	Plant fragments	TO-9185	12120 ± 100	12120 ± 100	13852-14076	marginal
Patricia Bay[5]	10	48.658	123.433	20	Shell	GSC-418	12750 ± 85	12200 ± 99	13919-14179	above
Rithets Bog[4]	11	48.483	123.383	15	Gyttja	GSC-945	11400 ± 95	10775 ± 112	12709-12876	below
Saanichton[5]	12	48.592	123.392	8	Shell	GSC-398	12440 ± 115	11890 ± 125	13606-13891	above
Cook St.[6]	13	48.413	123.353	1	Shell	GSC-1114	12100 ± 80	11550 ± 94	13275-13474	above
Cook St.[6]	13	48.413	123.353	1	Freshwater shell	GSC-1130	11200 ± 85	10990 ± 104	12857-13000	below
Cook St.[6]	13	48.413	123.353	1	Plant material	GSC-1131	11500 ± 80	11500 ± 80	13269-13413	below
Cook St.[6]	13	48.413	123.353	1	Gyttja	GSC-1142	11200 ± 95	11200 ± 95	13020-13193	below
Portage Inlet[7]	14	48.463	123.423	-2	Peat	GSC-4830	6220 ± 80	6220 ± 80	7015-7247	below
Helmcken Park[8]	14	48.460	123.428	-2	Peat	GSC-4731	8580 ± 65	8580 ± 65	9438-9739	below

Table 2.1. Radiocarbon ages of samples used for constraining postglacial sea level in the Victoria region (continued)

Location[a]	Site (Fig. 2.3)	Latitude (°N)	Longitude (°W)	Altitude (m)	Material Dated	Lab No.	Radiocarbon Age[b]	Corrected Age[c]	Calibrated Age (1 S.D.)	Sea level position
Portage Inlet[9]	14	48.463	123.422	-2	Peat	I-3673	5470 ± 115	5470 ± 115	6032-6404	below
Portage Inlet[9]	14	48.463	123.422	-2	Peat	I-3674	6670 ± 120	6670 ± 120	7435-7620	below
Portage Inlet[9]	14	48.463	123.422	-2	Peat	I-3676	9250 ± 140	9250 ± 140	10250-10575	below
Portage Inlet	14	48.459	123.422	-2	Shell (Ostrea Lurida)	TO-9885	4010 ± 50	3290 ± 103	3461-3727	above
Portage Inlet	14	48.459	123.422	-2	Peat	TO-9886	11170 ± 80	11170 ± 80	12972-13140	below
Portage Inlet	14	48.459	123.422	-2	Shell fragments	TO-9887	13140 ± 80	12190 ± 94	13921-14159	above
Anderson Cove	15	48.361	123.659	-4	Shell (Saxidomus Giganteus)	TO-9888	4430 ± 50	3710 ± 103	4009-4311	above
Anderson Cove	15	48.361	123.659	-4	Peat	TO-9889	6900 ± 60	6900 ± 60	7673-7792	below
Anderson Cove	15	48.361	123.660	-4	Plant and wood fragments	TO-9890	5100 ± 70	5100 ± 70	5749-5917	marginal
Anderson Cove	15	48.361	123.660	-4	Wood fragments	TO-9891	8160 ± 80	8160 ± 80	9011-9248	below
Anderson Cove	15	48.361	123.660	-4	Bark fragments(?)	TO-9892	7760 ± 80	7760 ± 80	8434-8600	below
Anderson Cove	15	48.361	123.660	-4	Peat	TO-9893	9010 ± 80	9010 ± 80	9941-10248	below
Juan de Fuca Strait[10]	16	48.420	123.430	-32.8	Shell	CAMS-62767	8910 ± 50	8190 ± 103	9118-9382	above
Juan de Fuca Strait[10]	16	48.415	123.427	-41.7	Shell	CAMS-62533	8490 ± 50	7770 ± 103	8535-8841	above
Juan de Fuca Strait[10]	16	48.415	123.427	-42.5	Shell	CAMS-62534	13370 ± 50	12420 ± 71	14212-14620	above
Juan de Fuca Strait[10]	16	48.415	123.426	-42.7	Shell	CAMS-58684	10640 ± 50	9690 ± 71	11029-11196	above
Juan de Fuca Strait[10]	16	48.415	123.426	-44	Shell	CAMS-58685	9880 ± 50	9160 ± 103	10296-10519	above
Esquimault Harbour[11]	17	48.398	123.381	-55	Shell	RIDDL-265	9670 ± 140	8950 ± 166	9949-10399	above
Juan de Fuca Strait[10]	18	48.400	123.414	-60.5	Shell	CAMS-58695	10720 ± 60	9770 ± 78	11114-11229	above
Juan de Fuca Strait[10]	18	48.400	123.414	-61.3	Shell	CAMS-58696	13690 ± 50	12740 ± 71	14912-15168	above

[a] All dates are from this study unless noted: [1]Monahan et al. (2000); [2]Hebda (1988); [3]Dyck *et al.* (1965); [4]Lowdon and Blake (1970); [5]Dyck *et al.* (1966); [6]Lowdon *et al.* (1971); [7]McNeely and Jorgensen (1993); [8]McNeely and Jorgensen (1992); [9]Buckley and Willis (1970); [10]Mosher and Hewitt (2004); [11]Linden and Schurer (1985)

[b] All dates ± 1σ limits

[c] Corrections applied include: -950±50 yr for marine samples >10 000 yr BP; -720±90 yr for marine samples < 10 000 yr BP; -625±60 yr for basal freshwater samples; 400-415 yr for GSC marine samples that were not normalized to $\delta^{13}C$ = -25.0‰

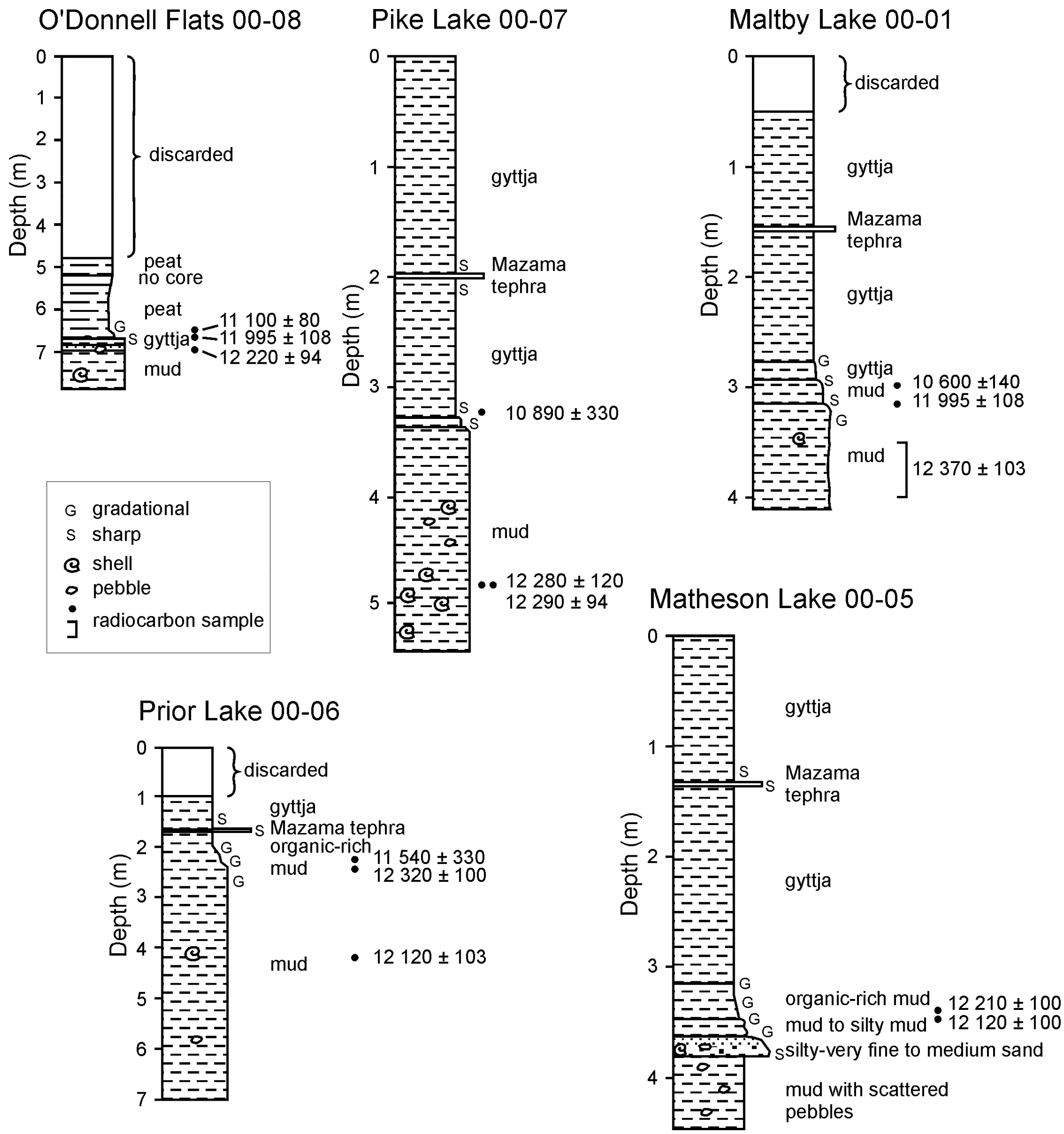

Figure 2.4. Sediment cores collected in 2000. Ages are in corrected radiocarbon years BP. S and G indicate sharp and gradual contacts, respectively.

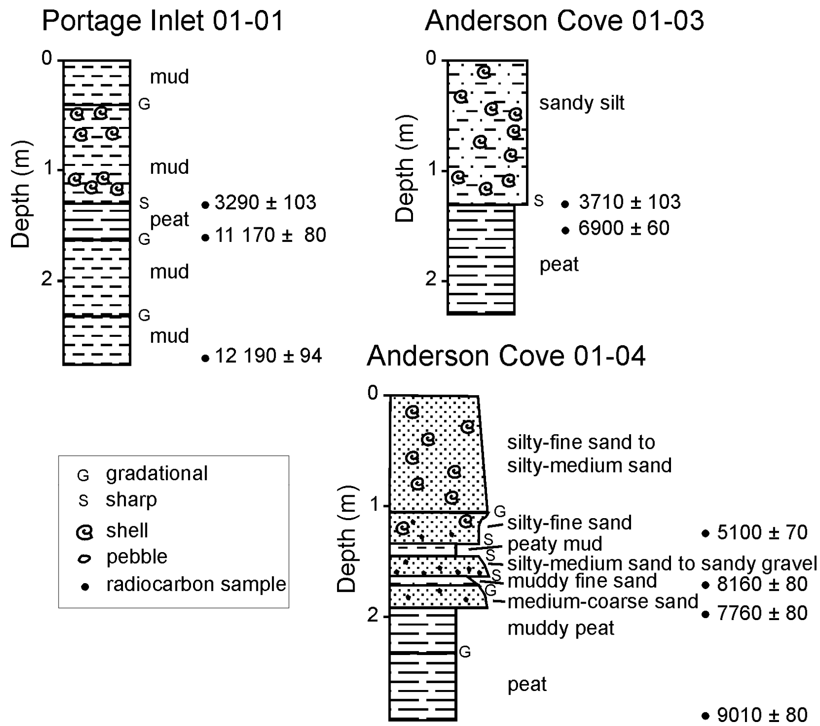

Figure 2.5. Sediment cores collected in 2001. Ages are in corrected radiocarbon years BP. S and G indicate sharp and gradual contacts, respectively.

present (yr BP). Ian Hutchinson (Department of Geography, Simon Fraser University), John Clague (Department of Earth Sciences, Simon Fraser University) and Thomas James (Natural Resources Canada; University of Victoria) interpreted the lithology of the cores. Figures 2.4 and 2.5 show the cores collected in 2000 and 2001, respectively. Table 2.1 lists the radiocarbon dated samples used in this study. The following section gives detailed stratigraphic information related to sea level for each locality given in Table 2.1. The descriptions are in order of highest to lowest elevation.

2.3.2 Colwood Delta

A radiocarbon sample of wood in the Colwood Delta provides an age for the maximum highstand in the study area. The sample was in a horizontally bedded sand and silt layer overlying foreset planar cross-bedded sand and gravel (Monahan *et al*., 2000; V. Levson, pers. comms., 2002). The elevation in the area is about 78 m, but the sample was collected at approximately 2 m depth. The sample has an age of 12 360 ± 70 yr BP. The wood is found in toplap deposits, coarse sediments that deposit when a river first enters a basin, possibly indicating that sea level was likely near this elevation during the formation of the delta. The delta formed when sea level was between 80 and 65 m elevation. Deposition ceased when Saanich Inlet became ice free (Howes and Naismith, 1983).

2.3.3 O'Donnell Flats

A vibracore from O'Donnell Flats at an elevation of 65 m was collected on June 30-31, 2000. The core was 7.8 m in length. The upper 4.8 m were discarded due to the homogenous peat composition. The core comprised marine mud overlain by gyttja and peat (Fig. 2.4). The mud was clayey silt with some very fine sand. The contact between the mud and gyttja occurred at 6.64 m depth and is sharp. The gyttja layer is 0.14 m thick and is weakly stratified. The contact between the gyttja and peat occurs at 6.50 m and is gradational. The peat contains abundant plant fragments.

Three radiocarbon samples were taken from this core. Marine shell fragments (possibly *Nuculana sp*) taken at 6.97 m depth in the mud yielded a corrected age of 12 220 ± 94 yr BP. A bulk sample taken from the base of the gyttja layer between 6.61-6.64 m depth had a corrected age of 11 995 ± 108 yr BP. This sample indicates that sea level dropped below 65 m at around 12 000 yr BP. A bulk sample of plant detritus from the base of the peat layer between 6.47-6.49 m depth had a corrected age of 11 100 ± 80 yr BP. The dates indicate that sea level likely dropped below 65 m sometime between 12 200 and 12 000 yr BP.

2.3.4 Pike Lake

A 5.45 m core was recovered from Pike Lake at an elevation of 60 m on June 30, 2000 (Fig. 2.4). The core comprised mud overlain by gyttja. The mud is mottled silty clay or clayey silt at depths below 3.36 m. Between the lower mud unit and the gyttja unit are a 0.04 m thick organic rich mud layer and a 0.03 m layer of weakly laminated gyttja and organic rich mud layers. The contacts between the layers are sharp. Above 3.29 m is a dark brown, massive gyttja that becomes less dense further up the core. Tephra from the Mount Mazama eruption occurs at 2.01 m depth.

Three radiocarbon samples were taken from the core at Pike Lake. Plant detritus taken from 4.81-4.82 m depth in the clayey silt gave an age of 12 280 ± 120 yr BP. An articulated marine shell (possibly *Nuculana sp*) taken from the same interval gave a corrected age of 12 290 ± 94 yr BP. The paired plant detritus and shell sample give the same date, suggesting that the reservoir correction is likely fairly accurate. These dates indicate that sea level was above 60 m at 12 300 yr BP. Plant fragments taken at a depth of 3.32-3.33 m in the transition between mud and gyttja gave an age 10 890 ± 330 yr BP. This sample indicates that sea level dropped below 60 m by 10 900 yr BP.

2.3.5 Maltby Lake

A 4.1 m core was recovered from Maltby Lake at an elevation of 53 m on June 2, 2000 (Fig. 2.4). The upper 0.5 m of core was discarded. The core comprised of gyttja overlying mud. A sharp contact between the mud and gyttja was at 2.94 m. Above 3.19 m, the mud becomes increasingly laminated and organic rich. Tephra from the Mount Mazama eruption occurs at 1.58 m depth.

Three radiocarbon samples were taken from this core. Marine shell fragments from between 3.49 and 3.97 m in the mud gave a corrected age of 12 370 ± 103 yr BP, indicating that sea level was higher at this time. A bulk sample of laminated organic mud, taken between 3.13 and 3.18 m gave a corrected age of 11 995 ± 108 yr BP. The laminated mud likely represents when sea level fell below 53 m. Plant fragments from 3.01 m in the mud just below the contact dated to 10 600 ± 140 yr BP.

2.3.6 Prior Lake

A 7.3 m core was recovered form Prior Lake at an elevation of 38 m on June 29, 2000 (Fig. 2.4). The upper 0.74 m of the core was discarded. The core comprised gyttja overlying mud. The contact between the units was gradational between 2.01-2.34 m. Tephra from the Mount Mazama eruption occurred at 1.58 m.

Three samples were taken from the core for radiocarbon dating. A marine shell (possibly *Nuculana sp*.) in mud from 4.25 m depth had a corrected date of 12 120 ± 103 yr BP. A twig taken at 2.40 m in mud dated to 12 320 ± 100 yr BP. This twig is just below the transition to gyttja, and is slightly older and inconsistent with the younger marine shell date located lower in the core. Another twig from 2.26 m in the transition from mud to gyttja had an age of 11 540 ± 330 yr BP. This sample is in an interval that likely indicates the transition from marine to freshwater conditions.

2.3.7 Gardner Pond

A bison skull was excavated from sediments at an elevation of about 30 m (Mackie, 1987). The skull was at a depth of 1.5 m in a marl layer overlying marine clay. The skull dates to 11 750 ± 110 BP (Hebda, 1988). This indicates that sea level dropped below 30 m by that time.

2.3.8 Blenkinsop Lake

Marine shells were collected from Blenkinsop Lake at an elevation of 27 m (Dyck *et al*., 1965). The shells (*Mya truncata)* were in a clay unit, and have a corrected date of 12 110 ± 94 yr BP. This date indicates that sea level dropped below 27 m sometime after 12 110 yr BP.

2.3.9 McKenzie Ave, Victoria

Marine shells were collected from a drillhole on McKenzie Ave in Victoria at an elevation of 26 m (Lowdon and Blake, 1970). The samples were whole shells (*Hiatella arctica*) in a shelly layer between a silty clay and peat. The corrected age of the sample is 12 170 ± 94 yr BP. This sample indicates that sea level stayed above 26 m until after 12 170 yr BP.

2.3.10 Matheson Lake

A 4.4 m core was recovered at Matheson Lake at an elevation of 23 m (Fig. 2.4). The core comprised mud and sand overlain by gyttja. Below 3.75 m was massive clayey silty mud with scattered pebbles. From 3.56-3.75 m was medium sand grading up to silty, very fine sand with rip-up clasts of clay, plant detrius and shell fragments. Between 3.28-3.56 m was silty and clayey mud that fines upwards to organic rich mud. From 3.13-3.28 m was a transitional layer between the mud and gyttja. Mazama tephra was at 1.37 m depth.

Two radiocarbon samples were taken from the silty and clayey mud layer overlying the sand layer. Plant fragments taken at 3.52 m dated to 12 120 ± 100 yr

BP. Another sample of plant fragments at 3.47 m dated to 12 210 ± 100 yr BP. The sand layer from 3.56-3.75 m suggests a high energy environment, indicating sea level was likely near 23 m when it was deposited. The mud layer immediately above the sand probably corresponds to when sea level dropped below Matheson Lake.

2.3.11 Patricia Bay

A marine shell sample was collected from a gravel pit at an elevation of about 20 m (Dyck *et al*., 1966). The marine shells (*Saxidomus sp.*) were taken from a shelly layer in the lower part of a gravely shore deposit that overlies marine clay. The shells have a corrected age of 12 200 ± 94 yr BP. The top of the gravel unit is at an elevation of 24 m, and the age of the shells likely corresponds to when sea level was near this elevation.

2.3.12 Rithets Bog

A gyttja sample was taken from Rithets Bog at an elevation of 15 m (Lowdon and Blake, 1970). The sample taken 5-8 cm above the contact between the gyttia and underlying marine clay had a corrected age of 10 775 ± 112 yr BP. This sample indicates that sea level was below 15 m by 10.7 kyr BP.

2.3.13 Saanichton

Marine shell fragments were taken from a gravel pit at an elevation of about 8 m (Dyck *et al*., 1966). The fragments were in clay below a deltaic deposit and have a corrected age of 11 890 ± 125 yr BP. The date indicates that sea level remained above 8 m until after 11 900 yr BP.

2.3.14 Cook Street, Victoria

An excavation along Cook Street, Victoria, revealed a section of freshwater sediments overlying marine clay at about 1 m elevation (Lowdon *et al*., 1971). Four radiocarbon samples were taken at this site. A marine shell (*Saxidomus giganteus*) taken 0.45 m below the contact has a corrected age of 11 550 ± 94 yr BP. Freshwater shells taken above the contact have a corrected age of 10 990 ± 104 yr BP. The gyttja correction was applied to the freshwater shells as they derive their carbon from plankton and material at the bottom of the basin (I. Hutchinson, pers. comms., 2006). Bulk plant material taken above the contact where the freshwater shells were located had an age of 11 500 ± 80 yr BP. No correction was necessary for the plant material, as they are vascular plants that derive their carbon directly from the atmosphere Gyttja taken 15-18 cm above the freshwater samples had an age of 11 200 ± 95 yr BP. No correction was made on the gyttja sample, as it was not a basal gyttja. The discrepancy in age between the freshwater shells and the plant material in the same interval indicates that a reservoir correction may not be appropriate for the freshwater shells. The dates indicate that sea level fell below 1 m elevation sometime between 11 500 and 11 000 yr BP.

2.3.15 Portage Inlet/ Helmcken Park

Three cores were taken at Portage Inlet on May 8-10, 2001, where the sill depth is about -2 m. One 4.19 m core (01-01) was logged and sampled (Fig. 2.5). The core comprised two mud layers separated by peat. Below 2.31 m was grey mud with olive grey organic mud phases, shell fragments and black organic streaks. From 1.36-2.31 m was grey organic-rich mud, with a transitional lower contact. Between 1.31-1.63 m was reddish brown to reddish grey muddy peat with a transitional lower contact. Above 1.31 m was a grey to black mud with abundant marine shells. Two other cores did not encounter a peat layer and were not sampled.

Three samples from the core were dated. Marine shell fragments from 2.7-2.73 m depth gave a corrected age of 12 190 ± 94 BP. A sample from near the base of the peat layer at 1.60-1.62 m dated to 11 170 ± 80 yr BP. A marine shell (*Ostrea Lurida*) taken at 1.29 m had a corrected age of 3290 ± 103 yr BP.

Several radiocarbon ages have been taken from Portage Inlet in previous studies. Three samples of peat were taken from a core collected in the late 1960s (Buckley and Willis, 1970). Peat directly overlaying the glaciomarine clay had an age of 9250 ± 140 yr BP. Peat overlaying Mazama tephra dated to 6670 ± 120 yr BP. Peat underlying marine sediments dated to 5470 ± 115 yr BP. A date from the base of freshwater peat at Helmcken Park on the west side of Portage Inlet gave an age of 8580 ± 65 yr BP (McNeely and Jorgensen, 1992). Another peat sample from the north shore of Portage Inlet underlying silty sand dates to 6220 ± 80 yr BP (McNeely and Jorgensen, 1993).

The data from Portage Inlet constrain the timing of the late Pleistocene sea-level fall and a mid-Holocene sea-level rise. The radiocarbon ages indicate that sea level dropped below 2 m sometime between 12 200 and 11 200 yr BP. It stayed below current sea level until sometime after 5500 yr BP.

2.3.16 Anderson Cove

Two cores were taken from Anderson Cove on May 9, 2001, where a barrier sill occurs at -4 m (Fig. 2.5). One 2.28 m core (01-03) comprised peat overlain by sandy silt. Below 1.52 m was muddy peat, grading upwards to greyish brown peat.

Dark grey, fine sandy silt sharply overlies the peat. A second 2.92 m core (01-04) comprised peat and sand. Below 1.90 m was peat. From 1.35-1.90 m was muddy sand and peat. Above 1.35 m was silty fine sand with occasional shell fragments and pebbles.

Two samples were dated from the first core (01-03). Peat from 1.54 m dated to 6900 ± 60 BP. A marine shell (*Saxidomus Giganteus*) from 1.29-1.34 m depth had a corrected age of 3710 ± 103 yr BP. Four samples were dated from the second core (01-04). Peat from a depth of 2.85 m dated to 9010 ± 80 yr BP. A piece of bark from 1.94 m depth dated to 7760 ± 80 yr BP. Wood fragments from 1.70 m depth dated to 8160 ± 80 yr BP. This anomalous age may indicate reworking of this unit, or the wood was old when it was deposited. Plant and wood fragments taken at 1.2 m depth within the silty fine sand had an age of 5100 ± 70 yr BP. The ages from the peat layer indicate that sea level remained below -4 m between 9000 and 6900 yr BP. If the silty fine sand unit represents when sea level was near -4 m, then sea level was at this level by 5100 yr BP. By 3700 yr BP, sea level was above -4 m.

2.3.17 Juan De Fuca Strait/ Esquimalt Harbour

Linden and Schurer (1988) and Mosher and Hewitt (2004) sampled marine sediments offshore of Victoria (table 1). The depth range of the samples is between -32.8 and -61.3 m. Eight dates from marine shells are used to determine lowstand range. The age of the samples ranges between 12 740 to 8190 yr BP. All of samples indicate that sea level was higher when the samples grew. Due to the lack of data, sea level position is not well constrained below -4 m.

2.4 Victoria sea-level curve

2.4.1 Previous work

Mathews *et al.* (1970) constructed the first radiocarbon constrained sea level curve for the Victoria area. Using a small amount of available data, they estimated that sea level fell from the highstand at 75 m to roughly present levels within a 2000 year period. Excavations at a water depth of -9 to -11 m in Esquimalt Harbour exposed leached marine shells and hardened sediments, indicating that the sediments were subaerially exposed at this depth. The authors also indicate that river mouths existed below present sea level in Saanich Inlet. Clague *et al.* (1982) expanded on the work of Mathews *et al*. (1970) and added that during the first half of the Holocene, sea level remained below -4 m elevation. They also indicated that sea level never rose above 1.5 m during the Holocene.

Linden and Schurer (1988) collected cores and seismic data in the Juan de Fuca Strait in the Victoria area. The seismic profiles identified an erosional unconformity between an acoustically transparent unit and stratified sediments to a depth of -70 m. Above -50 m it has an irregular appearance. The authors suggested that the unconformity was due to a drop in sea level to a depth of about -50 m based on an incomplete sediment record and dense clay from the seismically transparent unit found only above this level. They attributed the unconformity below that level to marine origins. They concluded that after 9000 yr BP, sea level in the Victoria area was influenced mainly by eustatic sea-level rise.

James *et al.* (2002) described the initial results of cores collected in 2000 (described in detail earlier). The modern 800 year reservoir correction (Southon, *et al.*, 1990) was used for marine samples, though it was noted that this correction may have been too small for late glacial samples. They also note an inconsistency in bulk basal gyttja ages, a problem addressed in Hutchinson *et al.* (2004b). James *et al.* (2002) noted that the rate of sea level fall decreased after 12 000 yr BP, and by 11 500 yr BP sea level dropped below present level.

Mosher and Hewitt (2004) did multibeam, seismic reflection and coring surveys to find the maximum sea level lowstand in the Victoria area. The multibeam and reflection surveys found a series of terrace and ridge features at -15, -35, -50 and -65 m depth in post-glacial sediments overlying glacial-marine sediments. The authors interpreted the terraces to be wave-cut erosional features when sea level was lower. They also found there were similar erosional features at -80 to -90 m depth, though they attributed those to shallow water erosion effects. Given the peak amplitude and period of waves in the Juan de Fuca Strait, they used this as evidence that sea level dropped to between -55 and -65 m elevation. The sea-level curve proposed by Mosher and Hewitt has a lowstand position at these depths.

2.4.2 New sea-level curve

Figures 2.6 and 2.7 show the interpreted postglacial sea-level curve in the Victoria area in radiocarbon and calibrated years respectively. The radiocarbon plot shows 1-sigma confidence limits, while the calibrated plot shows the probability distribution of the samples in calendar years. The samples provide tight constraints for determining the sea-level history for elevations above -4 m. The sea-level highstand in the Victoria area is somewhere between 75 and 80 m, given by the deposition of the Colwood Delta at this level. The wood sample provides a limiting age of when sea level was at this elevation. Between 14.5 and 13.2 cal kyr BP (12

500 and 11 500 yr BP), sea level dropped from its highstand to present sea level. There is overlap between some marine and terrestrial dates, with some terrestrial dates (Matheson Lake and Prior Lake) dating older than marine dates. The Prior Lake sample is a twig, and it may not be *in situ*. The Matheson Lake samples are unidentified plant material immediately above a sand deposit that likely corresponds to a beach. This material may need a reservoir correction. Other than these two points, the dates from the marine and terrestrial samples are consistent and indicate a rapid sea level drop. The rate of sea-level fall probably slowed after sea level dropped below about 30 m, as cores below this elevation have intervals of sand corresponding to beach deposits. Beach deposits are not evident at higher elevations as sea level was likely dropping so rapidly that there was not enough time to create developed beaches.

2.4.3 Lowstand position

The magnitude of the sea-level lowstand is poorly constrained, as there are few radiocarbon dates between -4 and -40 m. Subaerially exposed deposits occur to a depth of at least -11 m (Mathews *et al.*, 1970). If the assumed rate of sea-level fall is constant after 13.7 cal kyr BP (fig. 2.7), then the lowstand could have been as low as about -40 m, limited by the marine dates collected by Mosher and Hewitt (2004).

Though there are apparent unconformities to depths of -70 m (Linden and Schurer, 1988; Mosher and Hewitt, 2004), it is not likely the result of subaerial exposure because it would require sea-level fall to accelerate after 13.2 cal kyr BP. Figure 2.8 shows all the radiocarbon ages from Linden and Schurer (1988) and

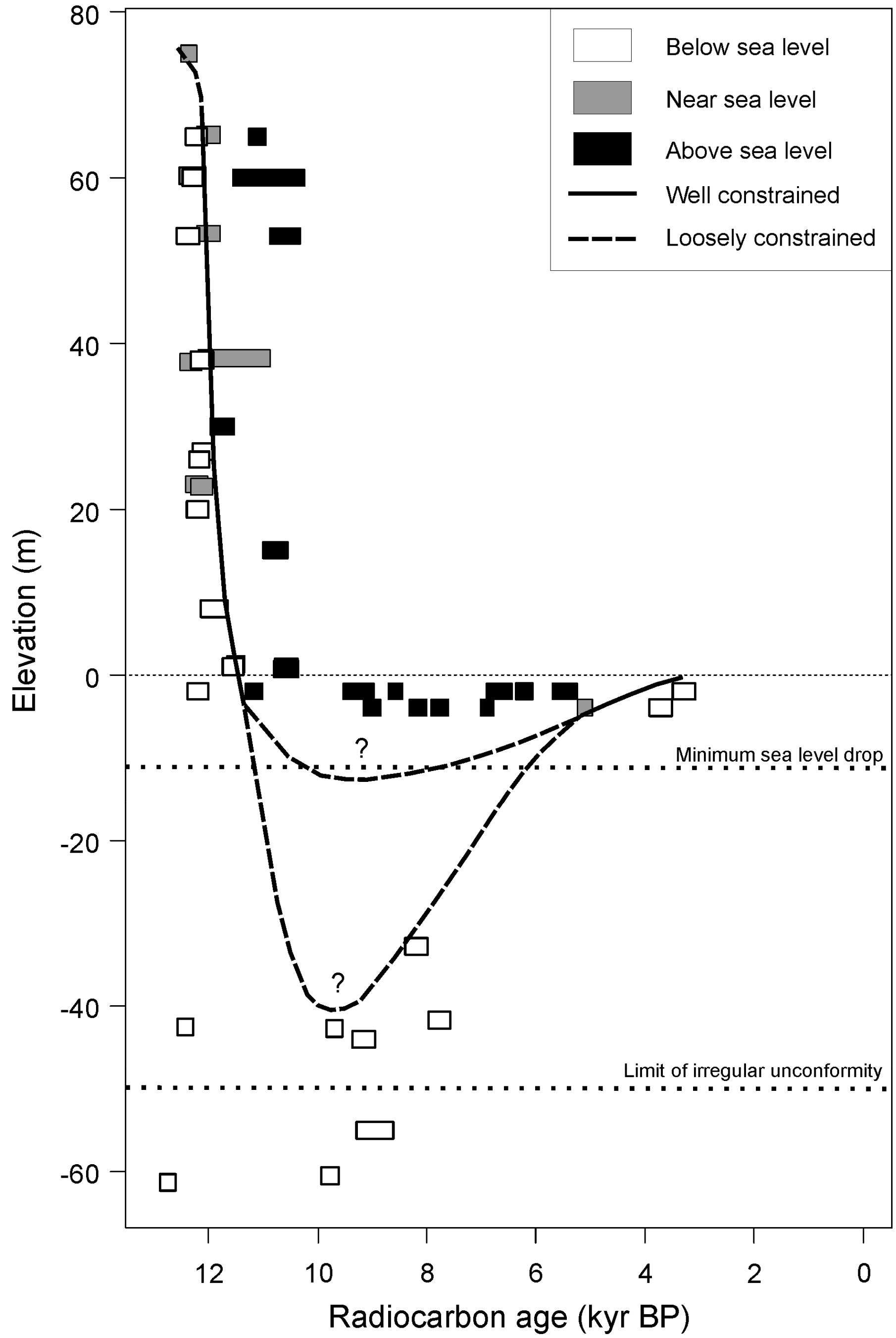

Figure 2.6. Sea-level curve for the Victoria area in radiocarbon years BP. The two curves below present sea level indicate the possible minimum and maximum sea level lowstand scenarios, based on subaerially exposed sediments found at -11 m depth and marine shell dates assuming a constant sea-level fall from Mosher and Hewitt (2004) respectively. Given the constraints on the rate of regression and radiocarbon dates from samples from offshore of Victoria, it is unlikely that the irregular conformity found to a depth of -50 m by Linden and Schurer (1985) was due to subaerial exposure.

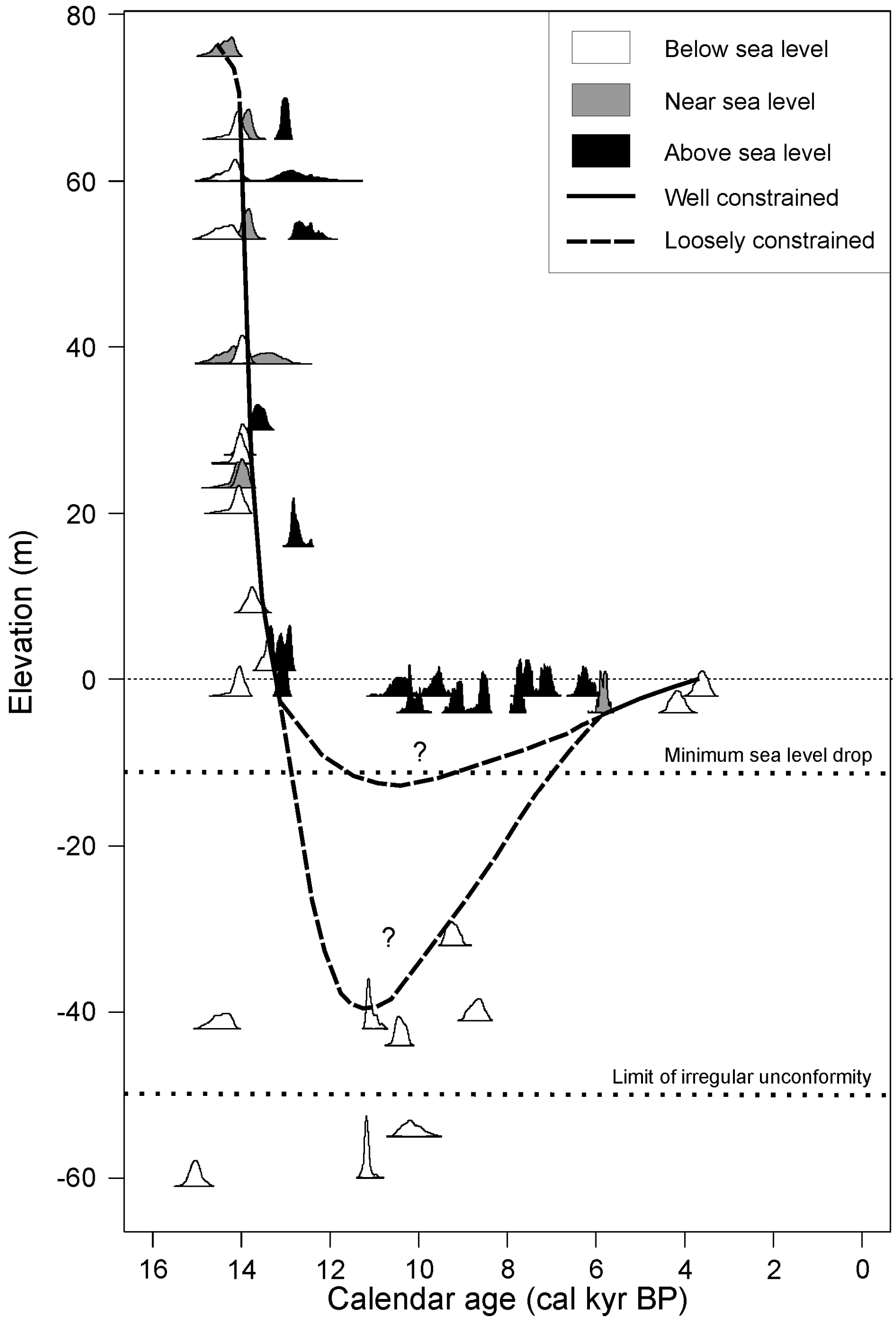

Figure 2.7. Sea level for the Victoria area in calibrated years BP. All dates are calibrated using Calib 5.0 (Stuiver and Reimer, 1993). The symbols correspond to the probability distribution of the sample age, scaled by a factor of 1000.

Mosher and Hewitt (2004) in the eastern Juan de Fuca Strait with respect to present water depth. There are no radiocarbon dates from 12.9-11.5 cal kyr BP, suggesting the change from glaciomarine to post-glacial sedimentation may correspond to the Younger Dryas period (Fairbanks, 1989). By 11.2 kyr BP, sea level was above -40 m. If sea level was lower than -40 m, it was short lived. The post-glacial sediments are interpreted to be derived mainly from reworking of older sediments (Hewitt and Mosher, 2001), so it cannot be ruled out that the unconformities are the result of submarine slumping or tidal currents.

Isostatic depression is caused by the flow of mantle material away from an area covered by ice sheets (Turcotte and Schubert, 2002). When the ice sheets melt away, the Earth slowly returns to its original form in an exponential fashion. The local crustal depression is determined by removing the eustatic (global) sea-level component from the local relative sea level. Sea level at Barbados is used as eustatic sea level (Bassett *et al.*, 2005; Fig. 2.9). Figure 2.10 shows the crustal response of the minimum and maximum uplift scenarios. The maximum sea level drop scenario has a steady exponential decay of crustal response. The minimum sea level drop scenario has an irregular form, with an initially slower decay between 9-13 cal kyr BP followed by a more rapid decay. This situation would require local ice sheets to grow between 11 and 8 cal kyr BP to slow the crustal response. This indicates that the minimum sea-level drop scenario is unlikely because local ice sheets were completely melted before 10 cal kyr BP (Clague, 1981).

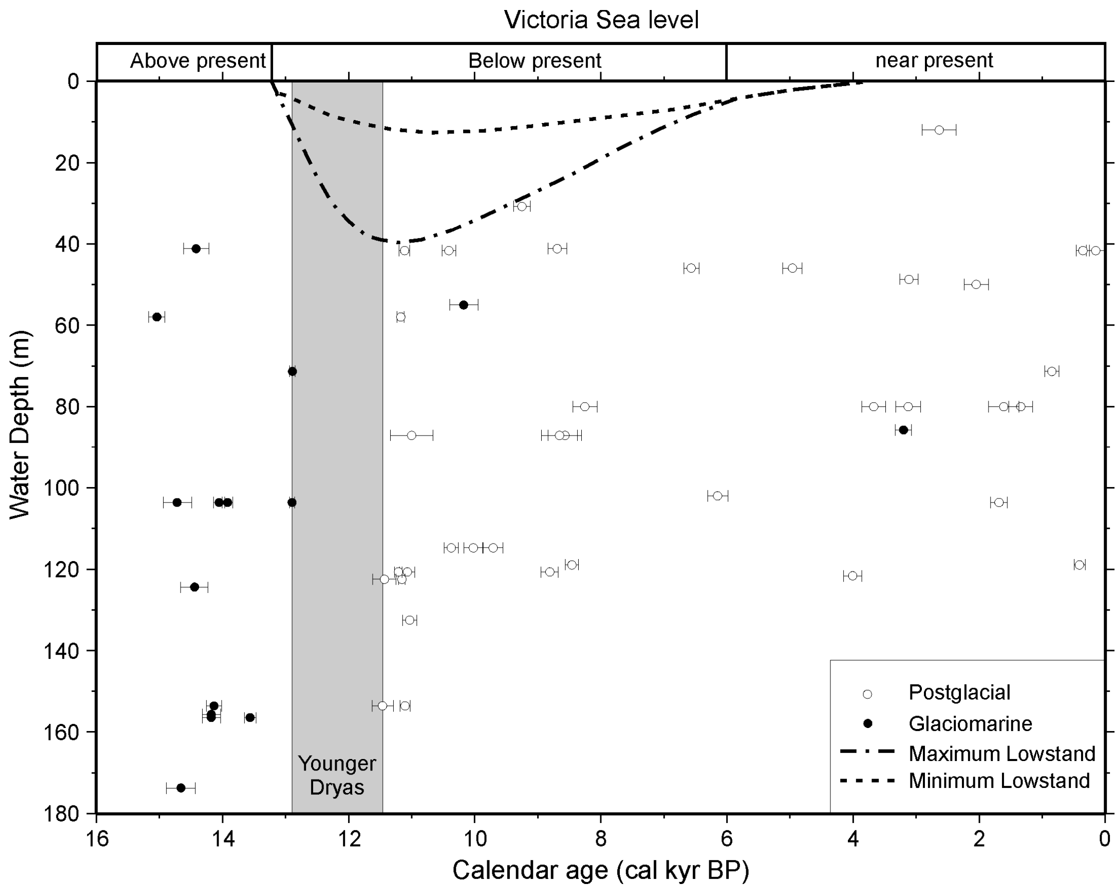

Figure 2.8. Radiocarbon age (calibrated 1σ limits) of marine shell samples from the eastern Juan de Fuca Strait (Linden and Schurer, 1988; Mosher and Hewitt, 2004) and inferred minimum and maximum sea-level lowstand positions scenarios for the Victoria area (Fig. 2.7). Also shown is the time period corresponding to the Younger Dryas (Fairbanks, 1989)

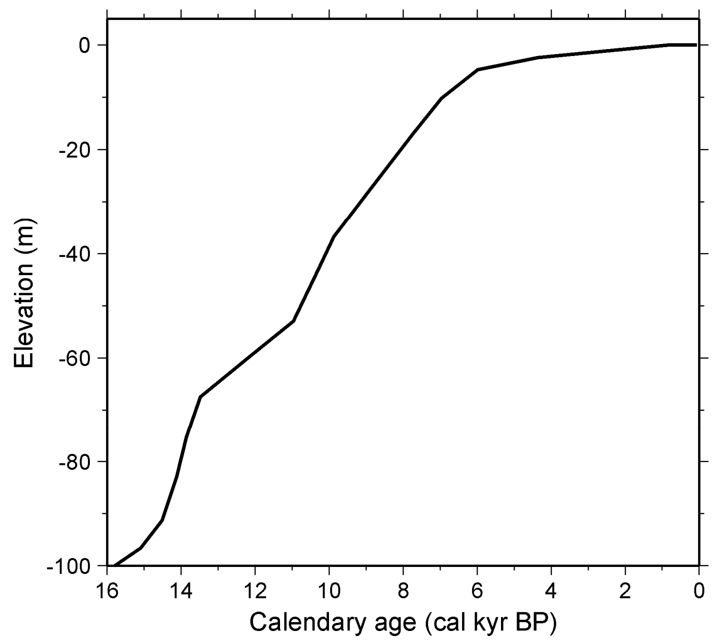

Figure 2.9. Eustatic sea level from Barbados (Bassett *et al.*, 2005). Eustatic sea level was over 100 m lower than present at 16 cal kyr BP, and rose to within a few metres of present 4-6 cal kyr BP.

The decay time of the maximum sea level drop scenario is 1250 years (Fig. 2.10), which is similar to the initial response in the northern Strait of Georgia (James *et al.*, 2005). There possibly is a shorter decay time of about 630 years during the early response, though a constant 1250 year decay fits the observed crustal response fairly well. In the northern Strait of Georgia, the initial decay time was found to be the combination of 500 and 2600 year times, which when combined produced an apparent early decay time of 1200 years. The effect of the shorter decay time was negligible within 1000 years after deglaciation. The 1250 year decay time observed in the response at Victoria is similar to the superimposed 500 and 2600 year decay times. If there is a longer decay time in the response at Victoria, it is not resolved due to the poor constraints on sea level after 13.2 cal kyr BP. The implication of a longer

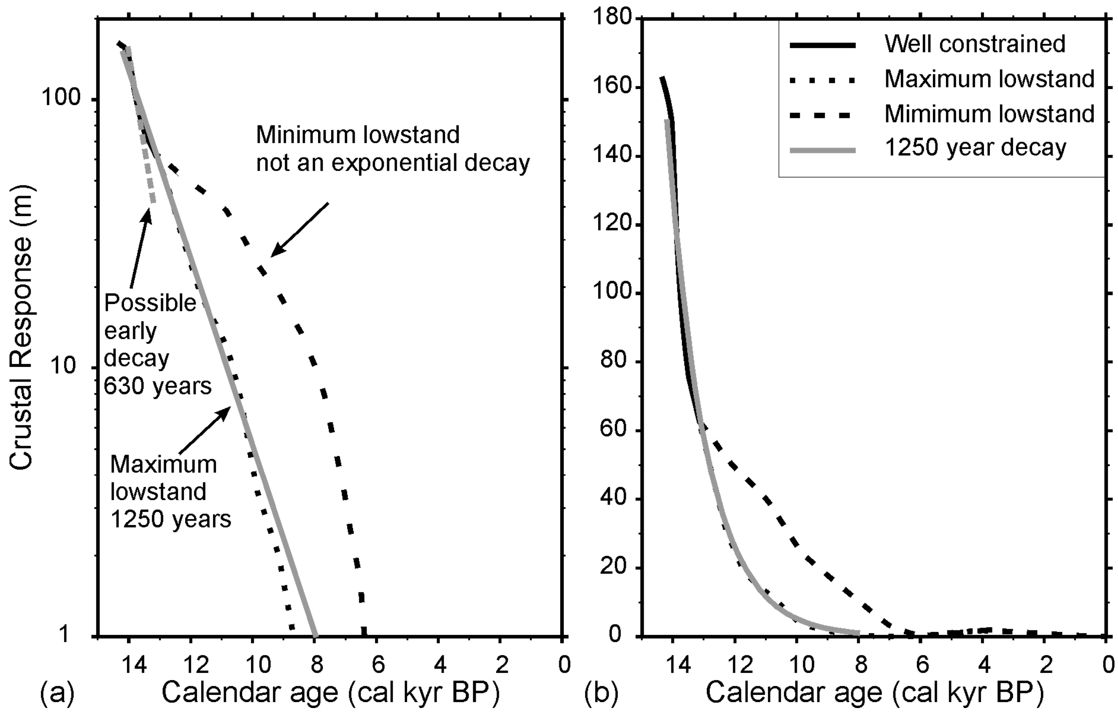

Figure 2.10. Crustal response from the Victoria area for the minimum and maximum sea-level lowstand scenarios. The best fit line for the maximum lowstand scenario has a decay time of about 1250 years. (a) log scale showing the exponential decay of the maximum lowstand scenario, versus the irregular behavior of the minimum lowstand scenario (b) crustal response with the predicted 1250 year decay curve.

decay time at later times would be that the lowstand position would be less than the maximum scenario.

2.4.4 Holocene sea level

During the early Holocene (10 to 6 cal kyr BP), the rate of sea-level rise is unknown, and depends on the assumed magnitude of the lowstand. A marine shell date indicates that sea level was higher than -33 m by 9.4 cal kyr BP. If the sea level lowstand was about -40 m, then sea-level rise was gradual and likely followed eustatic sea-level rise. If sea level did not fall much below 11 m below present, then sea level would have been relatively stable for about 4000 years before rising to present sea level sometime after 6 cal kyr. Sea level rose above -4 m sometime between 6.0 and 4.3 cal kyr BP. Once above this level, sea level stabilized, indicated by the mid-Holocene change from marine to freshwater sedimentation at Anderson Cove and Portage Inlet.

Hutchinson (1992) compiled dates relating to Holocene sea level in the Victoria area. These dates were recalibrated and plotted along with new dates from this study on Fig. 2.11. The dates indicate that sea level likely did not rise above present in the late Holocene, with the exception of a section of Island View Beach. Variability in the elevation of samples labeled as terrestrial come from uncertainty in measured elevation and choice of datum. Sea level has remained within 2 m of present since 4.5 cal kyr BP.

Island View Beach, located on the eastern shore of Sannich Peninsula, shows evidence of a recent sea-level rise that is anomalous compared to the rest of the Victoria area (Clague, 1989; Hutchinson, 1992). It is unknown whether or not the late Holocene sea level history at Island View Beach is due to tectonic motions or some local feature (Clague, 1989). The Southern Whidbey Island fault zone, which extends to just south of the Saanich Peninsula, had an earthquake about 2.8-3.2 cal kyr BP, and caused 1-2 m of uplift north of the fault (Kelsey *et al.*, 2004). Though this event predates the apparent sea-level rise at Island View Beach by at least 800 years, it shows that the region has active faults that can produce a local 1-1.5 m sea-level rise. A similar sea-level rise event happened west of the study area in Muir Creek, though the material dated there indicates that the sudden sea-level rise

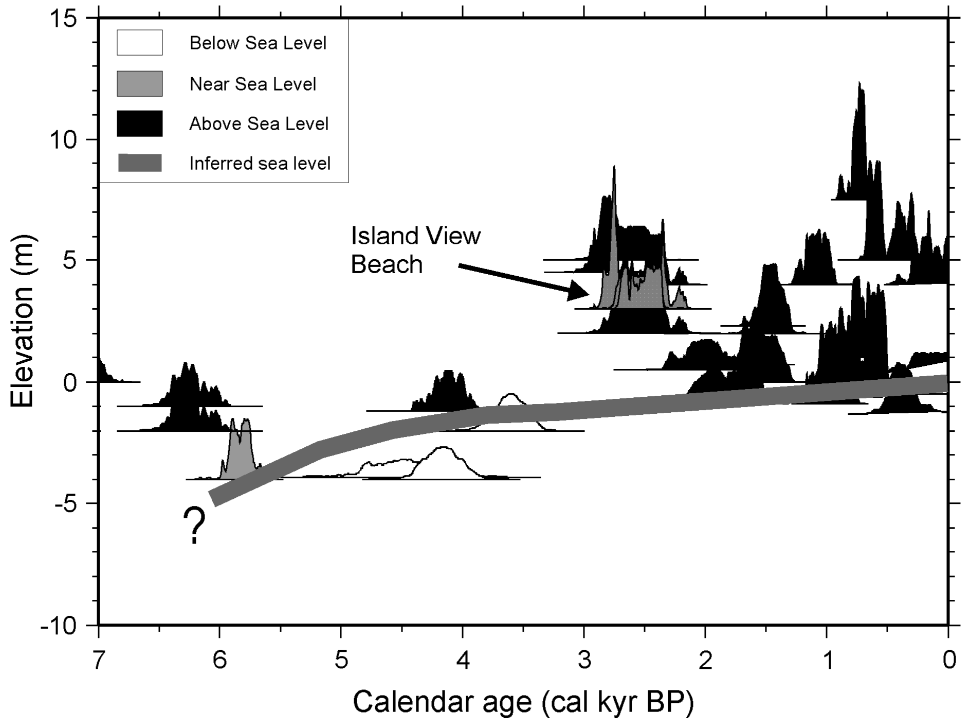

Figure 2.11. Age probability distribution (scaled by a factor of 1000) of calibrated radiocarbon samples that provide limits on sea level for the Victoria area in late Holocene time (Hutchinson, 1991). The data indicates that sea level remained relatively stable near present level for the past 4000 years. A transgression at Island View Beach appears to be a local event as it contradicts all other samples from the Victoria area.

happened at least 1000 years before Island View Beach (McNeely and Jorgensen, 1992). Due to this, any observed late Holocene sea level change in the Victoria area could be subjected to tectonic motions that exceed the rate of eustatic sea-level rise or postglacial rebound effects. Regardless, given the amount of terrestrial based dates from levels above present sea level (Hutchinson, 1992; Fig. 2.11), the samples at Island View Beach are likely a result of a localized feature.

2.4.5 Comparison with previous curves

Figure 2.12 compares the sea-level curve from this study with previous studies. Early studies (Mathews, 1970; Clague *et al.*, 1982; Linden and Schurer, 1988) did not use reservoir corrections and had fewer data points, so there is up to

1000 year difference in the initial timing of sea level fall. Due to the lack of data below present sea level, the sea level curves of Mathews *et al.* (1970) and Clague *et al.* (1982) had a smaller lowstand than this study. The sea level curve of Linden and Schurer (1988) is most similar to the present study. To construct their sea-level curve, they extrapolated between the observed highstand at 75 m and an irregular unconformity surface at -55 m using the timing from Clague *et al.* (1982) for the Victoria area and Peterson *et al.* (1984) for Alsea Bay, Oregon, respectively. The sea-level curve of Mosher and Hewitt (2004) use most of the same data as this study. The increased highstand position of 90 m is the result of an erroneous elevation of one of the samples (CAMS-33492), which is from a core in Saanich Inlet at a depth of -90 m (Blais-Stevens *et al.*, 2001). The earlier sea level drop and lowstand at -60 m instead of at a shallower depth is due to the sea level curve being drawn through marine samples, rather than above them.

2.4.6 Comparison with central and northern Strait of Georgia sea level

The late glacial sea level curve in Victoria shows that there are differences in sea-level history compared with the central and northern Strait of Georgia (Hutchinson et al., 2004a; James et al., 2005; Fig. 2.13). The sea-level highstand in Victoria is about 75 m, which is far less than the 150-175 m observed further north. There is a similar rapid drop in sea levels initially, but because of the smaller and earlier highstand in the Victoria area, sea level reached present level about 1000 yr before the central Strait of Georgia, and as much as 2000 yr before the northern Strait of Georgia. The observed sea-level lowstand of at least -11 m in the Victoria area is

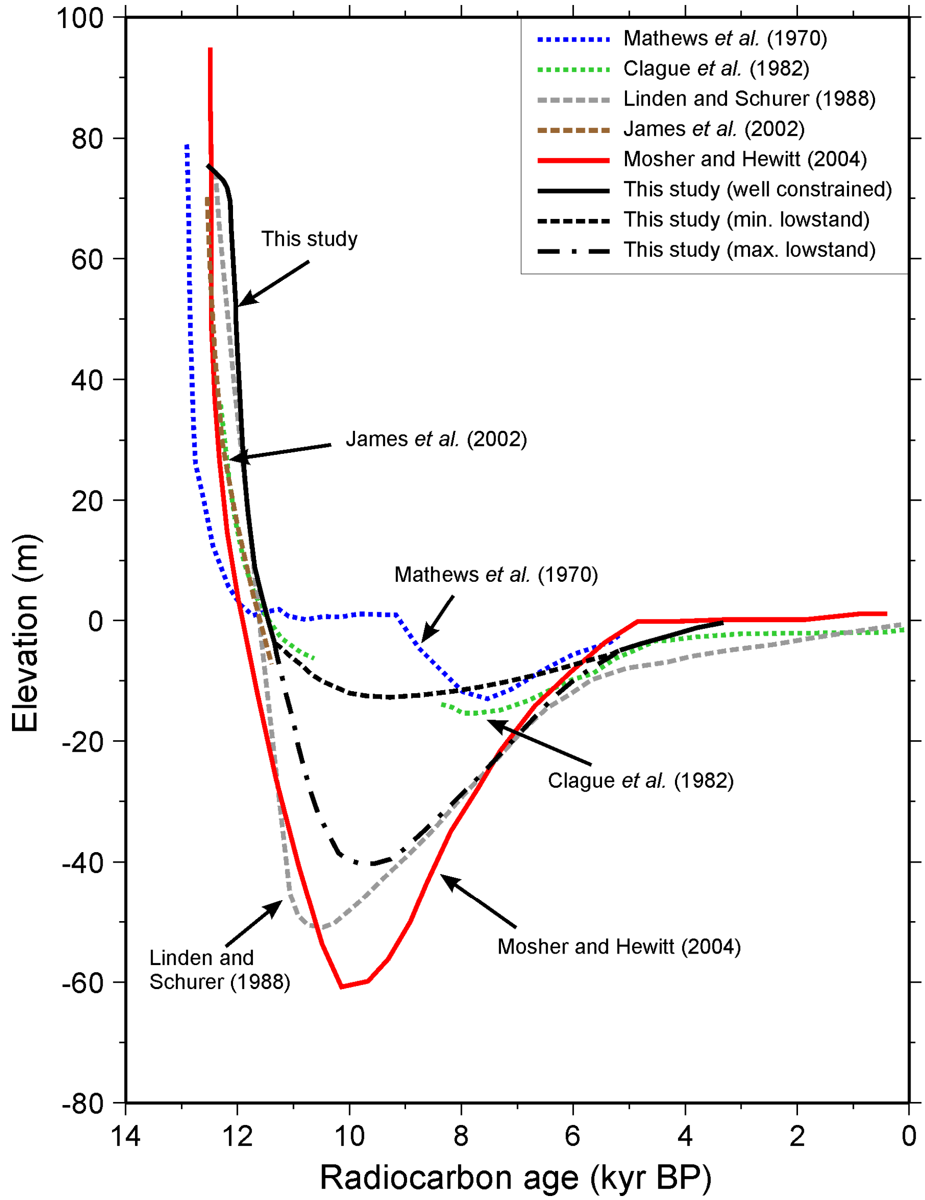

Figure 2.12. Comparison of the Victoria sea-level curve from this study with previous studies. The dashed and dotted dashed lines are the minimum and maximum sea-level lowstand scenarios, respectively.

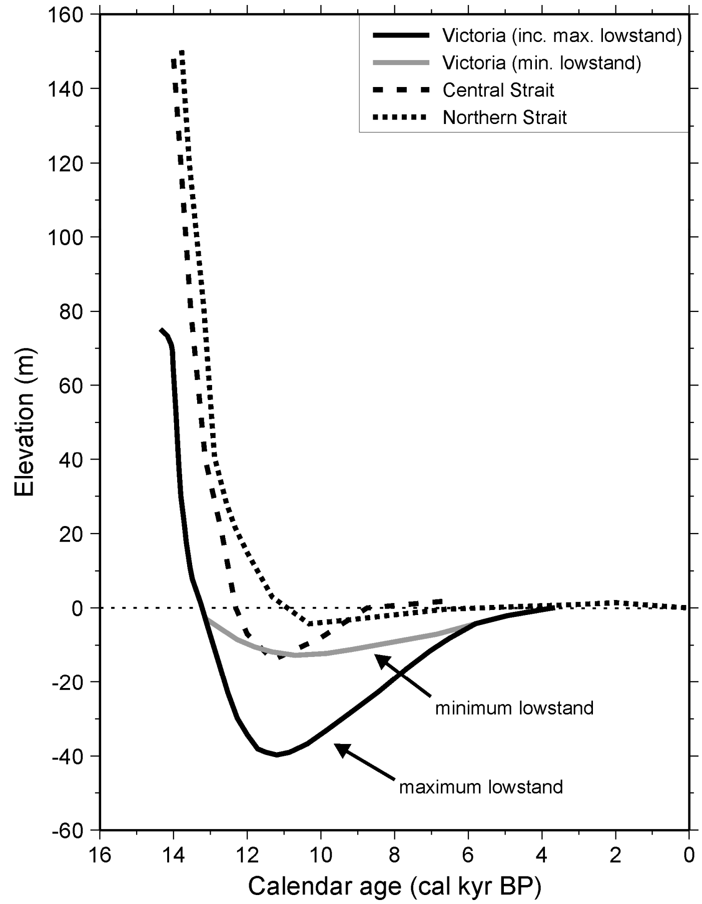

Figure 2.13. Comparison of sea level curves from Victoria, central Strait of Georgia (Hutchinson *et al.*, 2004a) and northern Strait of Georgia (James *et al.*, 2005).

lower than in the north Strait of Georgia (above -8 m), though it may be comparable to the central Strait of Georgia. Sea level in Victoria rose to within 2 m of present levels at least 2000 years after the central and northern Strait of Georgia.

Figure 2.14 shows the difference between the Victoria and the central and northern Strait of Georgia sea-level curves. The difference in sea level denotes the amount of crustal tilting between the locations. The maximum difference happened when the central and northern Strait of Georgia sea levels were at their highstand position, as the Victoria area was already undergoing significant rebound at that

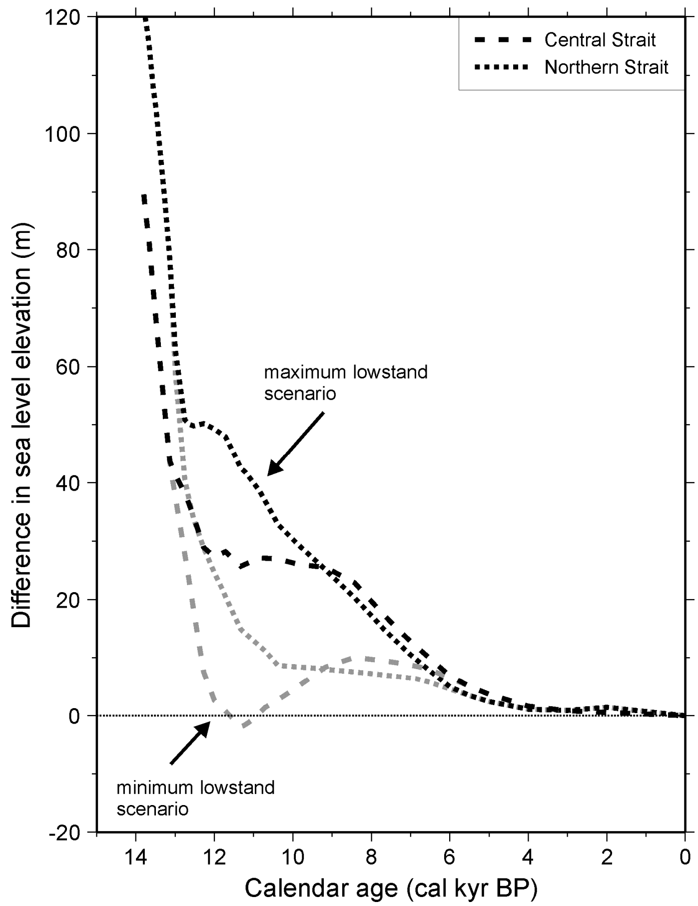

Figure 2.14. Difference between the Victoria sea-level curve and the central and northern Strait of Georgia curves. The curves are best constrained 13-14 cal kyr BP and after 4-6 cal kyr BP. The grey and black curves are the minimum and maximum sea-level lowstand scenarios, respectively.

point. Given the distance to the central Strait of Georgia from Victoria is about 150 km, this gives a maximum tilt of 0.6 m km^{-1}. The northern Strait of Georgia is about 230 km from Victoria, which results in a maximum tilt of 0.5 m km^{-1}. By the time that the sea level in Victoria reached present levels shortly before 13 cal kyr BP, there was still a difference of 40 m to the central Strait of Georgia and 70 m to the north Strait of Georgia.

Due to the poorly constrained lowstand position in Victoria, the difference in sea level varies between 6 and 13 cal kyr BP depending on the choice of lowstand scenario (Fig. 2.14). By 5 cal kyr BP, the difference in sea level between Victoria and the central and northern Strait of Georgia was less than 5 m. If isostatic rebound was largely complete in Victoria earlier than in the more northern locations, then the difference between the sea level curves should resemble an exponential decay at late times. The maximum lowstand scenario produces a closer approximation to an exponential decay than the minimum scenario for both curve comparisons. In the minimum lowstand scenario relative to the central Strait of Georgia, the difference between the curves approaches zero by 11.5 cal kyr BP, then rises to 10 m by 8 cal kyr BP. For this situation to happen, it would require 10 m of depression in the central Strait of Georgia relative to Victoria, which seems unlikely if the ice conditions were similar to present by the Holocene in southwestern British Columbia (Clague, 1981; Dyke, 2004). More likely, the minimum lowstand scenario underestimates the amount of sea-level drop in Victoria, and that it is closer to the maximum scenario.

2.5 Summary

A sea-level curve for Victoria is determined using recently collected isolation basin cores and data from previous studies. The sea level history is well constrained above -4 m elevation. The magnitude of the sea-level highstand was about 75-80 m at about 14.3 cal kyr BP, and rapidly fell to below present elevation by 13.2 cal kyr BP. This rapid sea-level fall after deglaciation is similar to that observed in the central and northern Strait of Georgia, though the highstand was smaller in magnitude and sea level dropped to below present elevation at an earlier time. After 13.2 cal kyr BP, sea level dropped to a lowstand position between -11 and -40 m elevation. Analysis of the crustal response and comparison with the central and northern Strait of Georgia relative sea-level curves indicates that the lowstand position was likely closer to the maximum scenario. Between 6 and 4 cal kyr BP, sea level rose near present elevation and remained there since.

Chapter 3 - History of the southwestern Cordilleran ice sheet and Quaternary Geology

3.1 Introduction

Many episodes of glaciation shaped the landscape and surficial geology in southwestern British Columbia and northwestern Washington during the Quaternary (Booth *et al.*, 2003). The last major glaciation, known as the Fraser Glaciation, began over 28 cal kyr BP, and reached a maximum about between 17 and 15 cal kyr BP. This glaciation correlates with the Wisconsin glaciation of eastern North America. The ice sheet retreated rapidly from its peak extent, and within about 5000-6000 yr the ice sheets attained their present extent. The history of the ice sheet extent and thickness is necessary to model glacio-isostatic adjustment. This chapter summarizes the limiting ages from radiocarbon dates and geological markers to determine the extent and thickness of the ice sheets.

3.2 Quaternary geology of southwestern British Columbia and northwestern Washington

3.2.1 Pre-Fraser glacial and interglacial sediments

Most Pre-Fraser sediments appear in sparse exposures and provide a relatively incomplete record for the Pleistocene (Booth *et al.*, 2003). In the Puget Lowlands, there are many isolated Pleistocene deposits that are magnetically reversed, indicating an age greater than 788 ka (Easterbrook, 1986; Booth *et al.*, 2003). Among these sediments are at least three drift units. The oldest Orting Drift, which may be over 2 Ma, shows evidence of a Canadian source by an abundance of garnet grains within the sediments. The Stuck drift dates to about 1.6 Ma, and is primarily derived from the Cascade Mountains. The Salmon Springs drift dates to about 1 Ma based on tephra dates overlying this unit. There are no known sediments that indicate that glacial events from about 1 Ma to later than 300 ka. The Double Bluff drift dates between 300 and 100 ka (Booth *et al.*, 2003). The Westlynn Drift, found in the Fraser Lowland, corresponds to a previous glaciation, possibly older than 128 ka (Clague, 1994). The drift comprises glaciofluvial sands and gravels, bedded silt and clay with sand and gravel lenses, massive glaciomarine diamicton, and till (Armstrong, 1975).

Before the Wisconsin glacial interval, there are well preserved sediments corresponding to the last interglacial and ice sheet advance (Fig. 3.1; Clague, 1994). The Muir Point formation on Vancouver Island, the Highbury Sediments in the Fraser Lowlands, and the Whidbey Formation in the Puget Lowland correspond to the last interglacial (Alley and Hicock, 1986). The Muir Point Formation contains gravel, silt, sand and peat, with abundant plant fossils, indicating a non-glacial origin. Radiocarbon ages from this unit are infinite, implying an age greater than 40 cal kyr BP. The Dashwood Drift on Vancouver Island and Semiahmoo Drift in the Fraser Lowland overlie the Muir Point Formation and Highbury Sediments respectively (Hicock and Armstrong, 1983). These units are comprised of till and glaciomarine sediments. Pollen analysis indicates that the Dashwood and Semiahmoo were deposited by the same glacial event. These units also correlate with Possession Drift in Washington, which has an age between 50 and 80 ka. These sediments likely represent the retreat of ice sheets in the last pre-Wisconsin glaciation.

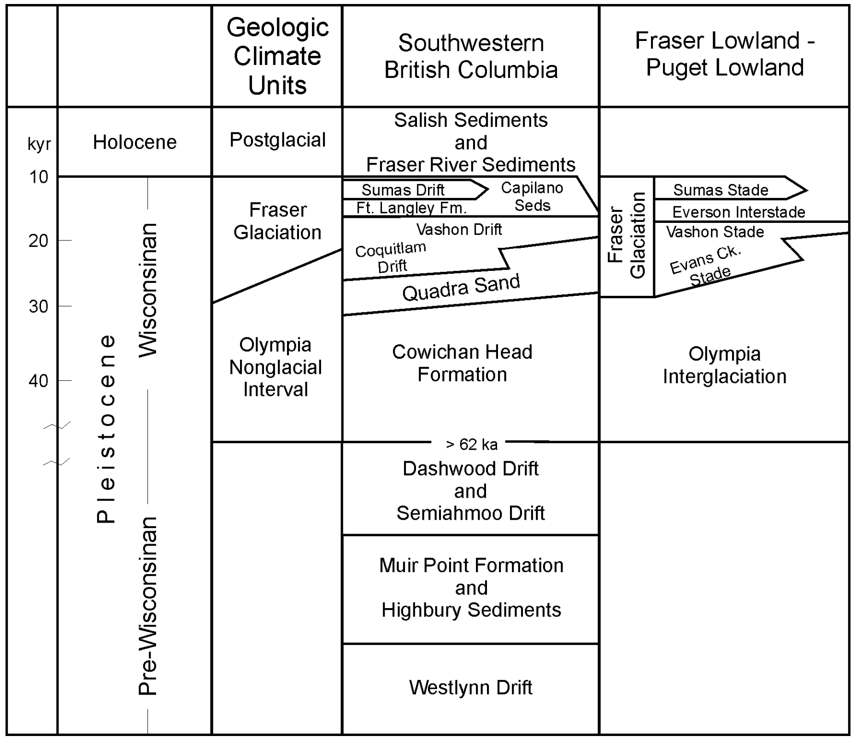

Figure 3.1. Late Quaternary stratigraphy of southwestern British Columbia (Clague, 1994).

3.2.2 Olympia nonglacial interval

The Cowichan Head Formation overlies the drift associated with the second last major glaciation, representing ice free conditions during the Olympia nonglacial interval (Armstrong and Clague, 1977; Clague, 1981). Radiocarbon dates from this formation range from 28 to over 45 cal kyr BP. The Cowichan Head Formation has two members; the lower member consists of sand and pebbly sand of marine origin and the upper member consists of silt, sand and gravel with disseminated organic matter representing a fluvial and estuarine origin. The Cowichan Head Formation represents a non-glacial period, and the contact with the underlying Dashwood Drift is an unconformity (Hicock and Armstrong, 1983). The time when the formation was deposited represented a relative fall in sea level after the last pre-Wisconsin glaciation. From the analysis of pollen, the climate at the time of deposition was cooler than present, equivalent to present day northern British Columbia and southern Yukon (Armstrong and Clague, 1977).

3.2.3 Fraser advance

The Quadra Sand comprises well sorted sand and gravel deposited at the onset of the Fraser glaciation in the Georgia Basin (Clague, 1976). It was deposited in a floodplain with braided rivers and streams and is marked by cross bedding and a lack of organic material. Exposures are limited, but they indicate that the floodplain likely encompassed the entire Strait of Georgia. The source material for the Quadra Sand is from the Coast Mountains on the basis of mineralogical and paleocurrent information, and does not have any significant contribution of material from Vancouver Island. The contact between the Quadra Sand and the underlying Cowichan Head Formation is sharp, distinguished on the basis of compositional differences and presence of crossbedding (Armstrong and Clague, 1977). The age of the Quadra Sand is progressively younger towards the south, with the northern Strait of Georgia deposits having ages over 34 cal kyr BP and the southern Puget Sound deposits having ages around 18 cal kyr BP (Clague, 1976). This progression reflects the advance of the ice sheets into the Georgia Strait from the north. At Point Grey in Vancouver, finer sediments and organic deposits in the lower portion of the Quadra Sand indicate that relative sea level was higher during the onset of glaciation, despite eustatic sea level being up to 85 m lower than present (Clague et al., 2005). Relative sea level rose at least 18 m higher than present between 27-30 cal kyr BP when the lower Quadra Sand was first deposited in the Vancouver area, indicating that isostatic depression was over 100 m. The upper part of the Quadra Sand contains no microfossils, but the balance between sediment accumulation and rate of deposition indicates that there was continuous sea level rise.

3.2.4 Fraser glacial and post-glacial sediments

The late Wisconsin Fraser glaciation deposited drift throughout southwest British Columbia (Armstrong, 1981). There are at least 3 major drift units: the Coquitlam Drift, Vashon Drift, and Sumas Drift (Fig 3.1). The drift units comprise a mixture of till, glaciofluvial, glaciolucustrine and ice-contact deposits. The Fort Langley Formation comprises mainly interbedded marine and glaciomarine sediments and glacial drift. These sediments represent the retreat of the ice sheets after the glacial maximum. The Capilano Sediments comprises glaciofluvial, glaciomarine and marine sediments. These sediments contain dropstones, but no diamiction or ice contact deposits. Deposition of glacial and glaciomarine deposits ended about 11 cal kyr BP when the ice sheets retreated a sufficient distance from the Georgia Basin.

3.3 Ice sheet history

3.3.1 Introduction

The Fraser glaciation is the last glaciation that occupied most of southwestern British Columbia and parts of the northwestern United States (Armstrong *et al.*, 1965; Clague and James, 2002; Fig. 3.2). There were several advances and retreats between 40 and 10.5 cal kyr BP. The glaciation lagged the Laurentide glacial maximum, which achieved maximum extent about 21.5 cal kyr BP, and reached a maximum between 15-17 cal kyr BP (Porter and Swanson, 1998; Dyke, 2004). After reaching

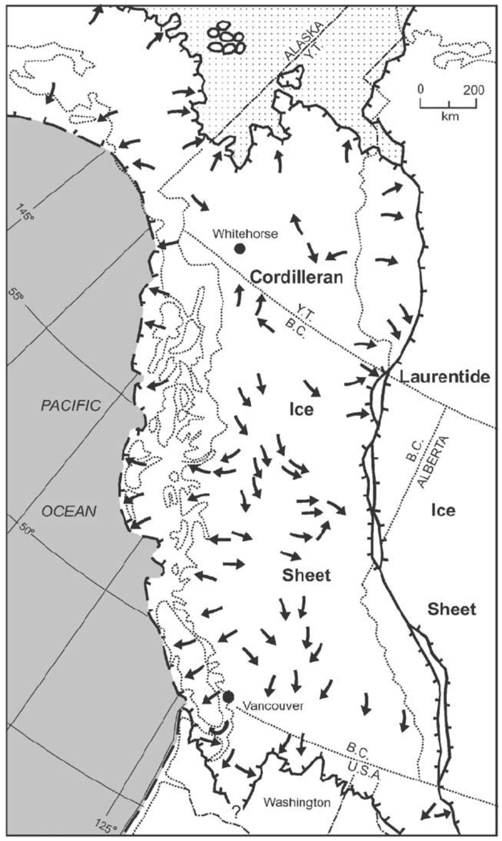

Figure 3.2. Maximum extent of the Cordilleran ice sheet during the Fraser glaciation and major ice flow directions (Clague and James, 2002).

its maximum, the ice sheet retreated to its present level by the start of the Holocene, interrupted by periods of stagnation and readvance (Clague, 1991; Dyke, 2004).

3.3.2 Early Fraser advance

The advance of the Fraser Glaciation is marked by the deposition of the Quadra Sand (Clague, 1994). Between 40 and 30 cal kyr BP, the climate progressively shifted from conditions similar to today to tundra-like in southern Vancouver Island (Alley, 1979). The ice sheet began to grow during this time, and advanced to the Fraser Lowland by 28 cal kyr BP (Clague *et al.*, 2005). The Fraser Lowland region was depressed over 100 m by 28 cal kyr BP, indicating that there was a significant ice load present during the early advance.

The earliest advance of the Frasier Glaciation did not persist, and by 23.5 cal kyr BP, the ice sheet retreated from the Fraser Lowland (Clague, 1994). The deposits from the earliest advance of the Fraser Glaciation are called the Coquitlam Drift (Hicock and Armstrong, 1981). The Coquitlam Drift lies within the Quadra Sand in the Fraser Lowland and dates between 26 and 22 cal kyr BP. The Quadra Sand deposited below and above the Coquitlam Drift is indistinguishable lithologically. The Coquitlam advance did not affect all areas in the Fraser Lowlands, such as the Chehalis River, probably due to a lack of precipitation further to the northeast (Ward and Thomson, 2002). Pollen records indicate temperature was 8°C lower than present during the recession, so the ice free conditions before 21 cal kyr BP in the Fraser Lowland probably represent a time when there was far less precipitation than during glacial advances (Hicock *et al.*, 1982). The period when glaciers retreated in the Fraser Lowlands is known as the Port Moody interstade (Ward and Thomson, 2002). In Washington State, the Coquitlam Drift correlates to the Evans Creek Drift, a drift produced from glaciers in the Cascades and Mt. Rainier (Armstrong *et al.*, 1965; Barnosky, 1984).

3.3.3 Olympic Mountains glaciation

There were at least six advances of Olympic glaciers in the Wisconsin (Thackray, 2001). The latest major advance happened sometime before 21.8 cal kyr BP, which is similar to the timing of the glacial maximum of the Laurentide ice sheet. This date indicates that the Olympic glaciers reached their maximum extent thousands of years before the Cordilleran ice sheet. By the time Cordilleran ice sheet reached the latitude of the Olympics, the Olympic glaciers may have retreated significantly. The difference in timing of the maximum of the Olympic glaciers is likely due to dryer conditions after 21.8 cal kyr BP, which impeded growth of the glaciers. There is one late undated advance (Twin Creeks 2), which may correspond to the same time as the Cordilleran maximum, though it was not of great extent (Thackray, 2001). The size of the Olympic glaciers was not likely significantly larger than present during the late glacial times.

3.3.4 Vashon Glaciation

The Vashon Stade represents the largest advance of ice in southwestern British Columbia and northwestern Washington (Armstrong *et al.*, 1965). At its maximum, the ice sheets covered Vancouver Island, the Juan De Fuca Strait, and extended south into the Puget Lowlands (Clague, 1981). The advance phase happened between 20 and 15 cal kyr BP. Ice free condition existed in the Chilliwack Valley in southwestern British Columbia until 19.1 cal kyr BP, when the ice sheet reached the Canada-United States border (Clague, *et al.*, 1988).

In order to analyze the history of the Cordilleran ice sheet, radiocarbon samples must be corrected for reservoir effects as mentioned in Chapter 2 (Hutchinson et al., 2004b). Previous analyses of ice sheet history did not correct for these effects or used early estimates of reservoir corrections (*e.g.* Alley and Chatwin, 1979; Clague, 1981; Booth, 1987; Easterbrook, 1992; Dethier *et al.*, 1995; Porter and Swanson, 1998; Swanson and Caffee, 2001). The retreat history in this study is up to 1000 yr different than in previous studies because of these corrections. Tables 3.1 and 3.2 lists dates pertaining to the advance and retreat of the Cordilleran ice sheet, respectively. Only dates with a corrected error less than 250 years were used to determine ice sheet history as samples with large errors are deemed to be unreliable.

Figure 3.3 shows the distribution of radiocarbon dates pertaining to the Vashon advance. The distribution of samples is small, though they do indicate that the ice sheets did not reach low lying areas before 19 cal kyr BP. Dates in Puget Sound indicate that the Puget Lobe did not reach a maximum until after 17 cal kyr BP. The dates from the Puget Sound are from proglacial deltas, so the ice sheets had entered the Sound by that time (Porter and Swanson, 1998). Given the sparse dataset, it is not possible to accurately map out an advance pattern.

Figure 3.4 shows the distribution of radiocarbon dates pertaining to the retreat of the Vashon glaciation in southwestern British Columbia and northwestern Washington State. Most samples are younger than 15 cal kyr BP except a few samples from the margins of the ice sheet, such as in Puget Sound, Olympic Peninsula and western Vancouver Island. Most of the dates from the eastern Juan de Fuca Strait and San Juan Islands are younger than 15 cal kyr BP. Within the Strait of Georgia, there is no apparent spatial pattern in the dates, indicating that organisms repopulated the area contemporaneously shortly before 14 cal kyr BP (Barrie and Conway, 2002). The range of ages indicates that initial deglaciation of the margins of the ice sheets was slow, and accelerated when the Strait of Georgia deglaciated. Because a lack of data near the margins of the ice sheets, it is not possible to constrain the exact time when deglaciation began, other than it began between 16 and 15 cal kyr BP. The ice sheets retreated rapidly and by about 14 cal kyr BP the ice sheets had retreated to the northern end of the Strait of Georgia.

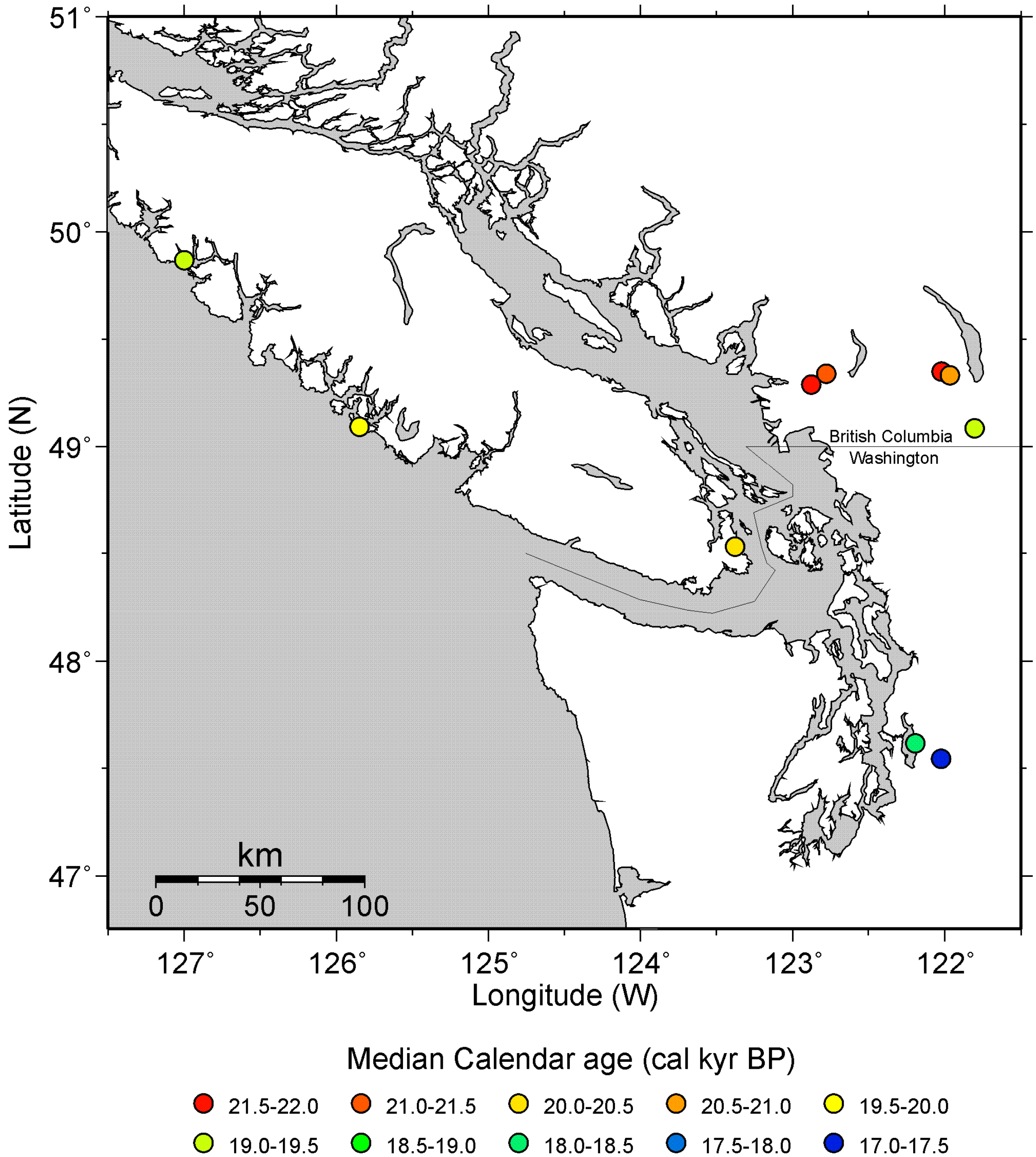

Figure 3.3. Distribution of radiocarbon dates pertaining to the Vashon advance of the Cordilleran ice sheet in southwestern British Columbia and northwestern Washington State. The dates are the median calibrated age BP (Table 3.1).

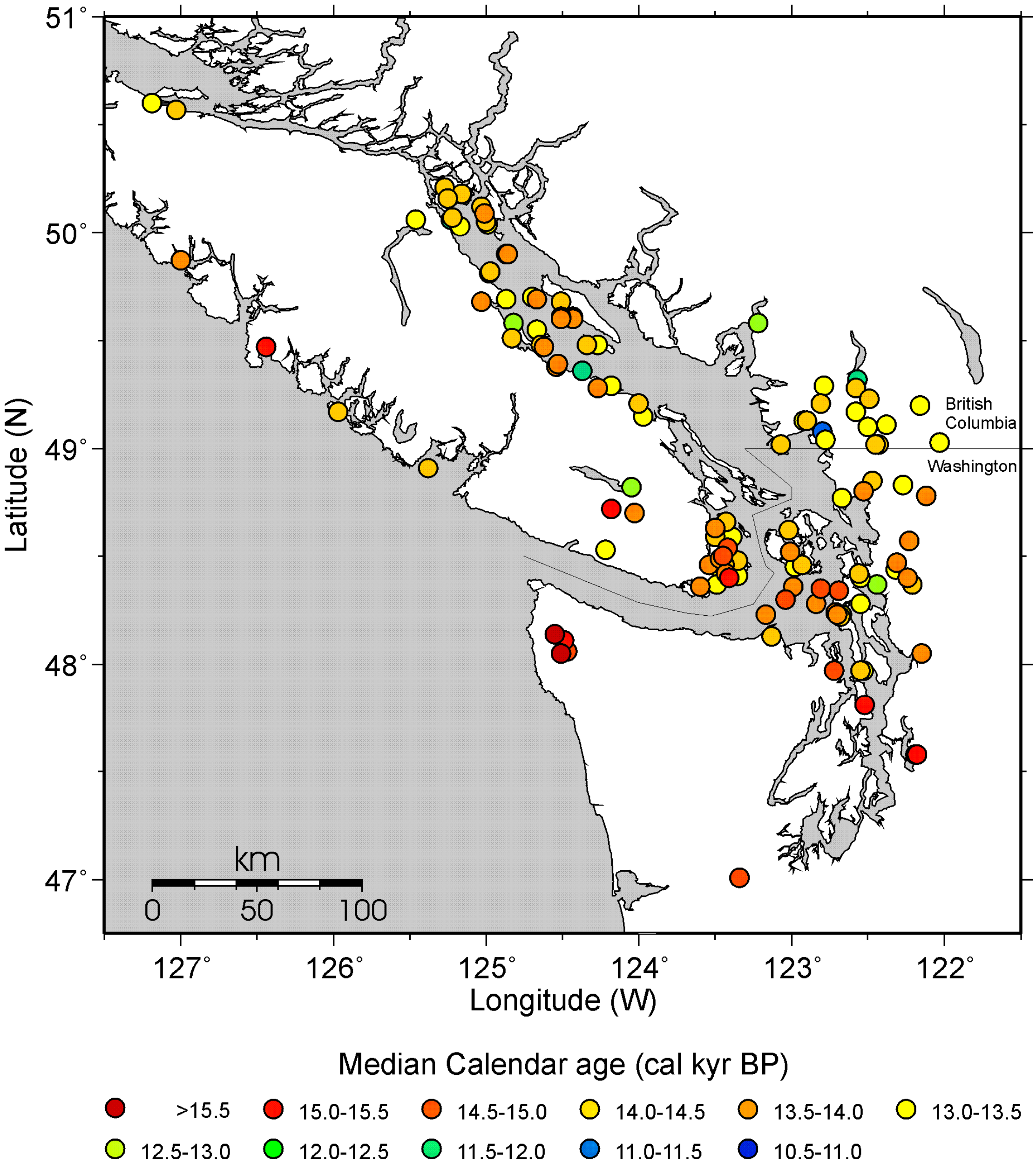

Figure 3.4. Distribution of radiocarbon dates pertaining to the deglaciation of the Cordilleran ice sheet in southwestern British Columbia and northwestern Washington State. The dates are the median calibrated age BP (Table 3.2).

3.3.5 Everson Interstade and Sumas readvance

Between 13.5 and 11 cal kyr BP, southwestern British Columbia experienced extremely variable climate with substantial temperature fluctuations (e.g. Pellatt *et al.*, 2002). The influx of glacial meltwater deposited glaciomarine, glaciofluvial, and marine sediments throughout southwestern British Columbia (Armstrong, 1981). During this time, ice sheet retreat slowed and at times ice readvanced down valleys and fjords (Mathews *et al.*, 1970; Clague *et al.*, 1997; Kovanen and Easterbrook, 2002b; Friele and Clague, 2002). Though these events indicate that ice sheet retreat was not uniform, by 10-11 cal kyr BP, the Cordilleran ice sheet was near its present extent (Clague, 1981; Dyke, 2004).

3.3.6 Holocene Advances

During the Holocene, temperatures in southern British Columbia remained 2-7° C higher than late glacial times, with a gradual cooling trend since 10 cal kyr BP (Walker and Pellatt, 2003). Fluctuations in climate allowed for minor readvances of mountain glaciers several times. The advances were not more than a few km from their present position on high elevation mountains and valleys (Osborn *et al.*, 2007).

3.4 Ice sheet thickness and extent

3.4.1 Ice sheet growth and decay

Ice sheet growth and retreat followed a four stage evolution (Clague and James, 2002). During interglacial times, ice was limited to mountain glaciers at high elevations, similar to present. As the climate changed to cooler and wetter conditions, the mountain glaciers began to migrate down valleys. As ice continued to build up, the Cordilleran ice sheet covered all but the highest peaks in the mountains. At the glacial maximum, ice built up enough to form an ice mass that flowed almost independent of topography (*e.g.* Stumpf *et al.*, 2000). Ice flow indicators suggest that there were several ice divides in the interior of the Cordilleran ice sheet.

There are two ways the Cordilleran ice sheet retreated: downwasting and calving (Fulton, 1967; Clague, 1981; Clague and James, 2002). In coastal areas, ice wasted away rapidly due to the influence of water, causing calving. In interior areas, the primary method of retreat was by downwasting. This process involves the ice sheets melting top down, eventually stagnating in valleys. Because of this, the volume of ice in the Cordilleran ice sheet diminished rapidly when downwasting started.

3.4.2 Ice sheet thickness

At its maximum, the Cordilleran ice sheet flowed over mountains as high as 2500 m above sea level (Wilson *et al.*, 1958; Mathews *et al.*, 1970; Booth, 1987; Stumpf *et al.*, 2000). The ice sheets sloped gently towards the Pacific Ocean, and may have been up to 1000 m thick at the margins. As the ice dome centers moved further inland, the ice surface gradient became gentler (Stumpf *et al.*, 2000). In low-lying areas, ice thickness exceeded 1500 m. When downwasting began, ice flow centers moved back to local mountains, and thickness of the reduced ice sheets did not exceed 700 m.

3.5 Summary

The Cordilleran ice sheet has a history that spans from 40-10 cal kyr BP. The largest advance reached a maximum sometime between 15 and 17 cal kyr BP, when ice was thick enough to flow independently of topography. The ice sheet attained a peak elevation of over 2500 m at the maximum in central British Columbia. The retreat of the ice sheets started before 15 cal kyr BP, and was initially slow. By 14 cal kyr BP, the ice sheets retreated out of the Strait of Georgia. Standstills and readvances slowed deglaciation between 14 and 11 cal kyr. By 10-11 cal kyr BP, the ice sheets were reduced to high elevation mountains and valleys and remained restricted throughout the Holocene.

Table 3.1. Dates pertaining to the advance of the Cordilleran Ice Sheet

Location	Latitude (°N)	Longitude (°W)	Laboratory number	Material dated	Corrected age (yr BP)[a]	Calibrated age (cal yr BP)[b]	Reference
Fraser Lowlands							
Allison Pool	49.085	121.803	TO-193	wood	15950 ± 110	19000 - 19246	Clague *et al.*, 1988
Allison Pool	49.085	121.803	GSC-4355	wood	16000 ± 90	19049 - 19284	Clague *et al.*, 1988
Allison Pool	49.085	121.803	GSC-4355	wood	16100 ± 75	19185 - 19403	Clague *et al.*, 1988
Chehalis Valley	49.331	121.967	TO-9158	wood	17380 ± 130	20327 - 20698	Ward and Thomson, 2004
Coquitlam Valley	49.338	122.778	GSC-2297	wood	17800 ± 75	20825 - 21210	Clague *et al.*, 1980
Chehalis Valley	49.331	121.967	TO-9157	wood	17820 ± 140	20799 - 21290	Ward and Thomson, 2004
Coquitlam Valley	49.338	122.778	GSC-2371	wood	18000 ± 75	21087 - 21483	Clague *et al.*, 1980
Chehalis Valley	49.349	122.019	AA-46118	wood	18180 ± 160	21371 - 21961	Ward and Thomson, 2004
Port Moody	49.288	122.878	GSC-2322	wood	18300 ± 85	21605 - 22029	Clague *et al.*, 1980
Chehalis Valley	49.331	121.967	AA-48004	wood	18380 ± 100	21618 - 21622	Ward and Thomson, 2004
Chehalis Valley	49.331	121.967	AA-46122	elderberry seeds	18600 ± 200	21954 - 22409	Ward and Thomson, 2004
Vancouver Island							
Port Eliza	49.867	127.000	CAMS-88275	Sparrow bone	16270 ± 170	19205 - 19564	Al-Suwaidi *et al.*, 2006
Port Eliza	49.867	127.000	CAMS-74625	Vole bone	16340 ± 60	19438 - 19536	Al-Suwaidi *et al.*, 2006
Port Eliza	49.867	127.000	CAMS-102798	Mountain Goat	16340 ± 60	19438 - 19536	Al-Suwaidi *et al.*, 2006
Tofino	49.092	125.847	CAMS-111667	wood	16430 ± 40	19485 - 19568	Al-Suwaidi *et al.*, 2006
Tofino	49.092	125.847	GSC-2768	wood	16700 ± 75	19610 - 19659	Clague *et al.*, 1980
Saanich Peninsula	48.532	123.380	GSC-2829	mammoth bone	17000 ± 120	19985 - 20257	Clague *et al.*, 1980
Puget Lowlands							
Issaquah Delta	47.543	122.025	CAMS-23160	wood	14450 ± 90	17116 - 17624	Porter and Swanson, 1998
Issaquah Delta	47.543	122.025	CAMS-23176	wood	14480 ± 70	17184 - 17657	Porter and Swanson, 1998
Issaquah Delta	47.543	122.025	CAMS-23177	wood	14550 ± 70	17351 - 17807	Porter and Swanson, 1998
Issaquah Delta	47.543	122.025	QL-4620	wood	14560 ± 60	17386 - 17817	Porter and Swanson, 1998
Issaquah Delta	47.543	122.025	CAMS-23171	wood	14580 ± 70	17425 - 17864	Porter and Swanson, 1998
Issaquah Delta	47.543	122.025	CAMS-23175	wood	14600 ± 90	17453 - 17917	Porter and Swanson, 1998
Issaquah Delta	47.543	122.025	CAMS-23170	wood	14620 ± 100	17482 - 17951	Porter and Swanson, 1998
Bellevue	47.617	122.192	BETA-112019	wood	14890 ± 70	17998 - 18203	Porter and Swanson, 1998
Seattle	47.633	122.317	W-1227	wood	15000 ± 400	17695 - 18752	Porter and Swanson, 1998
Seattle	47.625	122.325	W-1305	wood	15100 ± 400	17837 - 18831	Porter and Swanson, 1998

[a] All dates have a 1-sigma error

[b] Dates calibrated using Calib 5.0 (Stuiver and Reimer, 1993). Age range is 1-sigma limits

Table 3.2. Radiocarbon dates pertaining to the retreat of the Cordilleran Ice Sheet

Location	Latitude (°N)	Longitude (°W)	Laboratory number	Material dated	Corrected age (yr BP)[a]	Calibrated age (cal yr BP)[b]	Reference
Puget Lowlands, Washington							
Covington	47.352	122.070	L-269D	peat	10200 ± 500	11243 - 12637	Broecker *et al.*, 1956
Belmore	47.003	122.915	W-394	basal peat	10875 ± 306	12398 - 13167	Rubin and Alexander, 1958
Double Bluff	47.967	122.533	QL-4608	shell	11310 ± 78	13120 - 13250	Swanson and Caffee, 2001
Moss Lake	47.699	121.848	L-269A	basal peat	11275 ± 365	12854 - 13500	Broecker *et al.*, 1956
Cedarville	46.867	123.283	W-940	wood	11640 ± 275	13248 - 13766	Ives *et al.*, 1964
Double Bluff	47.968	122.545	USGS-64	shell	11720 ± 103	13446 - 13682	Robinson, 1977
Sequim	48.048	123.112	WSU-1866/1867	twigs, plant material	12000 ± 310	13425 - 14258	Peterson *et al.*, 1983
Marysville	48.054	122.152	USGS-808	shell	12350 ± 74	14101 - 14485	Dethier *et al.*, 1995
Simpson Lake	47.013	123.337	UW-146B	wood	12430 ± 160	14166 - 14771	Fairhall *et al.*, 1976
Basalt Point	47.967	122.717	AA-10077	shell	12520 ± 103	14386 - 14903	Swanson and Caffee, 2001
Simpson Lake	47.013	123.337	UW-147	wood	12620 ± 150	14489 - 15097	Fairhall *et al.*, 1976
Lake Carpenter	47.805	122.522	Ua-765	shell	12700 ± 182	14581 - 15253	Anundsen *et al.*, 1994
Simpson Lake	47.013	123.337	UW-146A	wood	12700 ± 160	14643 - 15231	Fairhall *et al.*, 1976
Lake Washington	47.582	122.187	QL-1517	organic clay (basal)	12805 ± 209	14739 - 15454	Leopold *et al.*, 1982
Mercer Slough	47.580	122.178	QL-1891	bog peat (basal)	12985 ± 100	15150 - 15510	Porter and Swanson, 1998
Lake Washington	47.633	122.250	L-346A	basal peat	13025 ± 553	14501 - 16178	Broecker and Kulp, 1957
Lake Carpenter	47.805	122.522	QL-4067	basal gyttja	13075 ± 162	15196 - 15707	Anundsen *et al.*, 1994
Lake Carpenter	47.805	122.522	T-6798	shell	13660 ± 345	15737 - 16729	Anundsen *et al.*, 1994
Lake Washington	47.633	122.250	L-330	peat	14000 ± 900	15526 - 18036	Broecker and Kulp, 1957
Western Olympic Peninsula, Washington							
Lake Dickey	48.055	124.467	UW-144	wood	12660 ± 220	14418 - 15198	Fairhall *et al.*, 1976
Olympic Penninsula	48.110	124.485	RL-139	wood	13010 ± 240	15039 - 15746	Heusser, 1973
Olympic Penninsula	48.052	124.506	Y-2449	wood	13100 ± 180	15208 - 15764	Heusser, 1973
Olympic Penninsula	48.140	124.549	RL-140	wood	13380 ± 250	15487 - 16240	Heusser, 1973
Olympic Penninsula	48.150	124.550	Y-2452	organic silt	14460 ± 200	17045 - 17794	Heusser, 1973
Western Juan de Fuca Strait							
Juan de Fuca Strait	48.450	124.475	I-2169	organic-rich mud	11300 ± 800	11051 - 13000	Clague, 1980
Juan de Fuca Strait	48.450	124.583	I-?	marine mud?	12200 ± 403	13719 - 14824	Anderson, 1968
Juan de Fuca Strait	48.367	124.383	I-?	marine mud?	13450 ± 403	15374 - 16504	Anderson, 1968
Southern Vancouver Island							
Cowichan Lake	48.817	124.050	I-8450	peat	10280 ± 150	11760 - 12385	Alley and Chatwin (1979)
San Juan Ridge	48.533	124.217	GSC-2041	peat	11200 ± 55	13054 - 13181	Alley and Chatwin (1979)
Lens Creek	48.700	124.033	GSC-2182	peat	12200 ± 70	13974 - 14145	Alley and Chatwin (1979)
Harris Creek	48.717	124.183	GSC-2223	peat	13100 ± 65	15300 - 15646	Alley and Chatwin (1979)
Victoria							
Matheson Lake	48.361	123.597	TO-9184	plant fragments	12210 ± 100	12395 - 12804	This study
Matheson Lake	48.361	123.597	TO-9185	plant fragments	12120 ± 100	12709 - 12876	Clague, 1980
Collwood Delta	48.455	123.540	B-109128	wood	12360 ± 70	12397 - 13197	This study
Saanich Inlet	48.591	123.503	CAMS-33490	shell	12130 ± 86	12850 - 12934	Mosher and Hewitt, 2004
Saanich Inlet	48.633	123.500	CAMS-33492	shell	12320 ± 78	12938 - 13083	This study
Juan de Fuca Strait	48.367	123.488	CAMS-58673	shell	10950 ± 71	13020 - 13193	Clague, 1980
Rithets Bog	48.450	123.483	GSC-945	basal gyttja	10775 ± 112	13214 - 13452	Clague, 1980
Pike Lake	48.488	123.468	TO-9192	shell	12290 ± 94	13269 - 13413	Clague, 1980
Pike Lake	48.488	123.468	TO-9191	plant detritus	12280 ± 120	13118 - 13735	This study
Pike Lake	48.488	123.468	TO-9190	plant fragments	10890 ± 330	13389 - 13727	Clague, 1980
Prior Lake	48.476	123.466	TO-9189	shell	12120 ± 103	13443 - 13666	Clague, 1980
Prior Lake	48.476	123.466	TO-9187	twig	12320 ± 100	13501 - 13728	Clague, 1980
Prior Lake	48.476	123.466	TO-9186	twig	11540 ± 330	13536 - 13769	Clague, 1980
Maltby Lake	48.497	123.449	TO-9183	shell	12370 ± 103	13845 - 14073	This study
Maltby Lake	48.497	123.449	TO-9182	mud (basal)	11995 ± 108	13852 - 14076	This study
Maltby Lake	48.497	123.449	TO-9181	plant fragments	10600 ± 140	13871 - 14072	Blais-Stevens et al., 2001
McKenzie Ave	48.460	123.443	GSC-763	shell	12170 ± 94	13925 - 14206	This study
Patricia Bay	48.658	123.433	GSC-418	shell	12200 ± 99	13941 - 14204	This study
Esquimault Harbour	48.415	123.427	CAMS-62534	shell	12420 ± 71	13982 - 14458	This study
Portage Inlet	48.463	123.422	I-3675	organic-rich mud	11700 ± 170	14055 - 14418	Blais-Stevens et al., 2001
O'Donnell Bog	48.541	123.416	TO-9195	shell	12220 ± 94	14046 - 14489	This study
O'Donnell Bog	48.541	123.416	TO-9194	basal gyttja	11995 ± 108	14128 - 14566	Monahan et al. (2000)
O'Donnell Bog	48.541	123.416	TO-9193	plant detritus	11100 ± 80	14129 - 14596	This study
South Victoria	48.400	123.414	CAMS-58696	shell	12740 ± 71	13665 - 15094	This study
Saanichton	48.592	123.392	GSC-398	shell	11890 ± 125	14212 - 14620	Mosher and Hewitt, 2004
Cook St Victoria	48.413	123.353	GSC-1131	plant material	11500 ± 80	14620 - 15084	This study

Table 3.2. (continued)

Location	Latitude (°N)	Longitude (°W)	Laboratory number	Material dated	Corrected age (yr BP)[a]	Calibrated age (cal yr BP)[b]	Reference
Eastern Juan de Fuca Strait – Southern Strait of Georgia – San Juan Islands – Northern Washington							
Bellingham	48.767	122.467	I-1035	wood	10370 ± 300	11758 - 12700	Trautman and Willis, 1966
Dodge Valley	48.365	122.438	USGS-124	shell	10380 ± 86	12035 - 12555	Dethier *et al.*, 1995
Bellingham	48.750	122.467	W-996	shell	10710 ± 354	12090 - 12996	Ives *et al.*, 1964
Penn Cover Park	48.233	122.667	I-1448	shell	10900 ± 245	12638 - 13134	Trautman and Willis, 1966
Cattle Point	48.450	122.983	I-2156	shell	10950 ± 177	12809 - 13077	Easterbrook, 1969
Lummi	48.767	122.667	I-2157	shell	11000 ± 187	12829 - 13100	Easterbrook, 1969
Little Sucia	48.767	122.917	I-1471	shell	11050 ± 294	12766 - 13282	Trautman and Willis, 1966
Davidson Head	48.617	123.133	I-1470	shell	11210 ± 294	12865 - 13345	Trautman and Willis, 1966
Polnell Pt	48.283	122.550	I-2154	shell	11350 ± 187	13058 - 13397	Easterbrook, 1969
Cattle Point	48.233	122.983	I-1469	shell	11400 ± 354	12954 - 13602	Trautman and Willis, 1966
Orcas Island	48.683	122.933	I-969	shell	11400 ± 403	12919 - 13667	Trautman and Willis, 1966
Everson	48.831	122.273	BETA-1324	pine stump	11455 ± 125	13199 - 13426	Dethier *et al.*, 1995
Hope Island	48.400	122.550	I-2286	shell	11450 ± 196	13110 - 13492	Easterbrook, 1969
Middle Fork-Deep Kettle Bog	48.776	122.116	AA-22210	wood	11520 ± 190	13214 - 13588	Kovanen and Easterbrook, 2001
Mount Vernon	48.443	122.322	BETA-1321	shell	11550 ± 139	13262 - 13549	Dethier *et al.*, 1995
Whidbey Island	48.233	122.767	I-1079	shell	11585 ± 304	13181 - 13751	Trautman and Willis, 1966
Orcas Island	48.617	123.017	I-1881	shell	11650 ± 196	13315 - 13694	Buckley *et al.*, 1968
Potholes	48.129	123.134	BETA-1323	shell	11650 ± 206	13309 - 13703	Dethier *et al.*, 1995
Coupeville Boat	48.221	122.678	USGS-1304	shell	11690 ± 158	13386 - 13706	Dethier *et al.*, 1995
Davis Bay	48.461	122.928	BETA-1717	shell	11790 ± 158	13453 - 13782	Dethier *et al.*, 1995
Axton Pit	48.850	122.467	B-145457	shell	11810 ± 64	13599 - 13758	Kovanen and Easterbrook, 2002b
Cedarville	48.867	123.283	I-1037	wood	11800 ± 400	13221 - 14121	Easterbrook, 1969
Kiket Island	48.421	122.560	BETA-1715	shell	11915 ± 121	13646 - 13914	Dethier *et al.*, 1995
Middle Fork-Deep Kettle Bog	48.776	122.116	AA-22209	wood	11940 ± 180	13610 - 14010	Kovanen and Easterbrook, 2001
Middle Fork-Deep Kettle Bog	48.776	122.116	AA-22204	wood	11945 ± 84	13723 - 13901	Kovanen and Easterbrook, 2001
South Fork-Cranberry Bog	48.567	122.233	AA-27075	Basal Peat	11971 ± 100	13738 - 13943	Kovanen and Easterbrook, 2001
Middle Fork-Deep Kettle Bog	48.776	122.116	AA-22207	wood	12035 ± 95	13795 - 13987	Kovanen and Easterbrook, 2001
Middle Fork-Deep Kettle Bog	48.776	122.116	AA-22205	wood	12045 ± 85	13809 - 13987	Kovanen and Easterbrook, 2001
Big Lake South	48.373	122.213	USGS-787	shell	12090 ± 82	13839 - 14021	Dethier et al., 1995
Deming, Wa	48.808	122.200	I-1447	shell	12020 ± 284	13461 - 14233	Easterbrook, 1969
South Fork-Cranberry Bog	48.567	122.233	AA-12733	Basal Peat	12108 ± 96	13845 - 14058	Kovanen and Easterbrook, 2001
Middle Fork-Deep Kettle Bog	48.776	122.116	AA-22206	wood	12120 ± 90	13861 - 14068	Kovanen and Easterbrook, 2001
Middle Fork-Deep Kettle Bog	48.776	122.116	AA-22203	wood	12145 ± 90	13890 - 14103	Kovanen and Easterbrook, 2001
Middle Fork-Deep Kettle Bog	48.776	122.116	AA-22208	wood	12150 ± 90	13895 - 14110	Kovanen and Easterbrook, 2001
Middle Fork-Deep Kettle Bog	48.776	122.116	AA-22202	wood	12160 ± 90	13906 - 14123	Kovanen and Easterbrook, 2001
Middle Fork-Deep Kettle Bog	48.776	122.116	AA-20749	wood	12165 ± 95	13903 - 14134	Kovanen and Easterbrook, 2001
Penn Cove, Wa	48.243	122.708	UW-32	shell	12150 ± 177	13761 - 14258	Fairhall *et al.*, 1966
North Bellingham	48.800	122.483	W-984	peat	12090 ± 350	13599 - 14599	Ives *et al.*, 1964
South Fork-Cranberry Bog	48.567	122.233	AA-27064	plant fragments	12215 ± 85	13961 - 14186	Kovanen and Easterbrook, 2001
Middle Fork-Deep Kettle Bog	48.776	122.116	AA-22199	wood	12230 ± 80	13979 - 14197	Kovanen and Easterbrook, 2001
South Fork-Cranberry Bog	48.567	122.233	AA-27077	plant fragments	12255 ± 84	13980 - 14253	Kovanen and Easterbrook, 2001
Juan de Fuca Strait	48.358	122.990	CAMS-58689	shell	12280 ± 71	14012 - 14257	Mosher and Hewitt, 2004
Juan de Fuca Strait	48.233	123.168	CAMS-58690	shell	12300 ± 71	14030 - 14320	Mosher and Hewitt, 2004
Pear Point	48.524	123.007	BETA-70791	shell	12290 ± 86	14012 - 14362	Dethier *et al.*, 1995
Penn Cove	48.233	122.700	PC-01 (UWAMS)	shell	12280 ± 103	13989 - 14396	Swanson and Caffee, 2001
Bellingham Bay	48.800	122.533	B-135695	shell	12300 ± 216	13955 - 14670	Kovanen and Easterbrook, 2002b
Seattle, Wa	48.472	122.305	UW-8	peat	12300 ± 200	13974 - 14654	Dorn *et al*, 1962
Sedro Woolley, Wa	48.565	122.214	W-398	basal peat	12275 ± 335	13834 - 14794	Rubin and Alexander, 1958
Middle Fork-Deep Kettle Bog	48.776	122.116	AA-20750	wood	12365 ± 115	14120 - 14615	Kovanen and Easterbrook, 2001
Middle Fork-Deep Kettle Bog	48.776	122.116	AA-22198	wood	12380 ± 90	14156 - 14596	Kovanen and Easterbrook, 2001
Big Lake	48.395	122.242	USGS-782	shell	12420 ± 86	14199 - 14641	Dethier *et al.*, 1995
South Fork-Cranberry Bog	48.567	122.233	AA-27065	plant fragments	12425 ± 90	14206 - 14662	Kovanen and Easterbrook, 2001
Juan de Fuca Strait	48.283	122.844	CAMS-58681	shell	12440 ± 71	14233 - 14653	Mosher and Hewitt, 2004
Juan de Fuca Strait	48.300	123.040	CAMS-58694	shell	12520 ± 78	14427 - 14893	Mosher and Hewitt, 2004
Juan de Fuca Strait	48.349	122.808	CAMS-58701	shell	12550 ± 71	14490 - 14943	Mosher and Hewitt, 2004
Whidbey Island	48.339	122.687	BETA-1716	shell	12645 ± 153	14499 - 15140	Dethier *et al.*, 1995
Whidbey island	48.324	122.653	BETA-1319	shell	12700 ± 354	14236 - 15337	Dethier *et al.*, 1995

Table 3.2. (continued)

Location	Latitude (°N)	Longitude (°W)	Laboratory number	Material dated	Corrected age (yr BP)[a]	Calibrated age (cal yr BP)[b]	Reference
Fraser Lowlands							
Nicomekl River Flat	49.083	122.797	GSC-519	shell	9880 ± 90	10619 - 10936	Clague, 1980
Surprise Lake	49.317	122.567	I-6967	basal gyttja	9715 ± 166	10772 - 11254	Clague, 1980
Furry Creek	49.583	123.217	GSC-2279	shell	10750 ± 107	11940 - 12544	Clague, 1980
County Line Overpass	49.100	122.500	GSC-186	shell	11130 ± 103	12677 - 12851	Clague, 1980
Burnaby	49.267	122.933	L-391C	shell	10950 ± 304	12412 - 13233	Clague, 1980
Fort Langley	49.167	122.583	GSC-168	shell	11380 ± 107	12846 - 13000	Clague, 1980
Coquitlam	49.293	122.787	GSC-2177	shell	11450 ± 71	12905 - 13037	Clague, 1980
Cultus Lake	49.033	122.025	GSC-2523	wood	11300 ± 50	13136 - 13232	Clague, 1980
Norrish Creek	49.195	122.157	L-331A	wood	11450 ± 150	13162 - 13446	Clague, 1980
North Delta	49.133	122.917	GSC-64	marine worm tubes	11510 ± 99	13253 - 13437	Clague, 1980
Deas Island Highway	49.042	122.783	GSC-226	wood	11590 ± 140	13301 - 13593	Clague, 1980
Sumas Mountain	49.067	122.192	L-221D	wood	11500 ± 1100	12059 - 15020	Clague, 1980
Mt. Lehman Road	49.105	122.380	GSC-1675	wood	11600 ± 140	13310 - 13603	Clague, 1980
Port Moody	49.210	122.812	GSC-2612	shell	12050 ± 78	13400 - 13601	Clague, 1980
Bradner Pit	49.017	122.450	B-144099	wood	11660 ± 50	13428 - 13584	Kovanen and Easterbrook, 2002b
Axton Pit	48.850	122.467	B-145455	wood	11670 ± 50	13438 - 13594	Kovanen and Easterbrook, 2002b
Bradner Pit	49.017	122.450	B-144097	wood	11680 ± 50	13447 - 13605	Kovanen and Easterbrook, 2002b
Axton Pit	48.850	122.467	B-145455	shell	11730 ± 64	13480 - 13664	Kovanen and Easterbrook, 2002b
Haney	49.275	122.583	I-5959	shell	11740 ± 196	13388 - 13775	Clague, 1980
Bradner Pit	49.017	122.433	B-120446	wood	11740 ± 70	13494 - 13688	Kovanen and Easterbrook, 2002b
East Delta	49.127	122.900	GSC-2604	shell	12150 ± 90	13483 - 13703	Clague, 1980
King George Highway	49.017	122.750	I(GSC)-6	shell	11675 ± 453	13078 - 14042	Clague, 1980
Axton Pit	48.850	122.467	B-145456	shell	11770 ± 64	13544 - 13726	Kovanen and Easterbrook, 2002b
Bradner Pit	49.017	122.450	B-144095	wood	11770 ± 40	13581 - 13717	Kovanen and Easterbrook, 2002b
Axton Pit	48.850	122.467	B-145460	wood	11790 ± 50	13598 - 13738	Kovanen and Easterbrook, 2002b
Axton Pit	48.850	122.467	B-145459	wood	11830 ± 50	13648 - 13764	Kovanen and Easterbrook, 2002b
Websters Corner	49.233	122.493	GSC-2193	shell	12350 ± 99	13713 - 13920	Clague, 1980
Bradner Pit	49.017	122.450	B-144094	shell	12000 ± 64	13780 - 13924	Kovanen and Easterbrook, 2002b
Bradner Pit	49.017	122.450	B-144096	shell	12000 ± 64	13780 - 13924	Kovanen and Easterbrook, 2002b
Bradner pit	49.017	122.450	B-144098	shell	12020 ± 64	13797 - 13943	Kovanen and Easterbrook, 2002b
Central Strait of Georgia							
Parksville	49.360	124.365	CAMS-51007	shell	9980 ± 71	11248 - 11617	Barrie and Conway, 2000
Denman Island	49.583	124.817	L-441B	shell	10550 ± 206	12214 - 12800	Clague, 1980
North Hornby Island	49.549	124.673	CAMS-52959	shell	10970 ± 71	12855 - 12950	Barrie and Conway, 2000
Wood Farm Bog	49.290	124.180	TO-9894	shell	10950 ± 112	12828 - 12982	Hutchinson *et al.*, 2004a
Lasqueti Island	49.477	124.269	TO-8282	basal gyttja	11225 ± 108	13025 - 13227	Hutchinson *et al.*, 2004a
Comox Bog	49.690	124.870	TO-9901	shell	11320 ± 103	13107 - 13277	Hutchinson *et al.*, 2004a
Nanaimo	49.150	123.970	GSC-80	shell	11870 ± 90	13239 - 13397	Clague, 1980
Strait of Georgia	49.696	124.696	TO-9315	shell	11550 ± 94	13275 - 13474	Guilbault *et al.*, 2003
Courtney	49.645	125.005	I(GSC)-9	shell	11550 ± 453	12952 - 13860	Clague, 1980
Buckley Bay	49.510	124.830	GSC-6496	shell	11650 ± 78	13400 - 13601	Hutchinson *et al.*, 2004a
Lasqueti Island	49.483	124.337	TO-8286	shell	11790 ± 121	13490 - 13759	Hutchinson *et al.*, 2004a
Wellington	49.205	124.000	GSC-389	marine worm	11790 ± 99	13505 - 13756	Clague, 1980
Texada Island	49.683	124.510	CAMS-52955	shell	11790 ± 71	13563 - 13747	Barrie and Conway, 2000
Boundary Bay	49.017	123.067	I(GSC)-248	shell	11850 ± 182	13468 - 13863	Clague, 1980
Courtney	49.642	125.003	I(GSC)-10	peat	11780 ± 450	13138 - 14166	Clague, 1980
Fanny Bay	49.483	124.817	L-391F	wood	11850 ± 300	13364 - 14026	Clague, 1980
Hornby Island	49.476	124.644	CAMS-33804	shell	11950 ± 78	13727 - 13892	Barrie and Conway, 2000
Strait of Georgia	49.607	124.430	LLNL51004	shell	12190 ± 71	13959 - 14132	Guilbault *et al.*, 2003
Texada Island	49.604	124.433	CAMS-51004	shell	12190 ± 71	13959 - 14132	Barrie and Conway, 2000
Strait of Georgia	49.387	124.527	TO-9326	shell	12190 ± 103	13903 - 14170	Guilbault *et al.*, 2003
Strait of Georgia	49.384	124.542	TO--9326	shell	12190 ± 103	13903 - 14170	Barrie and Conway, 2002
Puntledge River	49.683	125.033	GSC-24	wood	12200 ± 80	13959 - 14159	Clague, 1980
Strait of Georgia	49.607	124.508	LLNL51003	shell	12230 ± 71	13992 - 14173	Guilbault *et al.*, 2003
Texada Island	49.604	124.510	CAMS-51003	shell	12230 ± 71	13992 - 14173	Barrie and Conway, 2000
Texada Island	49.689	124.673	CAMS-50333	shell	12250 ± 71	14003 - 14199	Barrie and Conway, 2000
Parksville	49.283	124.267	GSC-1[a]	wood	12180 ± 190	13791 - 14389	Hutchinson *et al.*, 2004a
Hornby Island	49.470	124.615	CAMS-33803	shell	12320 ± 78	14055 - 14418	Barrie and Conway, 2000

Table 3.2. (continued)

Location	Latitude (°N)	Longitude (°W)	Laboratory number	Material dated	Corrected age (yr BP)[a]	Calibrated age (cal yr BP)[b]	Reference
Northern Strait of Georgia							
April Point Marina	50.063	125.228	TO-9909	shell	9840 ± 103	11123 - 11361	James *et al.*, 2005
Loveland Marsh	50.057	125.455	TO-10818	seeds	10830 ± 90	12795 - 12891	James *et al.*, 2005
North Comox	49.811	124.981	CAMS-52086	shell	11120 ± 71	12951 - 13087	Barrie and Conway, 2000
Graham's Gravel Pit	50.035	124.987	TO-9916	shell	11140 ± 103	12939 - 13120	James *et al.*, 2005
Whittington's Bog	50.027	125.174	TO-10817	poplar bud	11480 ± 90	13249 - 13408	James *et al.*, 2005
Piggott's Pond	50.045	124.995	TO-9915	shell	11660 ± 112	13389 - 13641	James *et al.*, 2005
Belansky's Well	50.118	125.028	TO-9897	shell	11670 ± 121	13392 - 13656	James *et al.*, 2005
Ballard's Bog	50.179	125.161	TO-9896	shell	11740 ± 112	13458 - 13707	James *et al.*, 2005
Gowlland Harbour	50.074	125.224	TO-11634	shell	11790 ± 112	13501 - 13756	James *et al.*, 2005
Strait of Georgia	49.818	124.974	LLNL33802	shell	11870 ± 78	13646 - 13812	Guilbault *et al.*, 2003
Saxon Creek Pond	50.207	125.266	TO-9895	shell	11880 ± 103	13618 - 13849	James *et al.*, 2005
Beaver Lake	50.156	125.248	TO-9911	shell	12030 ± 112	13774 - 13996	James *et al.*, 2005
Strait of Georgia	49.896	124.865	CAMS-52091	shell	12160 ± 71	13925 - 14101	Barrie and Conway, 2000
Strait of Georgia	49.895	124.860	LLNL52091	shell	12160 ± 78	13916 - 14107	Guilbault *et al.*, 2003
Gorge Harbour	50.092	125.012	TO-11637	shell	12360 ± 121	14102 - 14611	James *et al.*, 2005
Northern and Central Vancouver Island							
Port McNeill	50.600	127.194	WSU-2019	shell	11300 ± 226	12958 - 13347	Howes, 1981b
Port McNeill	50.567	127.025	WSU-1710	shell	11980 ± 168	13664 - 14027	Howes, 1981b
Tofino	49.167	125.967	BETA-42922	barnacle	12020 ± 94	13780 - 13971	Friele and Hutchinson, 1993
Broken Islands	48.906	125.381	GSC-3617	shell	12050 ± 74	13815 - 13978	Blake, 1982
Port Eliza	49.867	127.000	CAMS-97342	mountain goat	12340 ± 50	14112 - 14404	Al-Suwadi et al., 2006
Hesquiat Harbour	49.472	126.444	GSC-2976	wood	13000 ± 55	15193 - 15491	Blake, 1983
Bear Cove Bog	50.717	127.467	WAT-721	basal peat	13005 ± 316	14932 - 15891	Hebda, 1983
Offshore Vancouver Island							
Explorer Ridge	49.876	130.460	RIDDL-673	foraminifera	11710 ± 206	13356 - 13755	Blaise *et al.*, 1990
Explorer Ridge	49.876	130.460	RIDDL-674	foraminifera	12640 ± 206	14408 - 15148	Blaise *et al.*, 1990
Explorer Ridge	49.876	130.460	RIDDL-806	foraminifera	13580 ± 177	15841 - 16435	Blaise *et al.*, 1990
Explorer Ridge	49.876	130.460	RIDDL-807	foraminifera	14330 ± 187	16837 - 17557	Blaise *et al.*, 1990
Explorer Ridge	49.876	130.460	RIDDL-808	foraminifera	14620 ± 177	17309 - 18000	Blaise *et al.*, 1990
Central Shelf	48.900	126.883	LLNL-?	foraminifera	10260 ± 130	11720 - 12285	McKay *et al.*, 2004
Central Shelf	48.900	126.883	LLNL-?	foraminifera	10550 ± 121	12352 - 12745	McKay *et al.*, 2004
Central Shelf	48.900	126.883	LLNL-?	foraminifera	10650 ± 94	12620 - 12817	McKay *et al.*, 2004
Central Shelf	48.900	126.883	LLNL-?	foraminifera	11510 ± 130	13222 - 13479	McKay *et al.*, 2004
Central Shelf	48.900	126.883	LLNL-?	foraminifera	11690 ± 103	13421 - 13657	McKay *et al.*, 2004
Central Shelf	48.900	126.883	LLNL-?	foraminifera	12460 ± 94	14238 - 14720	McKay *et al.*, 2004
Central Shelf	48.900	126.883	LLNL-?	foraminifera	12570 ± 86	14576 - 14985	McKay *et al.*, 2004
Central Shelf	48.900	126.883	LLNL-?	foraminifera	13190 ± 86	15399 - 15797	McKay *et al.*, 2004

[a] All dates have a 1-sigma error. Reservoir corrections include 950±50 for marine organisms and 650±60 for basal gyttja and peat

[b] Dates calbrated using Calib 5.0 (Stuiver and Reimer, 1993). Age range is 1-sigma limits

Chapter 4 - Glacio-isostatic adjustment, sea level theory and tectonic setting

4.1 Introduction

Glacial loading on the surface of the Earth causes deformation as the crust and mantle respond to the weight of the load. In areas covered by ice sheets the sea level was locally high relative to present levels due to glacial depression and gravitational attraction due to the mass of ice sheets. This contrasts with areas far away from the ice sheet where sea level was lower than present due to water being transferred to continental ice sheets. The earth response due to the weight of the ice sheet is determined by subtracting the far-field sea level from the sea level near the ice sheet. When the ice sheets retreat, the Earth slowly returns to its original shape. The response is a combination of elastic effects of the lithosphere and the viscous mantle. The duration of postglacial rebound depends largely on the viscosity of the mantle and thickness of the lithosphere. The rate of sea-level fall during and after deglaciation can be modeled to determine the rheological properties of the earth.

4.2 Earth rheology

4.2.1 Elastic and viscous materials

An elastic material deforms instantly to an applied force, and returns to its original shape when the force relaxes. Mathematically, these materials act in a linear relationship of stress and strain, known as Hooke's Law. A simple case is for a body that has the same properties in all directions, known as an isotropic body. For this case, Hooke's Law is:

$$\sigma_{ij} = \lambda\theta\delta_{ij} + 2\mu\varepsilon_{ij} \tag{1}$$

where σ_{ij} is the stress tensor, ε_{ij} is the strain tensor, θ is the sum of the normal strain ($\theta = \varepsilon_{11+}\ \varepsilon_{22+}\ \varepsilon_{33}$), or dilatation, δ_{ij} is the Kronecker delta, μ is the shear modulus or rigidity, and λ is a Lamé parameter related to the compressibility of the material. The compressibility term only applies for normal stress (i=j) and involves a volume change. The mean normal stress, $\sigma_{0,}$ is obtained by taking the trace of (1) by setting i=j:

$$\sigma_0 = \left(\lambda + \frac{2}{3}\mu\right)\theta = -p \qquad (2)$$

where p is the pressure. For deviatoric stress ($i \neq j$), Hooke's Law becomes:

$$\sigma_{ij} = 2\mu\varepsilon_{ij} \qquad (3)$$

The mechanical analog of an elastic body is a spring (Fig. 4.1). A spring instantaneously shrinks in response to compression and will expand once the compression relaxes. At low pressure and temperature, such as near the Earth's surface, most rocks act elastically (Turcotte and Schubert, 2002).

A viscous body is one that is able to change shape over time depending on the amount of force exerted (Ranalli, 1995). The simplest viscous materials are known as Newton bodies, and expressed as:

$$\sigma_{ij} = -p\delta_{ij} + 2\eta\dot{\varepsilon}_{ij} \qquad (4)$$

where p is the confining pressure, η is the viscosity of the material and $\dot{\varepsilon}$ is the strain rate tensor. In this case, an instantaneous increase in stress will not amount to any deformation. A viscous material will flow when the stress is deviatoric ($i \neq j$).

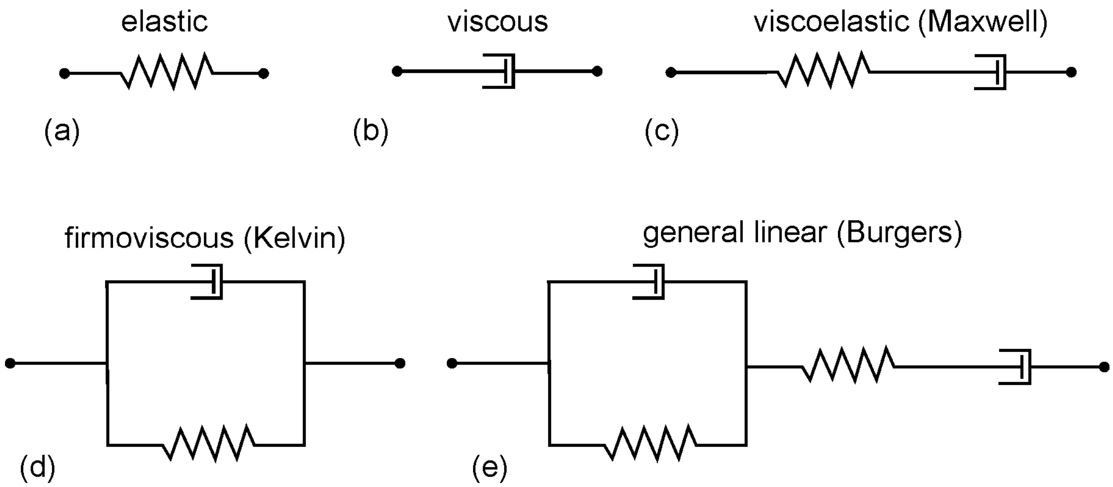

Figure 4.1. Mechanical equivalents of rheological models (Ranalli, 1995). (a) elastic or Hooke, (b) viscous or Newton, (c) viscoelastic or Maxwell, (d) firmoviscous or Kelvin, (e) general linear or Burgers

The mechanical analogue of a viscous body is a dashpot (Ranalli, 1995; Fig. 4.1), a device commonly used to prevent doors from slamming. In a simplified case where the applied stress is constant, the strain changes linearly with time. The deformation is permanent unless there is a restoring force.

4.2.2 Viscoelastic body

A viscoelastic, or Maxwell, body has both an elastic and viscous component. Mechanically, it is analogous to putting a spring and dashpot in a linear combination (Fig. 4.1). The formula that describes a Maxwell body is:

$$\dot{\varepsilon} = \frac{1}{2\mu}\dot{\sigma} + \frac{\sigma}{2\eta} \qquad (5)$$

In the case where the applied stress is constant, the strain will vary linearly with time. The elastic component of stress will respond instantly to the introduction of stress, while the viscous component will provide a continuous deformation. When there is a relief of stress, the elastic component will immediately relax, while the viscous component is permanent. A three-dimensional version of a viscoelastic body is used in this study to model postglacial rebound.

4.2.3 Firmoviscous body

A firmoviscous, or Kelvin, material is a combination of a viscous and elastic body. Mechanically, it is analogous to a parallel combination of a spring and dashpot (Fig. 4.1). The relationship is:

$$\sigma = 2\mu\varepsilon + 2\eta\dot{\varepsilon} \qquad (6)$$

In this case, there is damping of the elastic response. If the stress is constant, the strain will logarithmically reach a plateau equal to $\sigma/2\mu$. When there stress relaxes, the strain will exponentially decay to zero.

4.2.4 General linear body

A general linear, or Burgers, body is a linear combination of an firmoviscous and viscoelastic body (Ranalli, 1995; Fig. 4.1). If ε_1 is the firmoviscous strain component, and ε_2 is the viscoelastic strain component, the general equation for a general linear rheology is:

$$2\eta_1\ddot{\varepsilon} + 2\mu_1\dot{\varepsilon} = \frac{\eta_1}{\mu_2}\ddot{\sigma} + \left(\frac{\eta_1}{\eta_2} + \frac{\mu_1}{\mu_2} + 1\right)\dot{\sigma} + \frac{\mu_1}{\eta_2}\sigma \qquad (7)$$

In the case of a constant stress, the Burgers body simplifies to having elastic, viscous, and exponential transient creep components. In this situation, after the stress relaxes, the elastic component recovers instantly, the transient creep component decays over time, while the viscous component is permanent. Burgers rheology can explain the behavior of materials over a large frequency spectrum.

4.2.5 Non-linear rheology

In certain geological situations, strain rate varies non-linearly with stress (Turcotte and Schubert, 2002). Rocks that are under relatively low stress levels tend to flow by the diffusion of atoms or molecules within a crystal lattice, and behave as a linear Newtonian fluid. In high stress situations motion is predominantly through dislocation creep, where the motion of crystal defects cause flow. These situations are also known as power law rheology, as strain rate is proportional to the stress to some exponent. Experimental data on olivine crystals indicate that the mantle probably flows by dislocation creep, where high stress and high temperatures control the rheology.

4.2.6 Rheology for glacio-isostatic adjustment modelling

The behavior of the earth to stress depends on the time period involved (Turcotte and Schubert, 2002). The mantle acts elastically on short time scales ($<10^4$ s), as shear waves travel through the mantle with little attenuation. At the longest long time scales ($>10^{11}$ s), the mantle behaves like a viscous fluid as evident from mantle convection and the motion of lithospheric plates. Because the mantle acts elastically at short time periods and viscously at long periods, a viscoelastic rheology is appropriate to describe the behavior if non-linear effects are negligible.

Karato and Wu (1993) determined the response of various linear and non-linear mantle rheology models to postglacial rebound signals. Observations of seismic anisotropy to depths of 200-300 km indicate that the uppermost mantle undergoes dislocation creep to align minerals, which is a non-linear rheological deformation process. However, dislocation creep only happens in the uppermost mantle and at time scales less than plate tectonics, and may show effects on the time scale of postglacial rebound. Using a selection of linear, non-linear, and combination models, Karato and Wu (1993) found there is negligible difference in the response due to a uniform linear mantle or one with a thin (<200 km) layer of non-linear mantle overlying linear mantle. Models with a thick (>200 km) non-linear upper mantle do not fit observed sea-level data in areas affected by the Laurentide ice sheet, as the mantle flowed back to the center of deformation too quickly. Peltier (1998) argued that if the mantle was significantly non-linear, it would require different parameters for rotational momentum to explain glacio-isostatic adjustment and long-term mantle convection. He also suggested that any non-linear components, such as at the 670 km discontinuity, would be transparent to the observed glacio-isostatic adjustment effects. Since postglacial rebound is not sensitive to non-linear effects, this study uses an assumption that the mantle behaves visco-elastically.

The lithosphere behaves generally in an elastic manner (Ranalli, 1995). The thickness of elastic rheology depends on the local tectonic situation. For instance, in stable continental areas, the elastic thickness is more than 100 km. In areas where active tectonism occurs, it can be less than 20 km. There is also depth dependence, and towards the bottom of the lithosphere rocks become increasingly soft, approaching mantle viscosity. Near the surface, the lithosphere deforms in a brittle fashion. There also may be layers of weakness throughout the lithosphere controlled by temperature and lithology. The Moho acts as a decoupling layer between the crust and mantle and is rheologically weak. In general, rock strength increases to the middle of the lithosphere, and then slowly decreases to the base as the rocks act more ductile. Parts of the lithosphere deform plastically at times of the order of 10^7 years

(Turcotte and Schubert, 2002), so it is not significant on for postglacial rebound analysis.

4.3 Glacio-isostatic adjustment theory

4.3.1 Crustal motions due to loading

Adjustment of the Earth due to dynamic loading on the surface is a classic geophysical problem (Haskell, 1935; Niskanen, 1943; McConnell, 1965; Farrell, 1972; Peltier, 1974; Cathles, 1975, Peltier, 2004). The way the Earth deforms depends largely on the size and duration of the applied load and the rheology where the load is applied. For the simple case of a uniform halfspace, the vertical uplift after the removal of a sinusoidal load is (Turcotte and Schubert, 2002):

$$w = w_m \exp\left(\frac{-t}{\tau_r}\right) \tag{8}$$

where w_m the initial displacement, t is the time, and τ_r is the characteristic decay time. The response due to the load will decrease over time as the exponential function goes to zero. The decay time depends on density and viscosity, given by:

$$\tau_r = \frac{4\pi\eta}{\rho g\lambda} \tag{9}$$

where η is the viscosity of the half-space, ρ is the density of the earth, g is the gravity at the surface, and λ is the wavelength of the load.

4.3.2 Response of a layered Earth

Though the response of a uniform halfspace to a surface load is a simple calculation, a layered rheology is more realistic for the Earth (Niskanen, 1943; McConell, 1965). The Earth models used in this study use spherically symmetric layers that have uniform elastic properties, density and viscosity. The method to calculate the response follows the work of James (1991). Instead of one decay time as in a uniform halfspace model, a layered Earth has decay times associated with every rheological contrast. The expression for the response is a Legendre function, and each degree has its own decay time. At higher degrees, many of the decay times become very small in magnitude, and contribute little to the response.

The response due to a surface load is often expressed in terms of dimensionless Love numbers (Farrell, 1972; Peltier, 1974; James, 1991). The equation for this is:

$$\begin{bmatrix} U_n(r) \\ V_n(r) \\ \Phi_{2n}(r) \end{bmatrix} = \frac{ag_0}{m_e} \begin{bmatrix} h_n(r)/g_0 \\ l_n(r)/g_0 \\ -k_n(r) \end{bmatrix} \tag{10}$$

where U_n, V_n, and Φ_{2n} are the vertical displacement, horizontal displacement and gravitational potential due to deformation respectively, g_0 is the initial gravitational acceleration, a is the radius of the Earth, m_e is the mass of the Earth, r is the distance from the center of the Earth, and h_n, l_n, and k_n are the Love numbers. The Love numbers are related to the boundary conditions for the model. Like the decay times, the response of the Love numbers depends on the Legendre degree. Each Love number has an elastic and viscous component, though at large values of n, the elastic component becomes very small compared to the viscous component.

With the introduction of a layered Earth structure, there are decay times for each boundary where there is a density or rheology contrast (Peltier, 1985; James, 1991). The effect of increasing the density with depth creates decay modes that are longer than the homogenous model. At greater degrees, the magnitude of the displacement and potential dissipates. When a viscosity contrast is added, decay times known as T-modes are introduced. There are two T-modes for each interface between viscous layers. The T-modes generally have a rapid decay time and very little effect on the displacement and gravitational potential, except at small degrees. The small amplitude of the T-modes can cause calculation problems as the two T-modes expected between the layers become indistinguishable. This is especially prevalent when the viscosity contrast is very large (over two orders of magnitude). There is only one decay mode associated with a rheological contrast involving an elastic or fluid layer.

4.3.3 Sea level change

Many factors affect sea level including changing volume of continental ice sheets, gravitational attraction due to continental ice sheets, glacio-isostatic adjustment, ocean density changes (changes in temperature in the water column), tectonic motions, ocean circulation, atmospheric pressure, terrestrial water storage and human activities (Bindoff *et al.*, 2007). During the deglaciation of the large continental ice sheets in the late Pleistocene, continental ice mass changes, solid-earth response and gravitational effects of the ice load dominated sea-level change (Farrell and Clark, 1976). In areas near the ice sheets, sea level was higher than present due to the depression of the earth and gravitational attraction of the load (Fig. 4.2). In areas far away from the ice sheets, sea level was lower than present due to the removal of ocean water to the ice sheets. During deglaciation, the land in areas previously covered by ice sheets rebounded, lowering relative sea level, while sea level in far field locations rose due to the addition of water to the ocean.

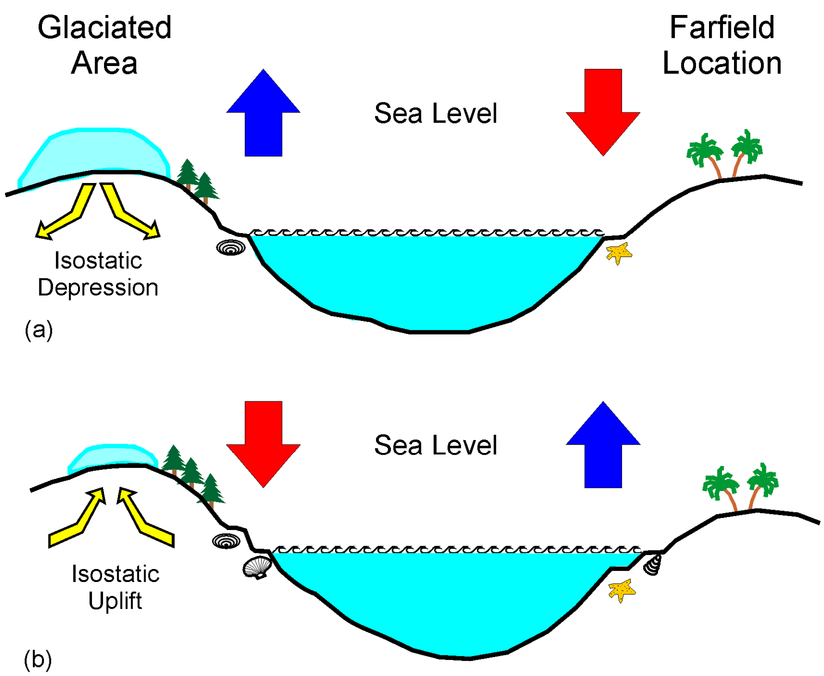

Figure 4.2. Sea level at glaciated and far-field locations (a) during a glacial episode and (b) during deglaciation. (modified from Farrell and Clark, 1976).

Sea level is defined as the relationship between the geoid, solid earth surface, and the volume of water in the ocean (Farrell and Clark, 1976; Mitrovica and Peltier, 1991; Mitrovica and Milne, 2003). Sea level is the difference between the geoid surface (*G*) and the surface of the solid earth (*R*):

$$SL(\theta,\phi,t) \equiv G(\theta,\phi,t) - R(\theta,\phi,t) + c(t) \quad (11)$$

The term *c(t)* is the conservation of mass term to account for the water mass balance between the ice sheets and oceans. This study uses the simplification that global far-field sea level represents this term. The geoid is an equipotential surface that defines the shape of the ocean surface. If there was enough water to cover the entire surface of the earth, this would be a smooth function. To account for land at elevations above the ocean surface and grounded ice, a delta function is applied to the sea level equation:

$$S(\theta,\phi,t) = SL(\theta,\phi,t)C(\theta,\phi,t) \tag{12}$$

The function *C* relates to height of the geoid relative to the solid surface. In places where the geoid height is greater than the solid earth height, it equals one, while where the solid surface is greater (basically where there is exposed land), the function equals zero. During times when the growth of continental ice sheets lowered global sea level, this function takes into account the sloping bathymetry of the continental shelf, and the surface area of the ocean surface decreases.

4.3.4 Global sea level

In order to find the glacio-isostatic response in an area, the globally averaged, or eustatic, sea level signal must be added to the local sea level to account for the conservation of mass (Farrell and Clark, 1976). An ideal far-field location should have minimal interactions with ice sheets and known tectonic motions. Figure 4.3 shows far field sea-level curves from Barbados from dated coral (Fairbanks, 1989; Bassett *et al.*, 2005), Barbados calculated from the ICE-5G model (Peltier, 2004), and Tahiti from dated coral (Bassett *et al.*, 2005). Despite different methods of analysis, the difference between the three curves at Barbados is less than 5-10 m after about 15 cal kyr BP. The sea-level history from Tahiti deviates greatly from the Barbados history, especially before 15 cal kyr BP and in the mid-Holocene.

Between 13 and 11 cal kyr BP, there is a 5-10 m difference between the Barbados and Tahiti sea-level curves. Bassett *et al.* (2005) suggest this discrepancy is due to an Antarctic source for meltwater pulse 1a (mwp-1a), a sudden increase of sea level due to the rapid collapse of ice sheets between 14.5 and 13.5 cal kyr BP, and isostatic adjustment due to the ocean load. The Barbados sea-level curve is relatively

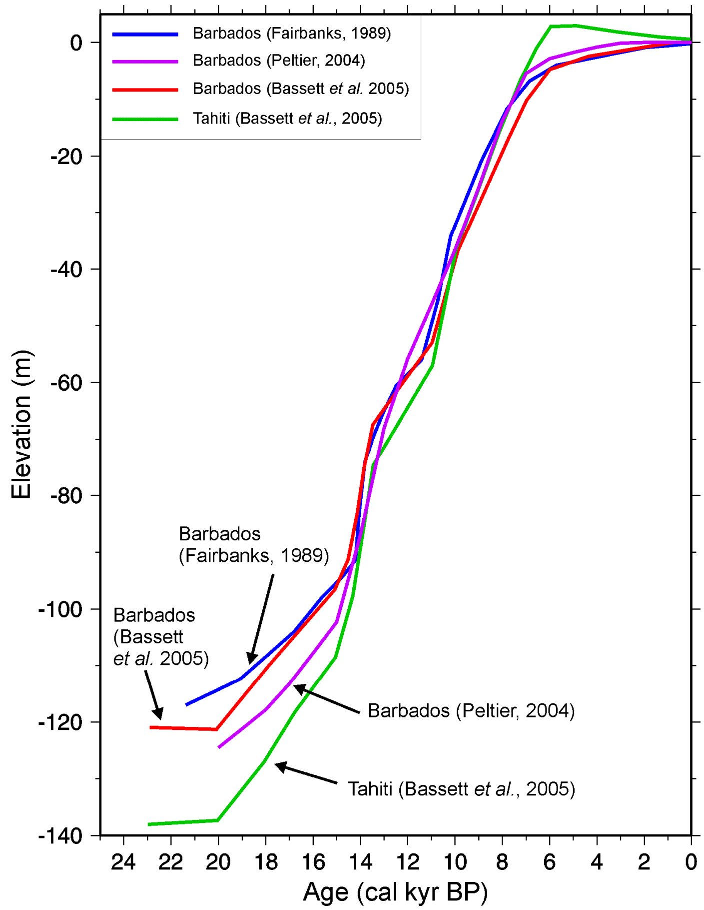

Figure 4.3. Comparison of three eustatic sea-sea level curves from Barbados and one from Tahiti.

insensitive to an Antarctic source for mwp-1a. The analysis also indicates that in southwestern British Columbia there is little change in predicted sea level regardless of the source of mwp-1a. The source of mwp-1a is a controversial topic, as some models suggest that an Antarctic source of the water cannot be proven (Peltier, 2005), so having a eustatic curve that is unaffected by the source of rapid sea-level change is necessary. Another issue is sea floor subsidence due to the increased ocean load when the ice sheets melt. This is evident in southern Pacific sea-level curves, as there is a slow fall in sea level from a mid-Holocene highstand (Bard *et al.*, 1996; Fig. 4.3).

Due to these issues, study uses a recently published Barbados sea-level curve (Bassett *et al.* 2005) to calculate relative sea level in southwestern British Columbia.

4.4 Tectonic setting

4.4.1 Cordilleran Orogen

The Canadian Cordillera has a complex history, spanning the past 2100 Ma (Gabrielse and Yorath, 1989). Throughout most of the Proterozoic and Paleozoic, the western margin of Canada was a passive margin with stages of rifting. The formation of the Cordillera began in the Late Triassic and early Jurassic. From the Jurassic to Paleogene, the accretion of ocean island terranes, thrusting of older margin sediments and the formation of volcanic arcs built the Cordillera. Throughout the Neogene, mountain building was primarily due to arc volcanism by the subduction of the Juan de Fuca Plate.

4.4.2 Cascadia subduction zone

The Cascadia subduction zone is the result of the convergence of the Juan de Fuca Plate with the North American plate (refer to Figure 1.2 in introductory chapter). The northern Juan de Fuca plate converges at a rate of 40-47 mm a^{-1} relative to North America (Riddihough, 1984). The subducting plate causes significant deformation along the coast of the Pacific Northwest due to the locking of the Juan de Fuca and North American plates between great earthquakes. There is evidence of a number of major subduction thrust earthquakes over the past few thousand years, the last being about 300 years ago.

Seismic profiles define the lithospheric structure of the Cascadia subduction zone in southwestern British Columbia (Clowes *et al.*, 1995; 1997). The data show that the upper crust is highly complex, and the lower crust has velocities between 6.4 and 7.4 km s^{-1} (Clowes *et al.*, 1995). Throughout most of the Cordillera, the crustal thickness is between 33 and 38 km with the central Cordillera having the lowest values. Closer to the plate margin, the crustal thickness shows along-strike variability, thinning slightly from south to north in Vancouver Island (Clowes *et al.*, 1997). This is likely due to the transition from the subducting Juan de Fuca Plate to the slower converging part of the Explorer Plate.

The depth to the subducting Juan de Fuca plate is defined to a depth of 60 km from seismic surveys and observations of seismicity in northern Cascadia (*e.g.* Flück *et al.*, 1997; McCrory *et al.*, 2004). Throughout most of northern Cascadia, the plate motion is roughly perpendicular to the subduction trench. In the Olympic Peninsula-southern Vancouver Island region there is a significant bend in the downgoing slab, and the angle of the subduction thrust is much shallower than the rest of Cascadia. In most of the forearc region between the continental crust and the subducting oceanic plate is a rigid mantle wedge (Wada *et al.*, in press). This wedge exists up to depths of about 80 km downdip of the subducting Juan de Fuca Plate. The angle of the descending plate becomes very steep at depths larger than 60 km.

4.5 Earth model

4.5.1 Introduction

Southwestern British Columbia presents a complicated earth structure with lateral variability due to the subducting Juan De Fuca Plate, interactions with the converging Explorer plate, and high heat flow in the backarc region. Due to these complications, it is necessary to simplify the earth model in order to make the determination of the response less complicated. The three dimensional earth is simplified into a simple one dimensional layered earth to accomplish this. The parameters for the uppermost layers are chose based on the average structure for the Strait of Georgia and Victoria area. Parameters for deeper layers are based on globally averaged values.

4.5.2 Density and rigidity

Earth models for this study use rigidity and density parameters based on the Preliminary Reference Earth Model (PREM) (Dziewonski and Anderson, 1981). PREM has nine boundaries based on sudden seismic velocity changes, and assumes that the properties between the interfaces are laterally homogenous. To simplify calculations, the core and lithosphere properties are volumetrically averaged together in this study. The mantle is split into two layers above and below the 670 km seismic discontinuity. For the purposes of this study, the rigidity and density is volumetrically averaged for each rheological layer.

4.5.3 Viscosity profile

The viscosity profile used in this study is a modified version of the VM2 model with the upper mantle allowed to vary in thickness and viscosity (Peltier, 1998). The determination of the VM2 viscosity model involved the inversion of relaxation times for the Laurentide and Fennoscandian postglacial sea levels, with the two-layer VM1 model used as a starting model. Figure 4.4 shows these models as well as the simplified model used in this study. For this study, the mantle was sectioned off into four parts, using a viscosity value based on VM2 except for the uppermost layer. All viscosity values are rounded to the nearest tenth of an order of

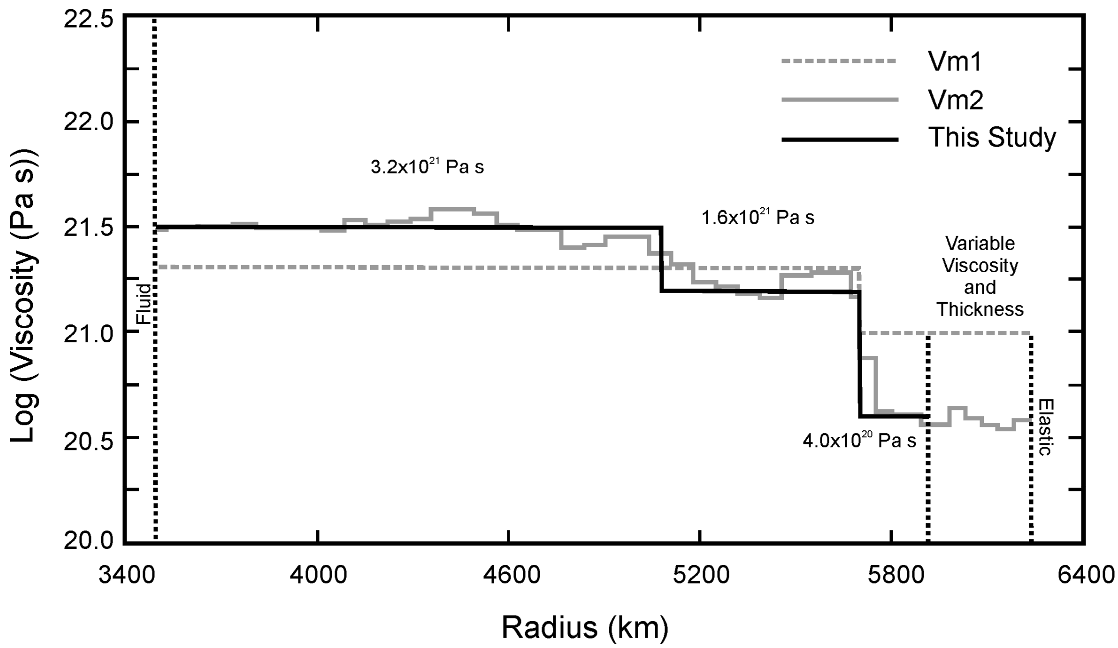

Figure 4.4. Viscosity profile on the mantle. The dashed and solid grey lines are the VM1 and VM2 models are from Peltier (1998), and the solid black line is the simplified model used in this study based on VM2.

magnitude. For the mantle above the 670 km discontinuity, there are two layers: an upper layer with variable thickness and viscosity (termed "asthenosphere"), and a lower layer that has a viscosity of $4x10^{20}$ Pa s. Below the 670 km discontinuity, there are two layers separated at 1291 km depth. The upper layer has a viscosity of $1.6x10^{21}$ Pa s, while the lower layer is $3.2x10^{21}$ Pa s. The core, assumed to begin at 2891 km depth, is fluid. In our models, the lithosphere is elastic, with a thickness as described in the next section.

4.5.4 Effective elastic thickness

The elastic thickness in the backarc of southwestern British Columbia is controlled by high heat flow from asthenospheric convection and water from slab dehydration, which results in a thin lithosphere (Hyndman *et al.*, 2005). The effective elastic thickness describes the average depth to the brittle-ductile transition in the crust or mantle (Flück *et al.*, 2003). One method to measure this is to find the coherence between topography and gravity field predicted to be caused by topography. In southern British Columbia backarc, the average elastic thickness, T_e, is less than 20 km. For instance, the observed crustal bulge in the Queen Charlotte Islands region due to Pleistocene glaciation indicates that the elastic thickness is between 10 and 20 km (Hetherington and Barrie, 2004).

The elastic thickness in the subduction zone is complicated by the combined effects of the continental and oceanic lithosphere. The best way to determine the depth to which elastic conditions prevail is by seismicity, as it indicates brittle behavior. Seismic tremors associated with silent slip events extend to depths over 40 km under southern Vancouver Island (Kao *et al.*, 2005). Seismicity associated with the subducting Juan de Fuca plate extends to depths of up to 65 km in southwestern British Columbia (Cassidy and Waldhauser, 2003). These events are located within the subducting oceanic crust and upper mantle, which becomes decoupled from the overriding continental plate at depths of less than 25 km (Wada *et al.*, in press). The crustal thickness in the Vancouver Island region is between 30 and 35 km (Clowes *et al.*, 1997). The effective elastic thickness calculated from gravity and topography data in southern Vancouver Island is about 40 km. Heat flow data from Vancouver Island and the Strait of Georgia have values between 25 and 45 mW m^{-2}, which is at least half the value in the backarc region (Lewis *et al.*, 1988). The lower heat flow is a result of a cool wedge that exists between the continental crust and the subducting Juan de Fuca Plate beneath Vancouver Island and the Strait of Georgia. Clague and James (2002) used a 60 km thick elastic layer, as this is average depth to the top of the Juan de Fuca plate in the study area and thus the maximum depth of the cool mantle wedge. The mantle wedge exists at depths of up to 80 km (Wada *et al.* in press), though the average thickness of the wedge over the study range is less than that. This also study also uses a consistent 60 km thick elastic layer (termed “lithosphere”) to reflect this.

4.6 Summary

This chapter describes the various parameters required for modelling glacio-isostatic adjustment in southwestern British Columbia. The PREM and VM2 models are the basis for the Earth models used in this study. The Earth models have an elastic lithosphere that is 60 km thick, Maxwell mantle with several layers of different viscosity and density, and a fluid core. In order to predict relative sea level due to glacial loading, this study uses the far-field sea-level curve from Barbados to account for global sea level since deglaciation.

Chapter 5 - Modelling of sea level in southwestern British Columbia

5.1 Introduction

James *et al.* (2000) completed the first detailed study of the relation between Earth viscosity structure and postglacial sea level in southwestern British Columbia and northwestern Washington State. This study modeled the tilts of dammed proglacial lakes in the Puget Sound, and some sparse sea level data from eastern Vancouver Island. The ice sheet model used disc loads similar to ICE-3G (Tushingham and Peltier, 1991), but used a smaller, uniform disc size with a diameter of 55 km to provide a more accurate coverage of the Cordilleran ice sheet. They assumed a uniform viscous mantle. They found that the mantle viscosity values in the area range between 5×10^{18} and 5×10^{19} Pa s. They calculated that the present day uplift rate was less than 0.1 mm yr^{-1} throughout southwestern British Columbia using this ice model.

Clague and James (2002) expanded the ice sheet model presented in James *et al.* (2000) to include a far field ice sheet. They also used a layered mantle model with interfaces at the major seismic discontinuities. They found that the modeled sea level observations were relatively insensitive to deep mantle stratification, but increasing the lithosphere thickness significantly lowered the magnitude of the modeled sea level. A low asthenosphere viscosity ($<10^{20}$ Pa s) still provided the best fit to the relative sea level observations. Using a low mantle viscosity ($<10^{20}$ Pa s), the present uplift rates due to glacio-isostatic adjustment were still less than 1-1.2 mm yr^{-1}.

Clague *et al.* (2005) studied the advance phase of the last major glaciation and the amount of glacial depression required to explain the sea-level observations. The ice sheet model was converted to calibrated age and included an earlier advance at 28 cal kyr BP. They based the amount of ice needed in the model on the elevation of the Quadra Sand in the Fraser Lowland, which occurs at elevations of up to 18 m above present sea level. Since global sea level at this time was at least 85 m below present at the time, there was at least 100 m of depression at the time. To account for this, the ice model assumes over 1 km of ice existed within the Strait of Georgia at 28 cal kyr BP.

Since these original modelling exercises, new observations from the central and northern Strait of Georgia (Hutchinson *et al.*, 2004a; James *et al.*, 2005) and Victoria (Chapter 2) provide tight constraints on relative sea level. New radiocarbon reservoir corrections determined by Hutchinson *et al.* (2004b) provide more accurate constraints on ice sheet history. The ice model of James *et al.* (2000) and Clague and James (2002) has also been converted to calendar years to provide a more realistic chronology.

In this chapter, the previous ice sheet models are used to predict sea level in regions where sea level is well constrained. Modifications to the ice sheet model are made to improve the sea level predictions. The modifications on ice sheet history are based on previously published radiocarbon data on the advance and retreat of the last glaciation and attempting to create smooth sloping ice sheet topography. The new ice model provides predictions that fit the observed sea-level observations over a variety of different asthenosphere thickness and viscosity values. Finally, there is a discussion of the various limitations of the modelling.

5.2 Initial sea level modelling

5.2.1 Modelling parameters

The first step in the modelling process is to compare the relative sea level data to the predicted sea-level changes of various earth models to the ice history used in James *et al.* (2000) and Clague and James (2002). The timing of the ice sheet history was converted to calendar years using Calib 5.0 (Stuiver and Reimer, 1993). The fit is derived using the root mean squared error misfit of the predicted sea-level curves to the observed curves:

$$RMS = \sqrt{\frac{1}{n}\sum_{1}^{n}\left(trueSL - predSL\right)^2} \qquad (1)$$

The sea-level curves are best constrained during the observed rapid sea level fall that happened shortly after deglaciation. The time periods corresponding to the rapid fall are 13.9-12.3 cal kyr BP for the central Strait of Georgia, 13.7-12.0 cal kyr BP for the northern Strait of Georgia and 14.1-13.1 cal kyr BP for Victoria. These intervals are used for determining how well the predicted sea level compares with observed sea level. The earth models use the VM2 model of Peltier (1998) for the viscosity below the asthenosphere, a 60 km elastic lithosphere and variable asthenosphere thickness and viscosity. All modeled sea-level curves use Barbados as the basis of eustatic sea level (Bassett *et al.*, 2005). The initial modelling focuses only on the well-constrained initial sea level fall.

5.2.2 Results of the unmodified ice model

Before changing any modelling parameters, it is necessary to assess the fit of predicted sea-level curves to observed sea level using the ice model of James *et al.* (2000) and Clague and James (2002). This ice model used the ice margin retreat history of Dyke (1996) for the Canadian portion of the ice sheet and Booth (1987) for the Puget Lobe. Ice elevation was based off the reconstruction by Wilson *et al.* (1958) and Thorson (1980). Figure 5.1 shows the calculated sea-level curves for earth models with an asthenosphere thickness of 300 km and variable asthenosphere viscosity. In general, the predicted sea level curves underpredict the maximum highstand positions observed in southwestern British Columbia. An asthenosphere viscosity of 10^{20} Pa s provides the best fit to the curves, but it underpredicts the highstand positions by over 60 m, and the sea-level drop is too slow. Viscosity values of 10^{17} and 10^{18} Pa s provide nearly identical responses with predicted sea levels that are too low and decay too rapidly. Though the misfit with a viscosity of 10^{21} Pa s is better than viscosity values less than 10^{20} Pa s, sea level does not drop fast enough to account for the observations. A viscosity of 10^{19} Pa s provides a sea-level drop that matches the shape of the observed fall in the sea-level record, though it still significantly underpredicts the observed highstand positions, especially in Victoria.

Figure 5.2 shows the RMS misfit of predicted sea level using Earth models with a range of asthenospheric thickness and viscosity to the sea-level curves in southwestern British Columbia. In all cases, the optimum fit is with an asthenosphere viscosity between 10^{20} and 10^{21} Pa s. There is only a weak dependence on asthenosphere thickness, as this viscosity range leads to a nearly uniform upper mantle. This viscosity is at least an order of magnitude larger than the preferred viscosity found by James *et al.* (2002) and Clague and James (2002).

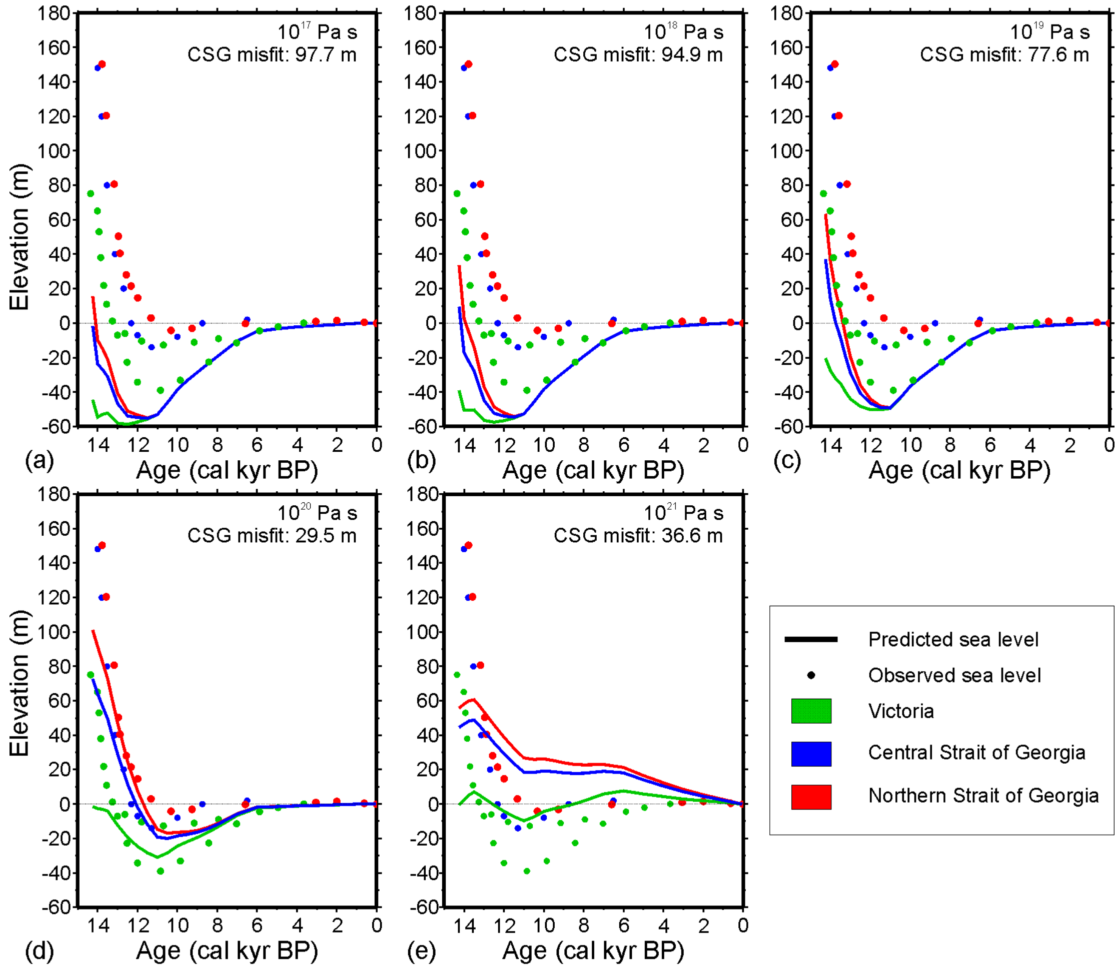

Figure 5.1. Comparison of predicted and observed sea levels in southwestern British Columbia using the ice model of James *et al.* (2000) and Clague and James (2002). The Earth models used to predict sea level have an elastic thickness of 60 km, asthenosphere thickness of 300 km and variable asthenosphere viscosity. RMS misfit of the central Strait of Georgia (CSG) sea-level curve is noted for each comparison. Asthenosphere viscosities are (a) 10^{17} Pa s, (b) 10^{18} Pa s, (c) 10^{19} Pa s, (d) 10^{20} Pa s and (e) 10^{21} Pa s.

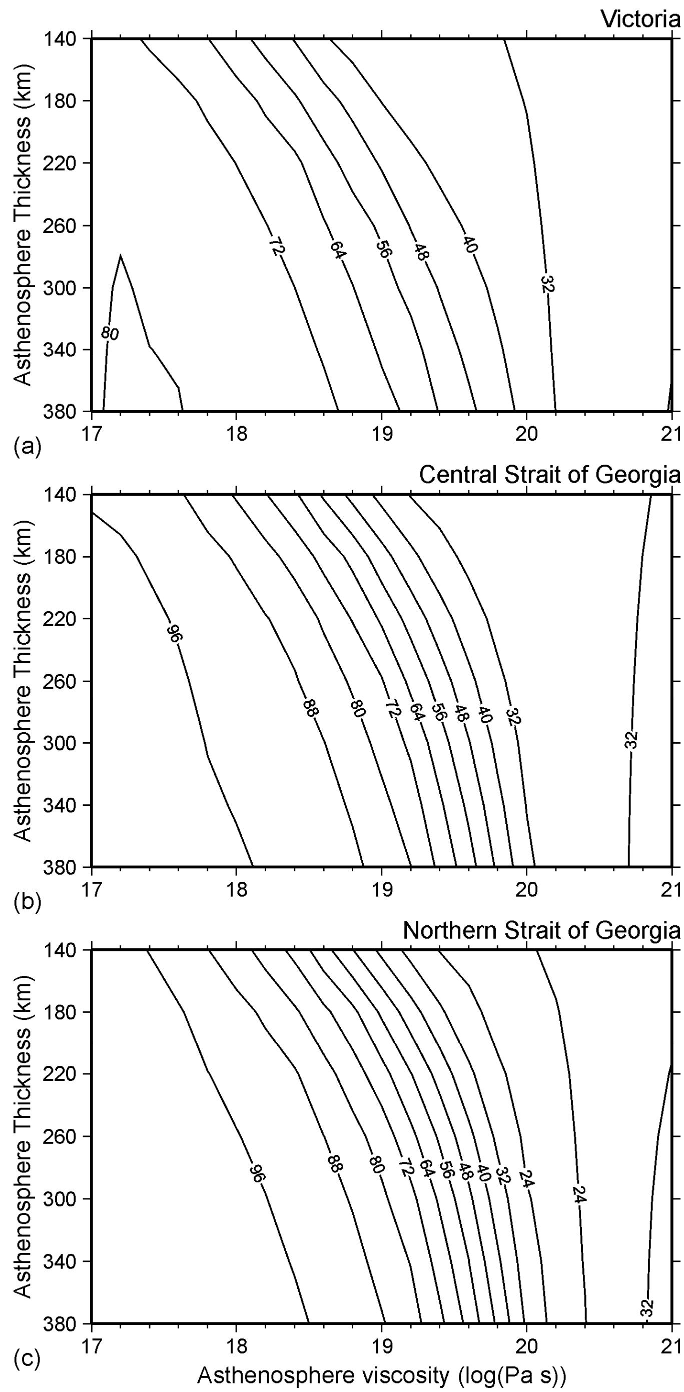

Figure 5.2. RMS misfit (m) of predicted sea-level curves to the well constrained sea-level curves for Earth models with a 60 km elastic lithosphere and a range of asthenosphere thickness and viscosity values using the ice model from James *et al.* (2000) and Clague and James (2002). (a) Victoria, (b) central Strait of Georgia and (c) northern Strait of Georgia

5.2.3 Results of the original ice model with increased ice thickness

Since there was a general underprediction of the magnitude of the highstand positions in the predicted sea-level curves for southwestern British Columbia, the next step was to increase the size of the load. To test the effect of increasing the ice load, each element from the ice model of James *et al.* (2000) and Clague and James (2002) was increased by 1.3 times. This change thickens the ice sheet by up to 450 m. Figure 5.3 shows the predicted sea-level curves with a 300 km thick asthenosphere and variable asthenosphere viscosity with the 1.3x load. Though there is a much larger modeled highstand position in all three curves, the extra load is not enough to match the observations. The response with a 10^{20} Pa s comes close to matching the sea level observations in the northern Strait of Georgia, though the sea level fall is too slow to match the observations. The best match to the speed of the sea level fall is the model with a viscosity of 10^{19} Pa s.

Figure 5.4 shows the RMS misfit of predicted sea level for various earth models with different asthenosphere viscosity and thickness when the original ice load thickness is multiplied by 1.3 times. The results of the central and northern Strait of Georgia curves have a much better fit better with lower viscosity and there is a clear relationship between asthenosphere thickness and viscosity. In particular, the minimum misfit of 16 m in the central Strait of Georgia and 24 m in the northern Strait of Georgia and Victoria is about 60% the RMS values for the thinner ice model.

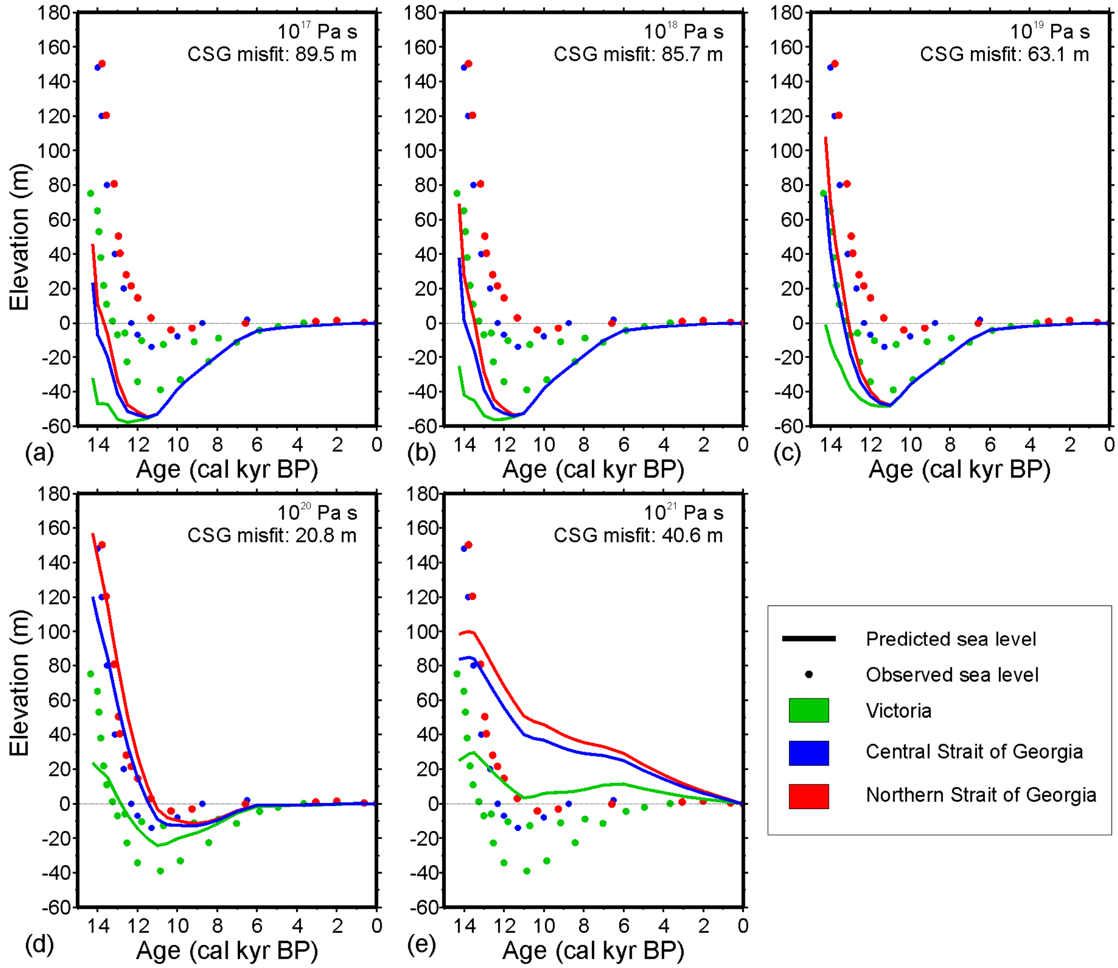

Figure 5.3. Comparison of predicted and observed sea levels in southwestern British Columbia using the ice model of James *et al.* (2000) and Clague and James (2002) with the thickness of the ice sheet multiplied by a factor of 1.3. The Earth models used to predict sea level have an elastic thickness of 60 km, asthenosphere thickness of 300 km and variable asthenosphere viscosity. RMS misfit of the central Strait of Georgia (CSG) sea-level curve is noted for each comparison. Asthenosphere viscosities are (a) 10^{17} Pa s, (b) 10^{18} Pa s, (c) 10^{19} Pa s, (d) 10^{20} Pa s and (e) 10^{21} Pa s.

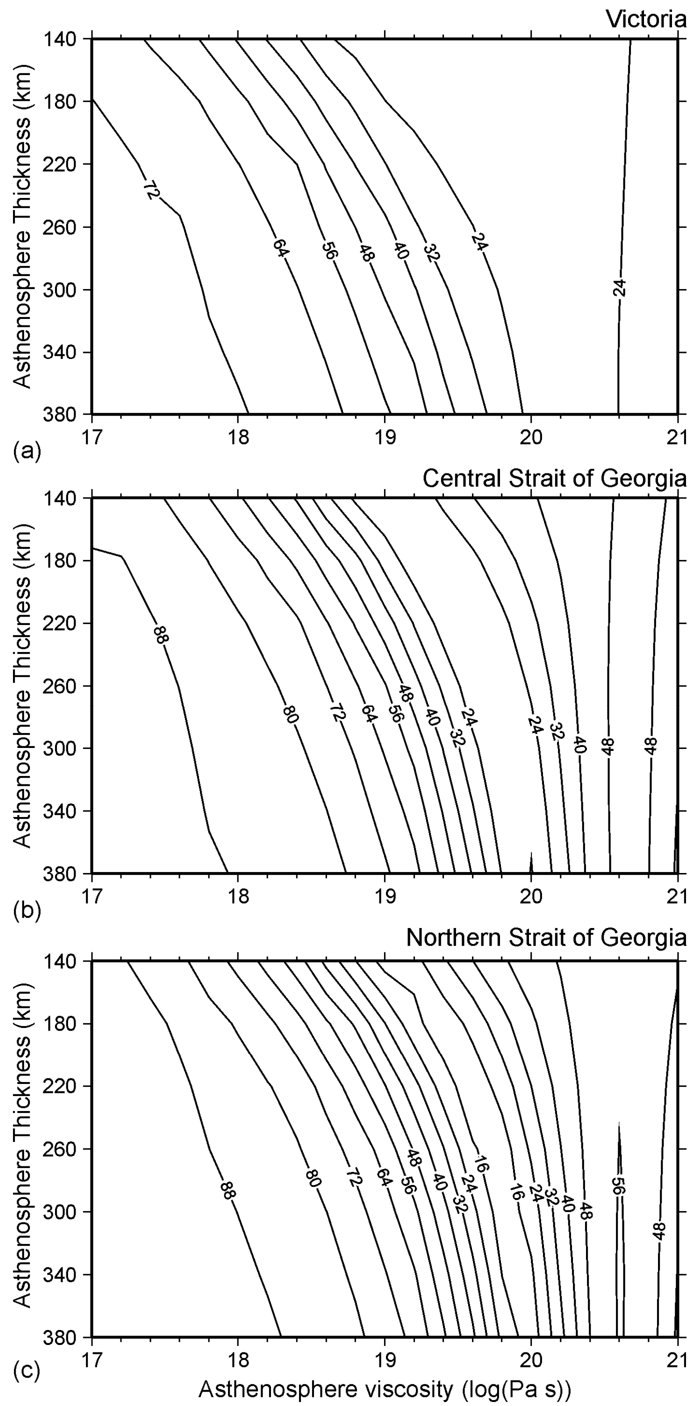

Figure 5.4. RMS misfit (m) of predicted sea-level curves to the well constrained sea-level curves for Earth models with a 60 km elastic lithosphere and a range of asthenosphere thickness and viscosity values using the ice model from James *et al.* (2000) and Clague and James (2002) with the thickness of the ice sheet multiplied by a factor of 1.3. (a) Victoria, (b) central Strait of Georgia and (c) northern Strait of Georgia

5.2.4 Initial changes to the ice model

The systematic misfit between the predicted and observed relative sea level using the ice model of James *et al.* (2000) and Clague and James (2002) indicate that the history and thickness of the ice load need modification. Gowan and James (2006) showed the results of the initial changes to the ice model. The goal was to match the observed sea level curves in the central and northern Strait of Georgia. The Victoria relative sea-level curve was not complete during this exercise and not used in the modelling. They added significantly more ice in and adjacent to the Strait of Georgia and increased the thickness of all other ice elements by 1.3-1.4 times. The timing of deglaciation was adjusted so that ice persisted for longer and deglaciated more rapidly in the Strait of Georgia, matching the nearly synchronous range of age of repopulation of the Strait of Georgia (Fig. 3.4 from Chapter 3). Ice elements within the Strait of Georgia were divided into a finer grid to allow for a more finely tuned deglaciation history. The timing of the maximum extent of the ice sheet was not changed.

Figure 5.5 shows the predicted sea-level curves for the model presented by Gowan and James (2006) with a 300 km thick asthenosphere. With a sufficiently low viscosity ($<10^{18}$ Pa s), the response to deglaciation is almost instantaneous. With larger viscosities ($>10^{20}$ Pa s), the response is too slow to account for the rapid drop in sea level after deglaciation. At 10^{19} Pa s, the modeled response closely follows the observed response, and reaches close to the observed highstand positions for the central and northern Strait of Georgia. The development of this ice model did not include the Victoria sea-level curve, and so for Victoria there is still a 40 m discrepancy between the predicted and observed highstand position.

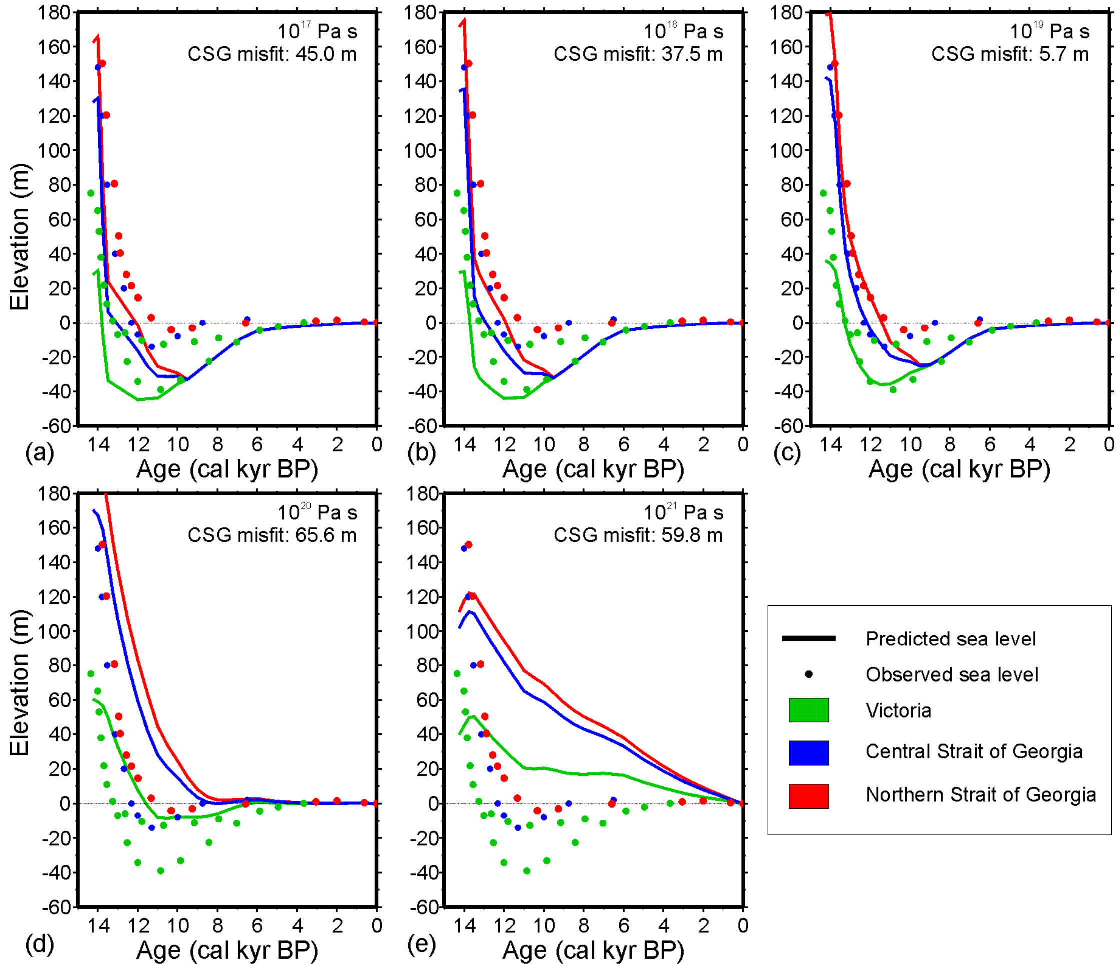

Figure 5.5. Comparison of predicted and observed sea levels in southwestern British Columbia using the ice model of Gowan and James (2006). The Earth models used to predict sea level have an elastic thickness of 60 km, asthenosphere thickness of 300 km and variable asthenosphere viscosity. RMS misfit of the central Strait of Georgia (CSG) sea-level curve is noted for each comparison. Asthenosphere viscosities are (a) 10^{17} Pa s, (b) 10^{18} Pa s, (c) 10^{19} Pa s, (d) 10^{20} Pa s and (e) 10^{21} Pa s.

Figure 5.6 shows the misfits of various earth models to the ice sheet history presented by Gowan and James (2006). Compared to the general 1.3 times load increase of the original model, the lowest misfit occurs with a viscosity that is about 0.6 orders of magnitude lower. Depending on the asthenosphere thickness, the optimal viscosity is between 10^{18} and $2.5x10^{19}$ Pa s. The best fits occur in the same viscosity range for the central and northern Strait of Georgia. The fit for the Victoria curve is not as good, though the fit follows the same asthenosphere viscosity-thickness relationship as the other two curves.

The Cordilleran ice sheet likely had a smooth topography that sloped gently down from the interior mountain belts to the ocean (Stumpf *et al.*, 2000). One way to test the validity of the ice sheet model is to determine the ice surface height. The ice surface is the sum of the elevation and model ice thickness, minus the isostatic depression due to the ice load. An earth model with a 300 km thick asthenosphere and a viscosity of 10^{19} Pa s produced the isostatic depression surface used for the ice surface calculation. Figure 5.7 shows the ice surface contour map for the model of Gowan and James (2006) at 16.8 cal kyr BP, when the Puget Lobe was at its maximum extent. The map shows that there is a 400-800 m depression of the ice surface within the Strait of Georgia. There is also a very steep dropoff of the ice surface on the west side of Vancouver Island. If the ice surface flowed smoothly over top of the Strait of Georgia and Vancouver Island from the Coast Mountains (*e.g.* Clague and James, 2002), then there should be a progressively decreasing ice surface height towards the southwest. Though this model fits the observed sea-level change in the central and northern Strait of Georgia, further changes appear to be needed to the ice model.

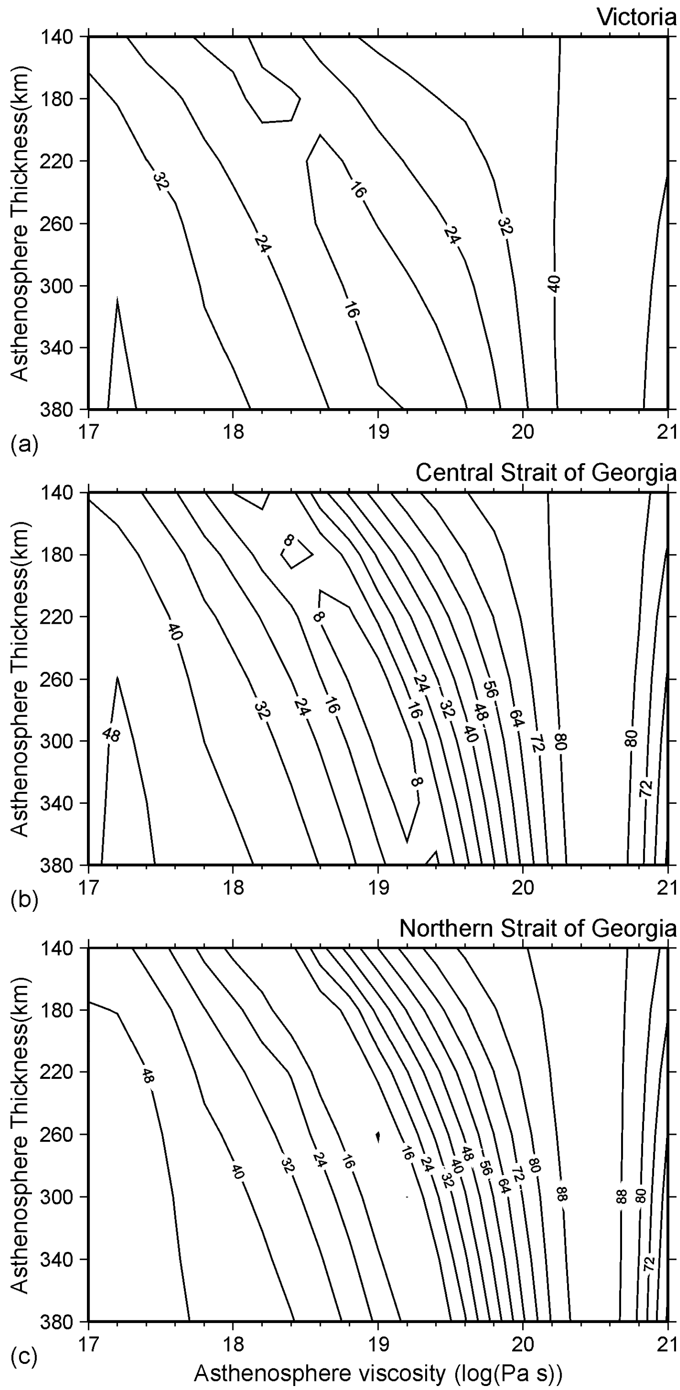

Figure 5.6. RMS misfit of predicted sea-level curves to the well constrained sea-level curves for Earth models with a 60 km elastic lithosphere and a range of asthenosphere thickness and viscosity values using the ice model of Gowan and James (2006). (a) Victoria, (b) central Strait of Georgia and (c) northern Strait of Georgia

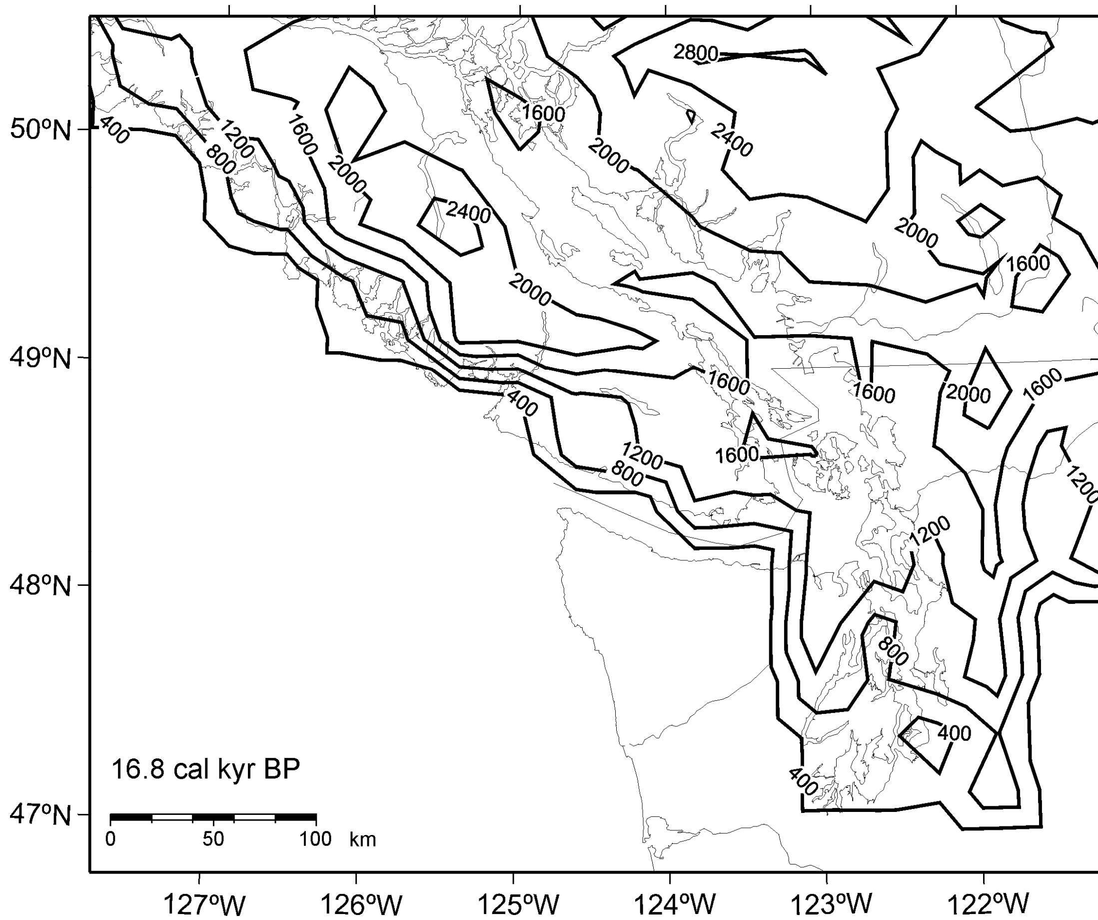

Figure 5.7. Ice surface elevation (in m) at the glacial maximum (16.8 cal kyr BP) in southwestern British Columbia for the ice model presented by Gowan and James (2006).

5.3 Review of ice sheet constraints

From above, the history and thickness of the ice sheet provides a strong control over the modeled sea-level response. The earth response to the original ice sheet model of James *et al.* (2000) and Clague and James (2002) were unable to match the observed postglacial sea levels in southwestern British Columbia regardless of the choice of earth model. Even with unrealistically high volumes of ice on Vancouver Island, the observed sea-level highstand in Victoria could not be matched with the modified ice sheet models. The isostatic response at a location due to the ice sheet has a strong dependence on the local ice thickness and history. This section provides an overview of the constraints on ice sheet history in southwestern British Columbia and northwestern Washington used for the development of a new ice model. Figures 5.8 and 5.9 show the location of areas described in the following sections. All chronologies are based on the assumption that deglaciation happened within 500 years of the oldest age constraints.

5.3.1 Puget Lobe

In the Puget Lowlands, the ice sheets reached their greatest extent sometime after 17.25 cal kyr BP and quickly retreated (Porter and Swanson, 1998; Swanson and Caffee, 2001). These authors suggest the Puget lobe reached its maximum extent about 16.9 cal kyr BP, and retreated to the northern limits of the Puget Sound about 400-500 years afterwards. This chronology is also based on older calibration methods, uncorrected or undercorrected basal freshwater and marine shell dates (see comments by Easterbrook, 2003). To determine how well constrained the ice sheet history is for the Puget Lobe, the dates used for ice sheet advance and retreat in Porter and Swanson (1998) and Swanson and Caffee (2001) were corrected for reservoir effects based on Hutchinson *et al.* (2004b) and re-calibrated (tables 3.1 and 3.2 chapter 3).

The advance history proposed by Porter and Swanson used dates from three locations (fig. 5.10). The recalibrated ages are up to several hundreds of years different than that determined by Porter and Swanson (1998). The dates from Seattle and Issaquah are from wood in an ice proximal delta. By using a 500 year limit on a linear advance, the Puget Lobe reached its maximum extent 16.2 to 16.7 cal kyr BP

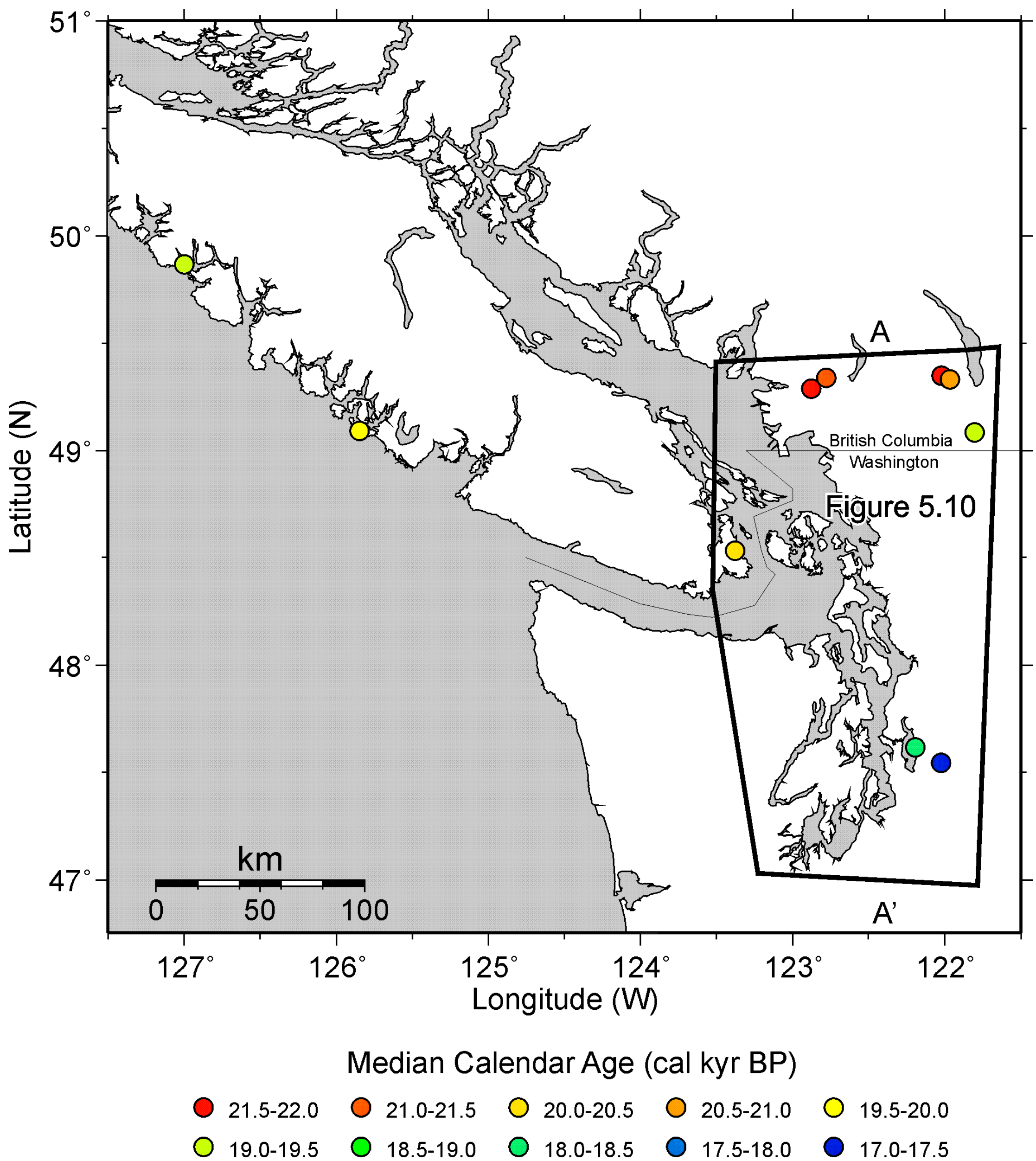

Figure 5.8. Distribution of radiocarbon dates that predate the Vashon advance. The location of the profile on Figure 5.10 is shown.

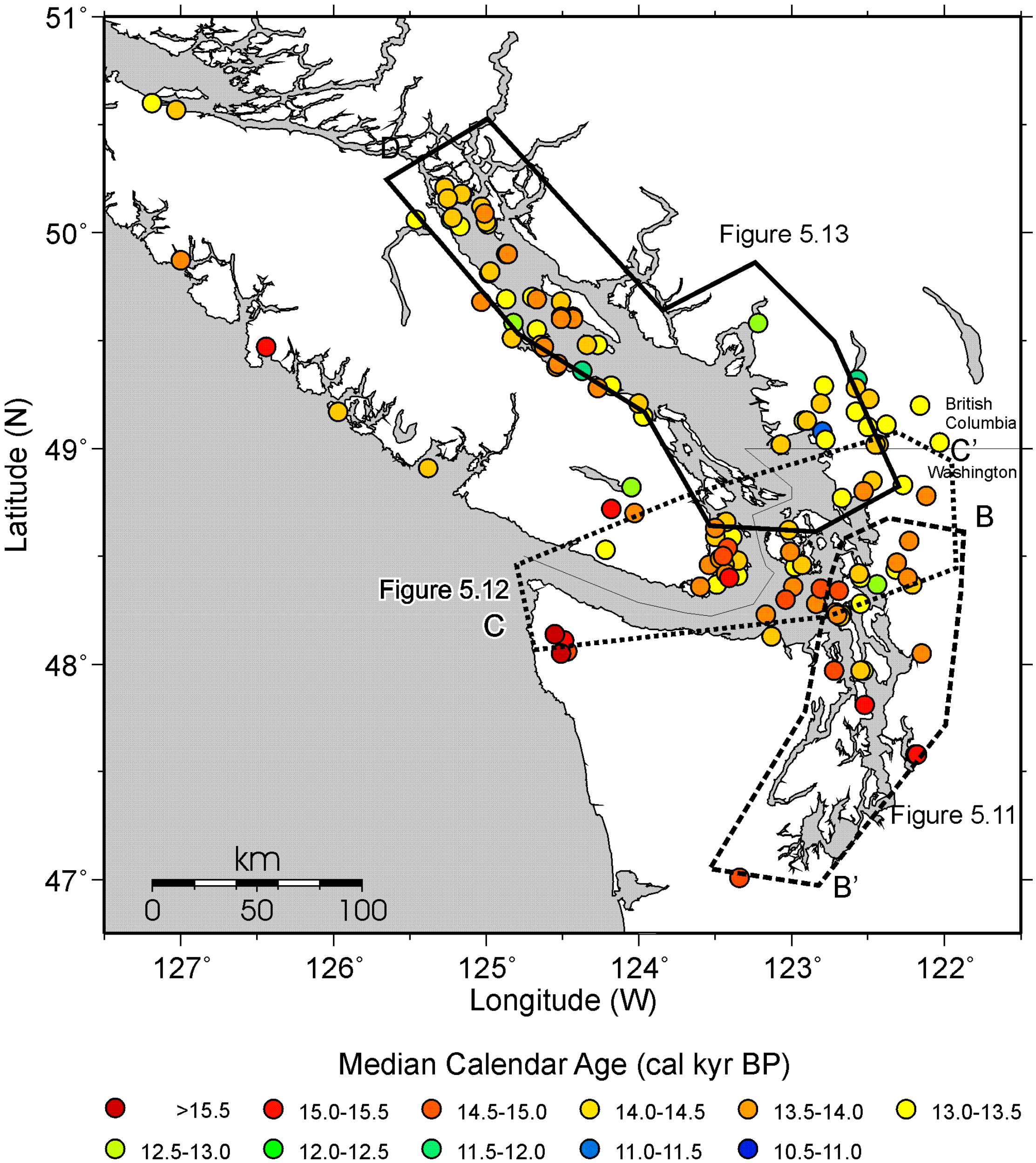

Figure 5.9. Distribution of radiocarbon dates that postdate the Vashon advance. The location of profiles on Figures 5.11, 5.12 and 5.13 are shown.

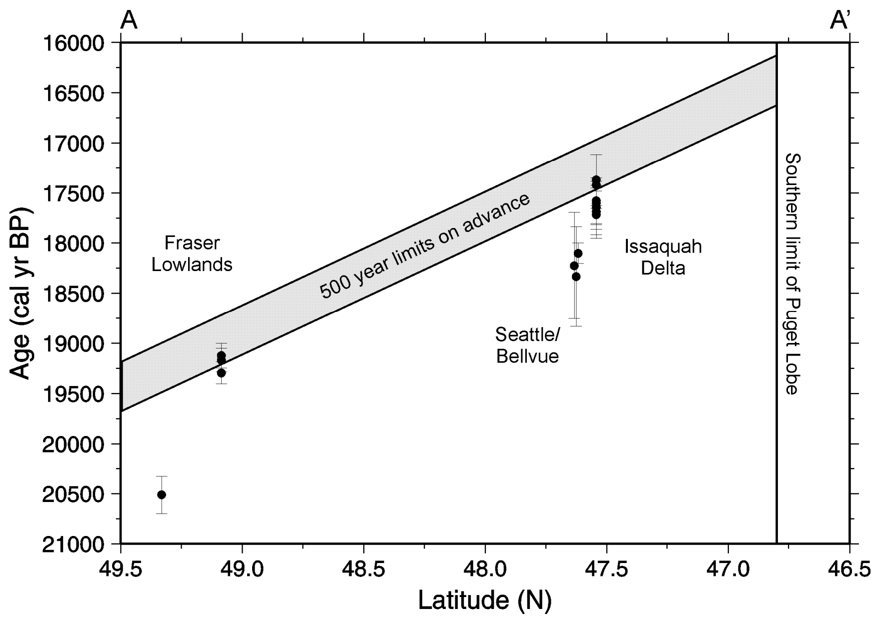

Figure 5.10. Constraints on the advance of the Puget Lobe. Calibrated dates are shown with 1 sigma limits. All samples are terrestrial dates.

(Fig. 5.10). The advance history is not well constrained by available radiocarbon dates, and given a likely complex advance history, this is only a rough estimate.

There are few dates that closely constrain the retreat of the Puget Lobe, as many samples have a large error (>250 years) and are not considered. The oldest sample is at Lake Carpenter with an age of about 15.5 cal kyr BP (Porter and Swanson, 1998; Fig. 5.11). The only samples that are over 15 cal kyr BP are dates from bulk basal freshwater material, which may not be the most reliable constraints given the uncertainty in the reservoir age of these samples. If these dates are not considered, all other dates are younger than 15 cal kyr BP and show no spatial pattern. Using the oldest marine shell samples as the limiting dates, deglaciation of the Puget Lobe began sometime between 15.7 and 15.2 cal kyr BP. Using a 500 year interval, the ice sheet retreated to the northern end of Whidbey Island between 15.3 and 14.8 cal kyr BP. Note that the basal dates still fall within this range at the one sigma confidence limits. The consequence of the new retreat history is that the dead ice terrain at Simpson Lake may have persisted for less than 700 years, which is 700 years less than suggested by Porter and Carson (1971). In the extreme situation, the dead ice terrain may have existed for only 100 years.

The retreat history of the Puget Lobe is also limited by the draining of glacial Lake Russell and Lake Bretz (Thorson, 1989). Lake Russell flowed southwards, and occupied the area south of about 48.5°. Once the Juan de Fuca lobe retreated eastward to the San Juan Islands, a spillway opened to allow water to flow northwards, and Lake Bretz formed. This means that the Puget Lobe did not fully retreat until after the Juan de Fuca Lobe had fully retreated.

Between 17.3 and 15 cal kyr BP, there are few reliably dated materials to determine the history of the Puget Lobe. This is the consequence of a combination of the area being covered in ice, glacial lakes, and having an environment that did not allow for the growth of organisms. The dead ice terrain at Simpson Lake (Porter and Carson, 1971) suggests that ice remained in Puget Sound until after 15 cal kyr BP. When basal freshwater samples are corrected for reservoir effects and samples that have 1σ errors larger than 250 years are excluded, the data suggests that retreat of the Puget Lobe did not begin until after 16 cal kyr BP. The best existing constraint is that the Juan de Fuca Lobe fully retreated before the Puget Lobe, which will be discussed in the next section.

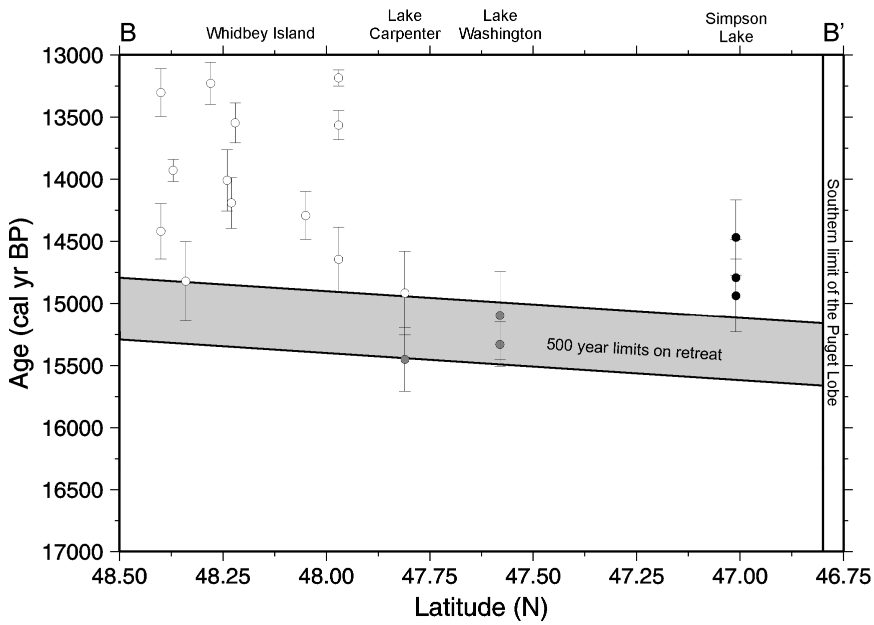

Figure 5.11. Constraints on the retreat of the Puget Lobe. Calibrated dates are shown with 1 sigma limits. Black symbols indicate terrestrial dates, grey symbols indicate a corrected basal freshwater sample, and white symbols indicate a corrected marine sample.

5.3.2 Glaciation of the Juan de Fuca Strait

At its maximum, the Cordilleran ice sheet covered the entire Juan de Fuca Strait, much of the Olympic Peninsula, and extended about 15-20 km into the northern limit of the Olympic Mountains (Bretz, 1920). Vashon till deposits are found as far south as Cape Johnson (47° 56' N, 124° 39' W) on the Olympic Peninsula. Granitic erratics found in the Northern Olympic Mountains at elevations up to 1500 m indicate that the ice was of considerable thickness in the Strait. Considering that the Strait is about 200 m deep (*i.e.* Mosher and Hewitt, 2004), there was at least 1700 m of ice in the eastern Juan de Fuca Strait.

The western extent of glaciation in Juan de Fuca Strait is difficult to discern due to high sedimentation rates found in the mouth of the strait (Herzer and Bornhold, 1982). Bretz (1920) proposed that it extended about 16-20 km offshore citing evidence of the western extent of Juan de Fuca ice on Vancouver Island. Strait-normal flutings along the coastal areas of Vancouver Island also indicate that the Juan de Fuca Strait was glaciated to a considerable distance beyond the Victoria area (Alley and Chatwin, 1979). Northwestward flowing ice in the strait likely coalesced with ice from Vancouver Island to produce the westernmost extension of the ice sheet (Herzer and Bornhold, 1982).

The Juan de Fuca Lobe of the Cordilleran Ice Sheet reached the western limit of the Strait, and covered part of the Olympic Peninsula and southern Vancouver Island (Heusser, 1973). Much of the northwestern Olympic Peninsula is covered with thick till derived from the Juan de Fuca Lobe, and it overlies till from Olympic alpine glaciers, indicating they coalesced. Glacial morainal sediments are found at the western mouth of the Juan de Fuca Strait, indicating that the entire Strait was covered in ice (Herzer and Bornhold, 1982). The ice sheets caused erosion at the mouth of the Juan de Fuca Strait, and deposited morainal features to depths of up to 400 m, indicating the ice sheet extended some distance onto the shelf.

The Juan de Fuca Lobe likely flowed from a Strait of Georgia source through much of its duration, and merged with ice from Vancouver Island. Ice flow indicators on southern Vancouver Island show a clear southwestward trend (Alley and Chatwin, 1979). When ice on Vancouver Island was thick enough, it likely flowed southwards over Juan de Fuca Strait onto the Olympic Peninsula. At its maximum extent, this southwestward flowing ice reached its maximum limit at the mapped boundary. After ice stopped flowing over Vancouver Island sometime after the glacial maximum, the Juan de Fuca Strait became dominated by northwestern ice flow from

Strait of Georgia sourced ice, and remained restricted to the Juan de Fuca Strait. This likely explains why dates from the northwestern Olympic Peninsula are significantly older than in the eastern Juan de Fuca Strait (Fig 5.12). Dammed glacial lakes on Vancouver Island indicate that the Juan de Fuca lobe remained at least 600 m above present sea level as ice was downwasting on the island (Alley and Chatwin, 1979).

The retreat of the Juan de Fuca Lobe is only constrained at the eastern end of the Strait. Herzer and Bornhold (1982), based on good preservation of meltwater troughs within the strait, suggest that the retreat of ice from the Juan de Fuca Strait was primarily by downwasting and not by calving. This indicates that the retreat of the lobe was likely slow. A shell from sediments in the eastern Juan de Fuca Strait south of Victoria dates to 15.04 cal kyr BP (Mosher and Hewitt, 2004). Other dates from the eastern Juan de Fuca Strait, Victoria region and San Juan Islands are younger than 14.8 cal kyr BP, indicating that the full retreat of the lobe did not happen until shortly after 15 cal kyr BP (Fig. 5.12).

The Juan de Fuca Lobe had to retreat far enough east to allow the draining of Lake Bretz northwards while ice still remained in the northern Puget Lowlands (Thorson, 1989). The age constraints indicate that the Juan de Fuca Lobe retreated almost contemporaneously with the Puget Lobe, though it reached the San Juan Islands slightly before the Puget Lobe did. This suggests that the Puget Lobe did not fully retreat until after 15 cal kyr BP.

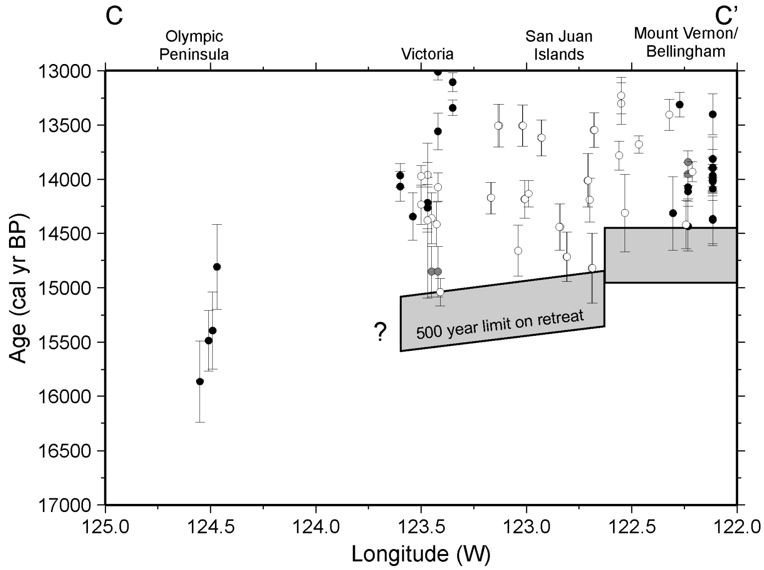

Figure 5.12. Constraints on the retreat of the Juan de Fuca Strait. Calibrated dates are shown with 1 sigma limits. Black symbols indicate terrestrial dates, grey symbols indicate a corrected basal freshwater sample, and white symbols indicate a corrected marine sample.

5.3.3 Strait of Georgia

After the Juan de Fuca and Puget Lobes retreated, ice retreat may have stalled. Flutings from Whidbey Island indicate that ice flow changed from a north-south direction to an east-west trend (Haugerud et al., 2003; Kovanen and Slaymaker, 2004). This indicates that after the Juan de Fuca Lobe retreated to the San Juan Islands, ice flow changed direction long enough to overprint the landscape to a certain extent. This probably represents a standstill or readvance of ice for a period of time. Furthermore, there appears to be a lag in the radiocarbon dates from the San Juan Islands and mainland Washington (Fig. 5.12). It appears that there is a 400 year delay between when the Juan de Fuca and Puget Lobes fully retreated and when the Strait of Georgia started to retreat. By 14.3 ka, the San Juan Islands were ice free (Fig. 5.13).

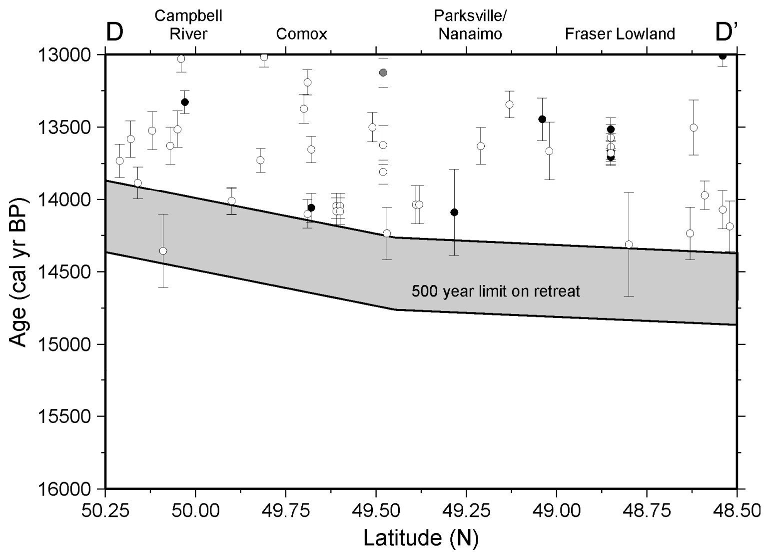

Figure 5.13. Constraints on the retreat of the Strait of Georgia. Calibrated dates are shown with 1 sigma limits. Black symbols indicate terrestrial dates, grey symbols indicate a corrected basal freshwater sample, and white symbols indicate a corrected marine sample.

When the Strait of Georgia deglaciated, it was primarily due to downwasting, evident from the thin ice proximal sediment layer conformably overlying till and the lack of iceberg scouring (Barrie and Conway, 2002; Guilbault *et al.*, 2003). There are few radiocarbon constraints between the southern Gulf Islands and Parksville, though they suggest that there is no spatial pattern of deglaciation along that part of the strait (Fig 5.13). The ice sheets retreated north of Parksville by 14.2 cal kyr BP. Other than one outlier, the radiocarbon dates suggest slowly progressive retreat of the ice sheets north of Parksville. By 13.8 cal kyr BP, the ice sheets retreated to the northern end of the Strait of Georgia. The data indicate it took about 500 years for the Strait to deglaciate.

5.3.4 Glaciation of Vancouver Island

Vancouver Island was extensively glaciated during the Vashon Stade (Clague, 1981; Howes, 1981a; 1981b). There are few dates pertaining to the advance of the ice sheets over Vancouver Island. Two wood samples from Tofino date between 19.8 and 19.4 cal kyr BP (Clague *et al.*, 1980; Al-Suwaidi *et al.*, 2006, Table 3.1 from Chapter 3). Three bone samples from a cave near Port Eliza date between 19.5 and 19.3 cal kyr BP (Al-Suwaidi *et al.*, 2006). These dates indicate that coastal Vancouver Island did not become glaciated until after that time.

There are few dates that constrain the deglacial history of northern and western Vancouver Island. A basal peat sample from Port Hardy has a corrected date of 15.4 cal kyr BP (Hebda, 1983), though the freshwater basal reservoir correction makes this uncertain. A wood sample from Hesquiat Harbour dates to 15.4 cal kyr BP (Blake, 1983), which is a better constraint due to the lack of reservoir age. This date indicates that the ice sheets retreated sufficiently by that time to allow forests to grow along the northwest coast of Vancouver Island. A mountain goat bone from Port Eliza dates to 14.3 cal kyr BP (Al-Suwadi *et al.*, 2006), further indicating that the ice sheets had retreated far enough back to support land mammals. Marine shells from northern and western Vancouver Island date between 14.0 and 13.1 corrected cal kyr BP (Howes, 1981b, Blake, 1982; Friele and Hutchinson, 1993).

Previous studies by Alley and Chatwin (1979) suggested that the ice sheets on southern Vancouver Island had melted down to an elevation of 400 m above current sea level by 15.5 cal kyr BP, based on a single date at Harris Creek (Table 3.2 chapter 3). Two other dates in that study taken at elevations greater than 700 m gave significantly younger dates of 14.1 and 13.1 cal kyr BP. It is possible that these samples require a reservoir correction to account for old carbon influx when the bogs formed (Hutchinson *et al.*, 2004b). When reservoir corrected, the age of the Harris

Creek sample is 13.9 cal kyr BP. Without the reservoir correction, this date is anomalously old compared to other samples in southern Vancouver Island.

Blaise *et al.* (1990) examined a core offshore of northern Vancouver Island to determine the sedimentation patterns during the Fraser glaciation. They found that there was a marked increase in sedimentation rate from before 17.6 to 14.7 ka, indicating a time period of extensive ice rafted debris deposits. This indicates that ice sheets were on the continental shelves during this time period. Due to the distance offshore of Vancouver Island, this record likely includes ice rafted debris from further north, and therefore may not record the exact timing of retreat from Vancouver Island.

Kienast and McKay (2001) and McKay *et al.* (2004) analyzed a core offshore western Vancouver Island to determine the sedimentation changes in the late glacial and deglacial times. These samples were recalibrated using the reservoir correction of Hutchinson *et al.* (2004b) for comparison with other data (Table 3.2 from Chapter 3). The authors state that the climate record interpreted from the core matches the climate record found in Greenland. A significant increase in terrestrial and marine carbon material in sediments happened between 14.7 to 13.5 cal kyr BP, coinciding with a large increase in sedimentation rate. Before that time, the terrestrial carbon accumulation was high, while the marine carbon accumulation was low. McKay *et al.* (2004) suggest that this increase in marine carbon accumulation indicates the start of deglaciation on Vancouver Island. In the preceding paragraphs, samples from coastal Vancouver Island suggest that deglaciation started by 15.4 cal kyr BP, and that Vancouver Island had an environment suitable for land mammals by

14.3 cal kyr BP. The timing of the high sedimentation rate suggests that early ice sheet retreat was restricted to coastal areas, and was not continuous. After 14.7 cal kyr BP, ice sheet retreat accelerated, and by 13.5 cal kyr BP, the ice sheets had retreated enough that little terrestrial material reached the offshore setting.

5.4 New glacio-isostatic adjustment results

5.4.1 Ice model

The creation of the new ice sheet model involved matching the history constrained by radiocarbon dates and sea level change, and creating a smooth ice sheet surface at the glacial maximum. The development of the model involved fitting each constraint progressively. The ice sheet model was first changed so that the earth response fit the Victoria sea level curve. Once this was done, the ice model was changed so that it produced a smooth surface that tapered off towards the edge of the ice sheet. This involved adjusting the models so that the sum of the land elevation and ice thickness, minus the isostatic depression due to the ice load produced a smooth surface. Finally, the model was refined to fit the radiocarbon constraints described in the previous section.

The finer grid areas allowed the ice thickness to reflect the high variability of the topography. Figure 5.14 shows the ice model at the glacial maximum in southwestern British Columbia and northwestern Washington. The grid is finer in the areas adjacent to where there are detailed sea level data. The ice is significantly thicker in the low lying areas than in mountainous regions. In some areas of the Strait of Georgia, there is in excess of 2500 m of ice. Figure 5.15 shows the ice surface produced by the combination of the elevation, isostatic depression and ice thickness. Where the grid is finer, the ice surface from the Coast Mountains to the Pacific Ocean is a gently sloping surface. Where the ice model is less fine, the ice surface is not as smooth, though it averages out to about 2400-2700 m, which is consistent with the model by Stumpf *et al.* (2000).

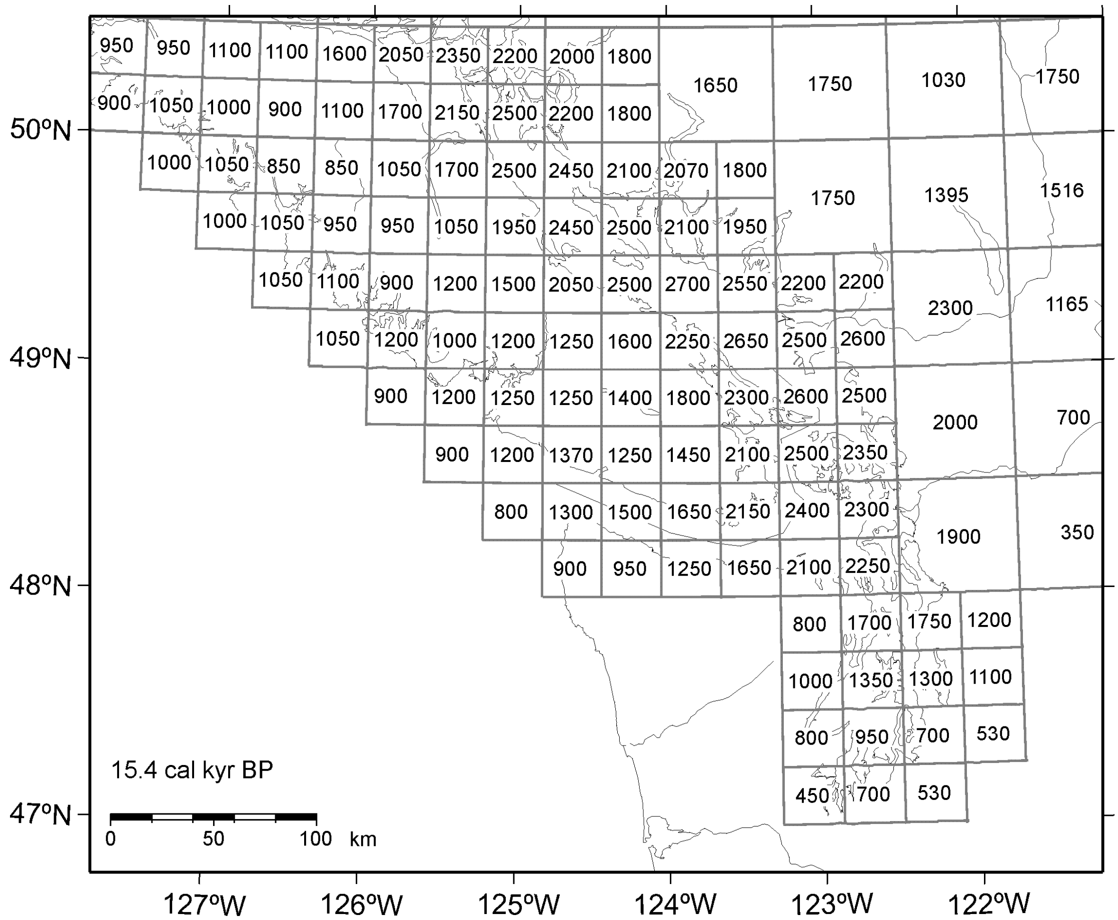

Figure 5.14. Ice sheet model for the southwestern Cordillera at the glacial maximum (15.4 cal kyr BP). The size of the elements is increased where there are few constraints on deglaciation and less impact on the study area.

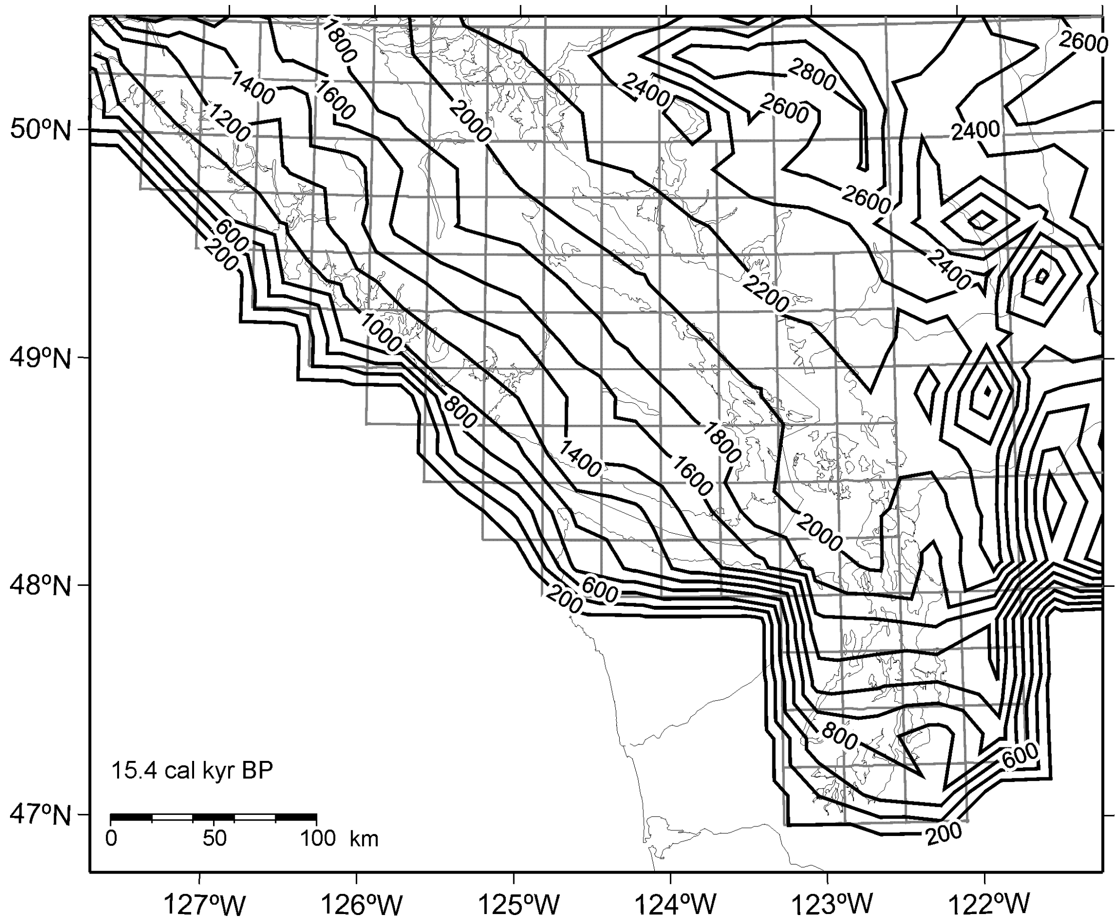

Figure 5.15. Ice surface elevation (in m) at the glacial maximum (15.4 cal kyr BP) in southwestern British Columbia. The grey outlines represent the ice model grid.

The final ice model consists of twenty time periods starting at 35 cal kyr BP, based on the chronologies discussed in the previous section. The glacial maximum is set to be between 17 and 15.4 cal kyr BP. The deglaciation of the Puget Lobe, Juan de Fuca Lobe and Strait of Georgia is split up into eight sections between 15.2 and 13.9 cal kyr BP to fit the constraints discussed earlier. Between 13.9 and 12.9 cal kyr BP, there is significant ice loss on all grid elements. Between 12.9 and 11.5 cal kyr BP, there is an increase of ice thickness on grid elements in mainland British Columbia to simulate readvances that happened during this time. Since the sea-level data from this time period are of low resolution, there was no attempt to simulate the various readvances and retreats discussed by Clague *et al.* (1997), Kovenan and Easterbrook (2002b) and Freile and Clague (2002). After 10.7 cal kyr BP, the ice model has no ice on any grid element to signify the return to present ice levels.

5.4.2 Earth modelling

Figure 5.16 shows the predicted sea-level curves for earth models with the optimal viscosity for various asthenosphere thicknesses. With the exception of the model with the thinnest asthenosphere, the response is almost identical. With an asthenospheric thickness of 140 km, the fit to the Victoria sea level curve is not as good as the thicker models. This is likely due to increasing sensitivity of the mantle below the asthenosphere as it gets thinner.

Figure 5.17 shows the fit of earth models with variable asthenospheric thickness and viscosity. The optimal viscosity values with thickness are slightly higher than what was found with the previous modelling attempts. The optimal viscosity lies between 3×10^{18} and 4×10^{19} Pa s. The results show that there is no apparent optimal asthenosphere thickness and viscosity pairing. This range is consistent with the results of postseismic deformation models of subduction zones around the world (Wang, 2007). For example, in the Chilean subduction zone, the viscosity of the continental mantle is 2.5×10^{19} Pa s (Hu *et al.*, 2004). Overall, the optimal misfit range is tighter in the central and northern Strait of Georgia sea-level curves than the Victoria sea-level curve. The Victoria sea-level curve fits slightly better with a thicker asthenosphere.

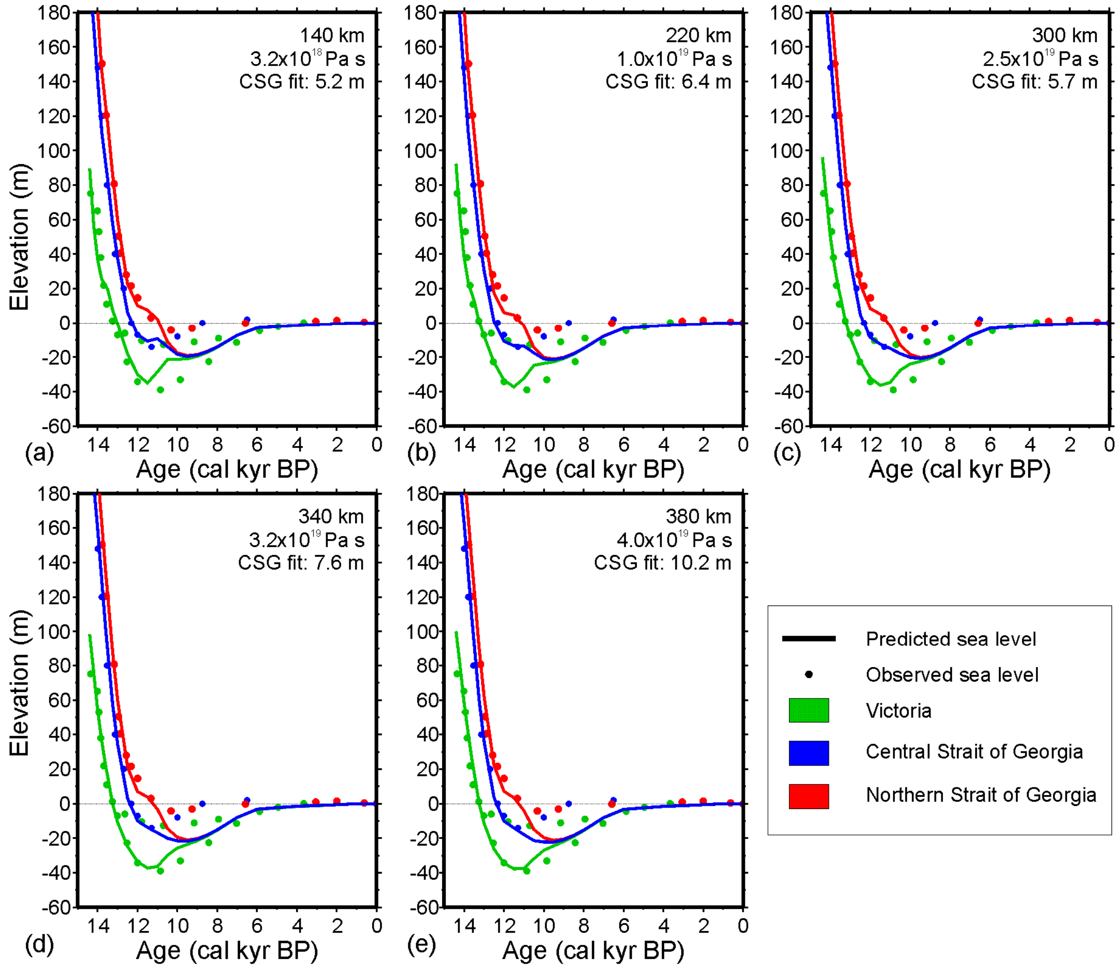

Figure 5.16. Comparison of predicted and observed sea levels in southwestern British Columbia using the final ice model. RMS fit of the central Strait of Georgia (CSG) sea-level curve is noted for each comparison. The predicted sea levels are determined with asthenospheric thickness and viscosity values of (a) 140 km and 3.2×10^{18} Pa s, (b) 220 km and 1.0×10^{19} Pa s, (c) 300 km and 2.5×10^{19}, (d) 340 km and 3.2×10^{19}, (e) 380 km and 4.0×10^{19}.

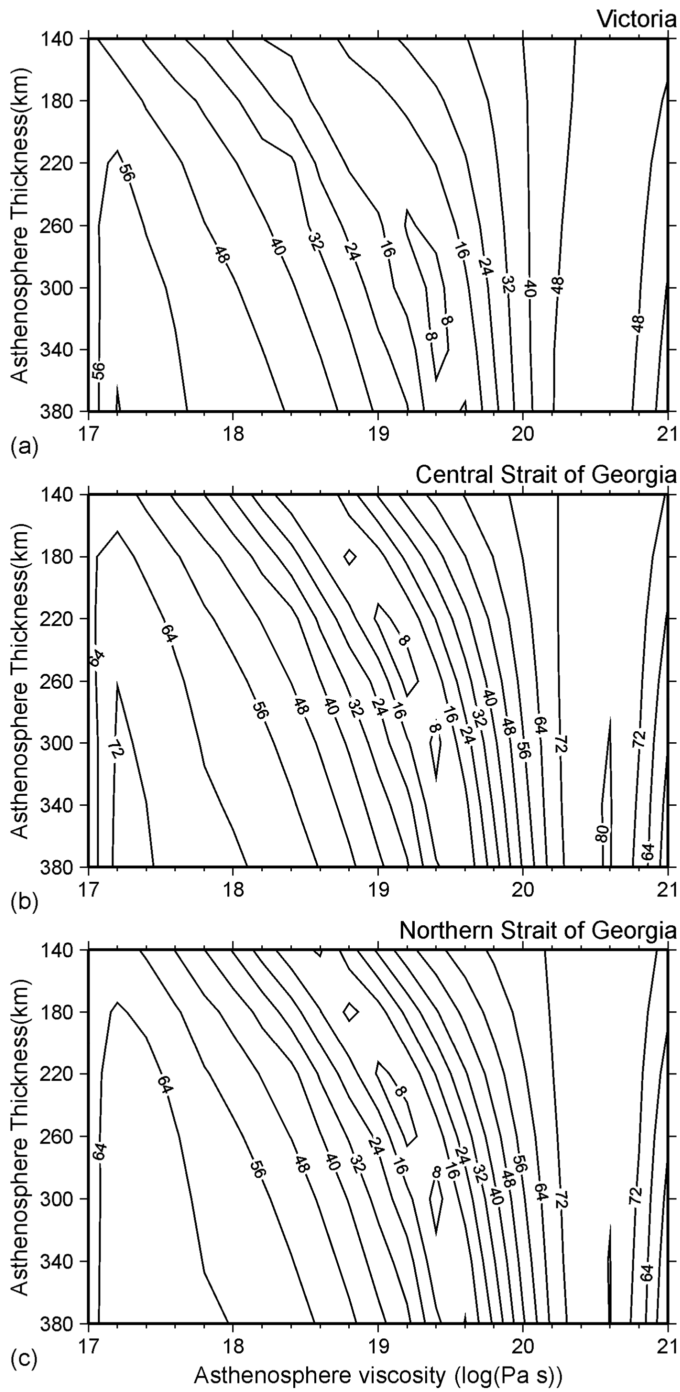

Figure 5.17. RMS misfit of predicted sea-level curves to the well constrained sea-level curves for Earth models with a 60 km elastic lithosphere and a range of asthenosphere thickness and viscosity values using the final ice model. (a) Victoria, (b) central Strait of Georgia and (c) northern Strait of Georgia with the final ice sheet model.

5.4.3 Assessment of fit

To get a better assessment of the fit, the radiocarbon constraints are plotted against the predicted relative sea-level (Fig 5.18). The model used to predict sea level has a lithosphere thickness of 60 km, asthenosphere thickness of 300 km and asthenosphere viscosity of $2.5x10^{19}$ Pa s. The sea level highstand positions fit well with the timing of deglaciation in the ice model. The modeled sea-level fall is consistent with the radiocarbon dates from the highstand positions to present sea level in all cases.

After 12 cal kyr BP, there are few constraints in the sea-level position at the three sites. The predicted Victoria sea level curve favours the maximum lowstand scenario, and reaches a position of -35 m. Sea level comes within 4 m of present levels at about 6 cal kyr BP, which is consistent with the observations. In the central Strait of Georgia, the modeled sea level drops to -20 m before rising to within 2 m of present by 6 cal kyr BP. The radiocarbon dates suggest that sea level rose to with 2 m of present by 8 cal kyr BP. The modeled sea-level curve for the northern Strait of Georgia violates none of the radiocarbon constraints, but the lowstand position of -20 m is probably too low. According to James *et al.* (2005), the maximum possible lowstand position for the northern Strait of Georgia is -8 m.

The sea-level modelling was successful in fitting the tightly constrained late glacial sea-level fall in southwestern British Columbia. The modelling also closely fits the mid-Holocene sea level rise in the Victoria sea-level curve. This indicates that the southwest Cordilleran ice sheet and simple spherically symmetric earth

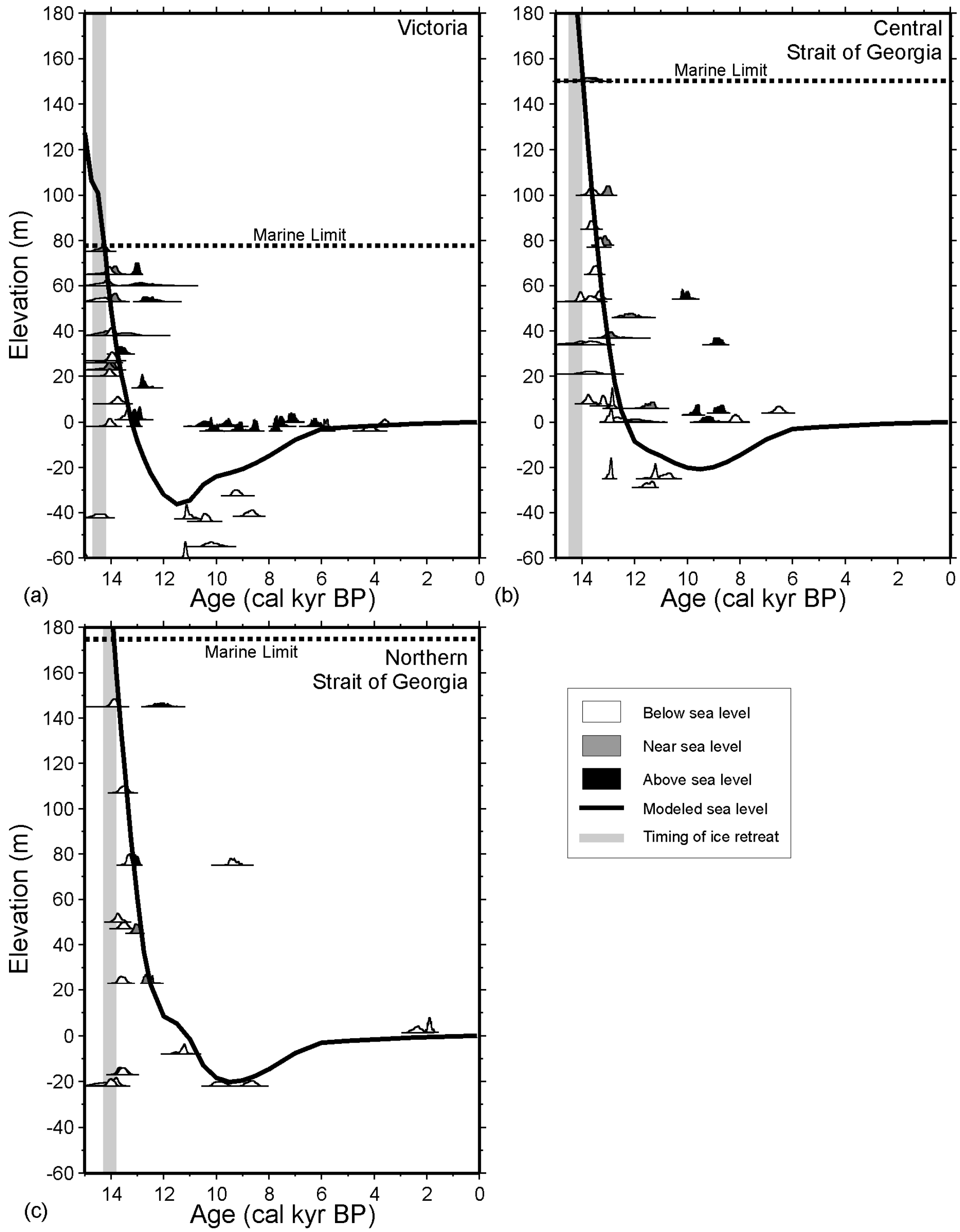

Figure 5.18. Predicted sea level curves using the final ice sheet model and radiocarbon constraints on sea level. The Earth model used to predict sea level has a lithosphere thickness of 60 km, asthenosphere thickness of 300 km and asthenosphere viscosity of 2.5×10^{19} Pa s. The symbols represent the probability distribution of the age of the sample scaled by 1000. (a) Victoria, (b) central Strait of Georgia and (c) northern Strait of Georgia.

models work well in explaining the crustal motions in the late Pleistocene. However, the magnitude of maximum sea-level fall and the sea level rise from early Holocene to present in the central and northern Strait of Georgia was not successfully modeled. This might be due to the lack of a far-field ice sheet in the ice model. Another possibility is that the assumption that the Cordilleran ice sheet returned to roughly present levels by 10.7 ka is not correct. There also may be problems with assuming a constant lithospheric thickness and mantle viscosity structure throughout the study area. There may be complex changes in rheology due to the variability in curvature of the subduction zone. It is also possible that the VM2 viscosity model below the asthenosphere might be not be appropriate. Though it is not yet possible to investigate lateral variability in rheology structure, the other issues are examined in the following sections.

5.4.4 Viscosity below the asthenosphere

Figure 5.19 shows the result of changing the viscosity of the mantle below the asthenosphere. In all cases, the asthenosphere thickness was set to 300 km, and the asthenosphere viscosity was 2.5×10^{19} Pa s. The viscosity of the mantle had the same magnitude of viscosity contrasts as VM2, but was increased by the factor indicated. The results show that increasing the viscosity of the mantle by 4.0 times produces the largest difference in the calculated sea-level curves, corresponding to a transitional zone viscosity of 1.6×10^{21} Pa s. Increasing the viscosity by this amount reduced the lowstand position by 5-7 m. The effect on the calculated sea level immediately following deglaciation is negligible. Increasing the viscosity more than this has virtually no effect on the calculated sea level. Decreasing the transitional zone viscosity to 2.5x10^{20} Pa s had a somewhat more profound effect, increasing the lowstand position by about 5 m. From visual analysis, the response of the Earth is relatively insensitive to the choice of viscosity below the asthenosphere, though it has a slight impact on the highstand and lowstand positions.

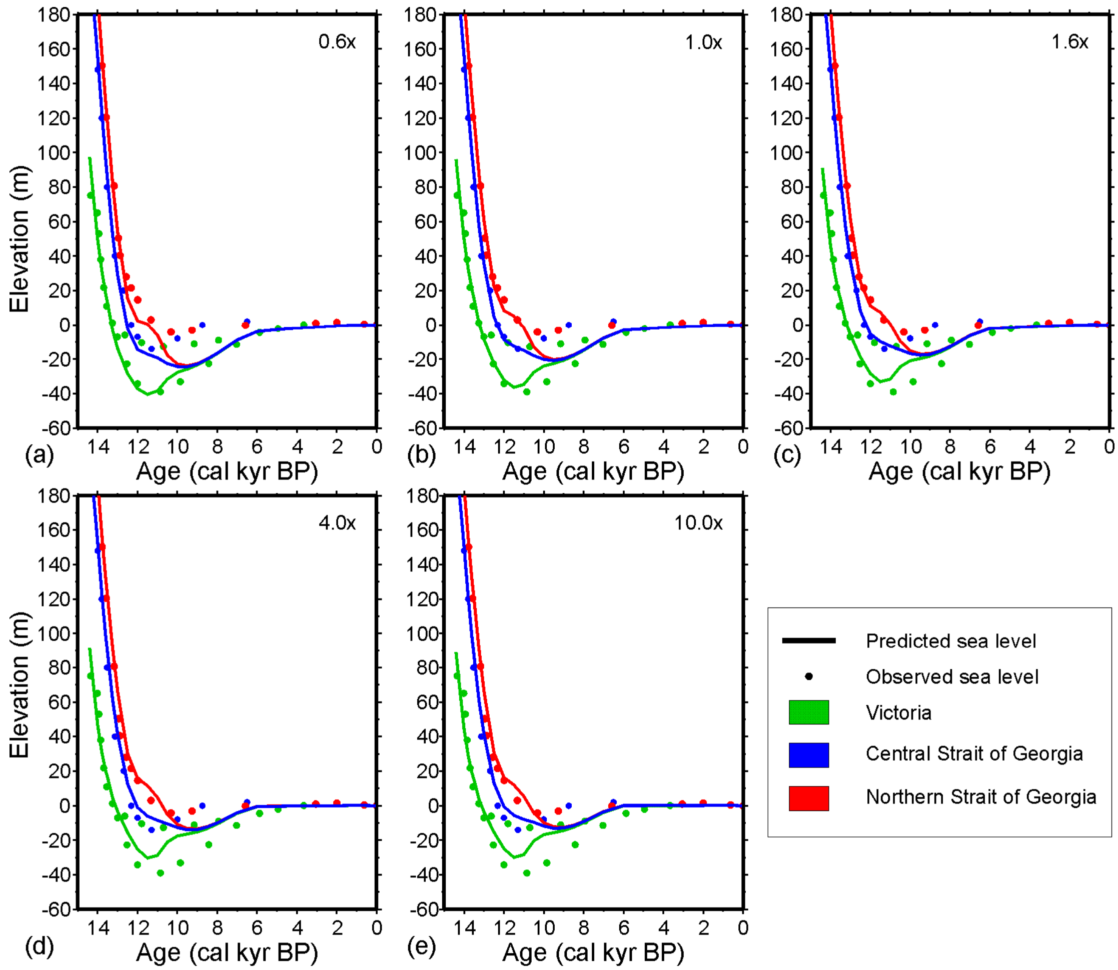

Figure 5.19. Modeled sea level curves for earth models with a lithosphere thickness of 60 km, asthenosphere thickness of 300 km, and asthenosphere viscosity of 2.5x10^{19} Pa s. The viscosity below the asthenosphere is increased from the VM2 model by a factor of (a) 0.6, (b) 1.0 (no change), (c) 1.6, (d) 4.0 and (e) 10.0.

5.4.5 Far-field effects

The Laurentide ice sheet occupied most of continental Canada and the northern United States, reached its maximum extent between 19 and 22 cal kyr BP and was greater than 3000 m thick over much of its area (Dyke *et al.*, 2002). Retreat of the Laurentide ice sheet from its maximum extent began by 14 kyr BP (16.4-16.9 cal kyr BP), and thinning may have started as early as 16.5 kyr BP (19.5-19.8 cal kyr BP). This indicates that by the time the Cordilleran ice sheet reached its maximum, the Laurentide ice sheet was already retreating. Clague and James (2002) calculated the response of the farfield signal and suggested it was very small due to the low viscosity of the mantle and thin lithosphere. The rheological structure changes significantly east of the Cordillera. For example, the effective elastic thickness determined from gravity and heat flow data varies between 20 and 60 km in the Cordillera and Interior Plains region, and thickens to over 120 km in the Precambrian cratonic areas (Flück *et al.*, 2003).

Figure 5.20 shows the response of the ICE-3G ice model (Tushingham and Peltier, 1991) with the southwestern Cordilleran portion removed. Since lateral variations in viscosity structure cannot be taken into account, the plot shows the response of a uniform VM2 model and a representative viscosity model from southwestern British Columbia with an asthenopheric thickness of 300 km and viscosity of 2.5×10^{19} Pa s. The VM2 model produces 35-48 m of uplift at 14 ka. There is about 13 m more uplift in Victoria than in the northern Strait of Georgia. The difference in response between the different areas becomes negligible in mid-Holocene times. With a thinner lithosphere and lower asthenosphere viscosity, the

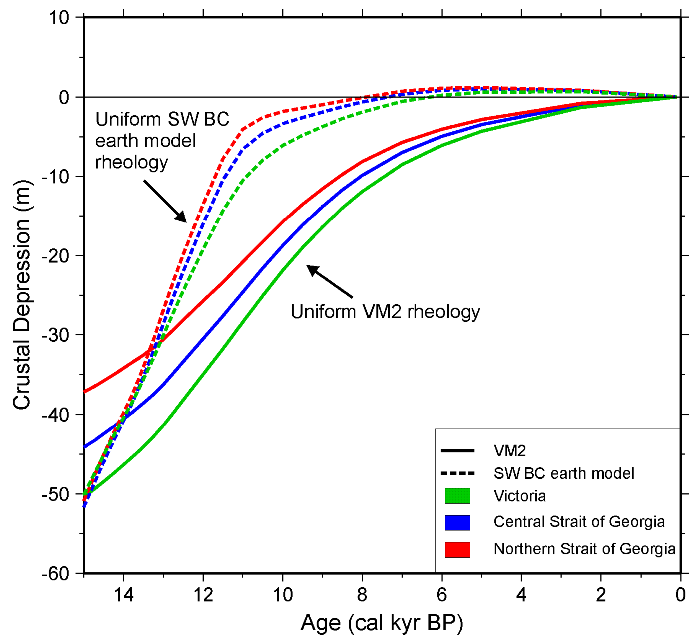

Figure 5.20. Modeled response of ICE-3G with the southwestern British Columbia elements masked out. The response of a uniform earth with a lithosphere thickness of 60 km, asthenosphere thickness of 300 km, and asthenosphere viscosity of 2.5×10^{19} Pa s (SW-BC) and a lithosphere thickness of 120 km, asthenosphere thickness of 320 km and asthenosphere viscosity of 4×10^{20} Pa s (VM2) are shown.

response is more uniform. There is still a significant forebulge of 40 m at 14 cal kyr BP. This quickly decays to less than 10 m by the start of the Holocene.

Either of the preceding cases produces a significant forebulge in late glacial times, which would significantly lower sea-level in southwestern British Columbia. If there was a significant forebulge, then in late Pleistocene and early Holocene times, there should be evidence of sea levels dropping below eustatic sea level for an extended period of time. This is not the case in the central and northern Strait of Georgia, and unlikely the case for Victoria from the compiled radiocarbon constraints. Significantly more ice in the southwestern Cordillera ice sheet would be needed to account for the observed high sea levels if there was a large forebulge. This is not realistic given the geological constraints on ice surface elevation.

There are few studies that look into the role of mantle heterogeneities in the postglacial response. Wu *et al*. (2005) and Wang and Wu (2006) found that lateral variations in the lithosphere and upper mantle can have a significant impact on the calculated earth response. In areas where the lithosphere is thinner and the mantle viscosity is lower, the late glacial response was up to several 10s of m different from using a uniform VM2 earth model. For instance, in Newfoundland, a laterally heterogeneous earth model produced a calculated sea level that was about 50 m higher than with the VM2 model. Having a thinner lithosphere and a lower mantle viscosity at the margins the Laurentide ice sheet appears to dampen the forebulge effects. Therefore, the assumption that the far-field ice sheets has only a minimal effect on Earth deformation in southwestern British Columbia is probably sound.

5.4.6 Slower deglaciation

The timing of deglaciation of the Cordilleran ice sheet away from coastal areas is based on several widely distributed samples that date earlier than 9000 yr BP (10 cal kyr BP) (Clague, 1980). Hetherington and Barrie (2004) noted there were areas in the Queen Charlotte basin where significant crustal depression persisted well into the Holocene, similar to that observed in the central and northern Strait of Georgia. One possible cause for continued crustal depression is that stagnant ice persisted in the central part of the Cordillera in the early Holocene. Figure 5.21 shows the results of having ice persist north of 51° well into the Holocene. In both cases shown, up to 1000 m of ice remains in central British Columbia. In the first case, ice persists until 4000 cal yr BP. There is negligible response at Victoria,

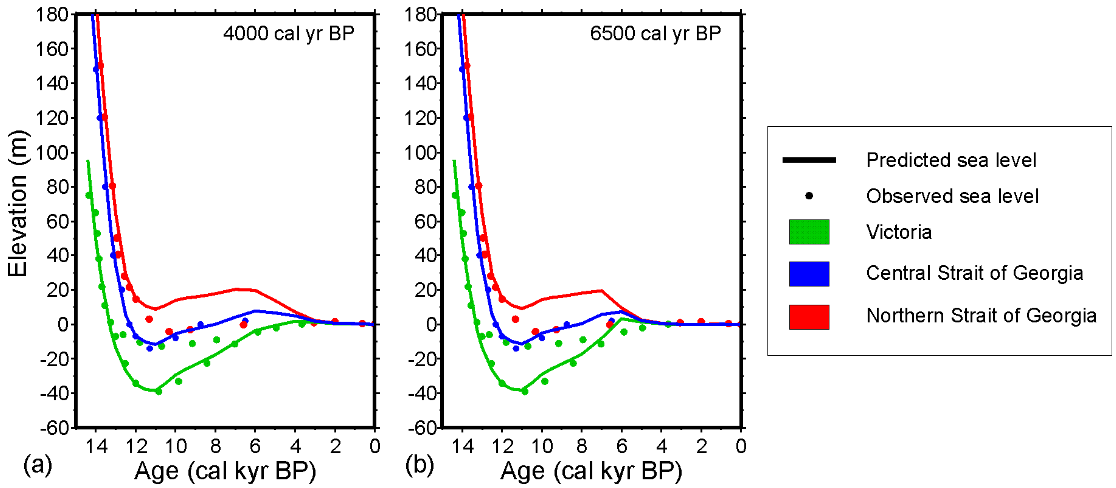

Figure 5.21. Modeled sea level for scenarios where the full deglaciation of central British Columbia is delayed to (a) 4000 cal yr BP and (b) 6500 cal yr BP.

though the sea level reaches up to 8-10 m above present in the central Strait of Georgia. This case is unlikely, as sea level remained below 6 m throughout the Holocene in the central Strait of Georgia (Hutchinson *et al.*, 2004a). Given the number of radiocarbon constraints in central British Columbia (*i.e.* Clague, 1980; Dyke, 2004), it seems unlikely that stagnant ice persisted until 4000 cal yr BP. The second case shows the predicted sea level reaching 0 m elevation at 6500 cal yr BP. Rapid deglaciation causes the mantle to flow quickly towards the rebounding area, and causes up to 10 m of additional depression in the Victoria area at 6000 cal yr BP.

From these results, it seems that delayed deglaciation of the Cordilleran ice sheet in central British Columbia might be responsible for some of the differences in the observed Holocene sea levels in the study area. It is unlikely that it is fully responsible for the observed differences, as it requires significant amounts of ice to remain in central British Columbia throughout the first half of the Holocene, which contradicts geological observations (Hetherington and Barrie, 2004; Dyke, 2004).

The observed forebulge indicates the lithospheric thickness in the Queen Charlotte region is very thin, possibly a low as 10-20 km. It is possible that a complex response due to differing rheology structure between the Queen Charlotte Islands area and the Cascadia subduction zone may be responsible for spatial difference in Holocene sea level within the Strait of Georgia.

5.4.7 Current crustal uplift

Determining the uplift rates due to incomplete postglacial rebound is important in making accurate assessments of contemporary tectonic motions (James *et al.*, 2000). Figure 5.22 shows the uplift rates due to incomplete glacial rebound of the Cordilleran ice sheet using an asthenospheric thickness and viscosity of 300 km and 2.5×10^{19} Pa s respectively. The results show that there is a present uplift rate of about 0.09-0.1 mm/yr. Measured contemporary uplift rates from GPS data for the central Strait of Georgia and Victoria area range between 1 and 2 mm yr^{-1}, though these estimates have a large error range (Mazzotti *et al.*, 2003). This means that incomplete rebound from the Cordilleran ice sheet might make up 5-10% of the measured uplift rates. Ultimately, the calculated uplift rate is so small that it probably cannot be differentiated from other sources, such as tectonism.

Due to the problem with lateral changes in rheology, predicting the uplift rates due to far-field ice sheets is difficult. Figure 5.22 shows the results of the contemporary uplift rates for the masked ICE-3G model using a asthenospheric thickness and viscosity of 300 km and 2.5×10^{19} Pa s, as well as the VM2 Earth model. These results are combined with uplift rates from the southwest BC ice model. Using a uniform, thin lithosphere and mantle viscosity representative of southwestern

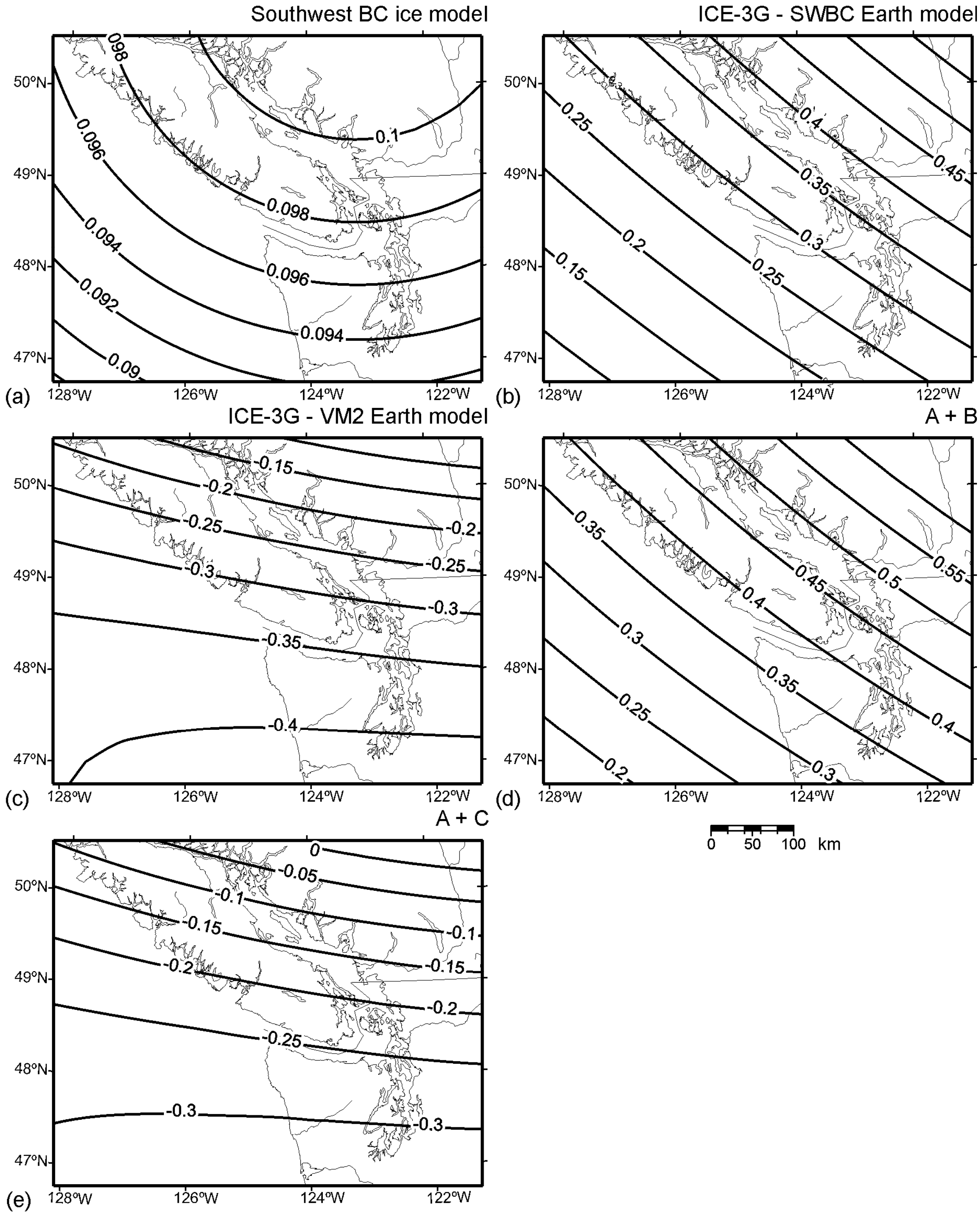

Figure 5.22. Uplift rates (mm yr^{-1}) calculated for the (a) southwestern Cordilleran ice sheet model with a lithosphere thickness of 60 km, asthenosphere thickness of 300 km, and asthenosphere viscosity of 2.5×10^{19} Pa s, (b) masked ICE-3G model with the same viscosity profile and (c) masked ICE-3G model with the VM2 viscosity model, (d) combination of a and b, (e) combination of a and c.

British Columbia causes an uplift rate of 0.35-0.5 mm yr^{-1} in eastern Vancouver Island. This is likely due to mantle flow towards the former center of the Laurentide ice sheet. As noted in figure 5.20, the far-field ice sheet causes a forebulge, which still exists at present if the VM2 earth model is used. In this case, there is a 0.05-0.25 mm yr^{-1} subsidence rate in eastern Vancouver Island. In reality, the true vertical motion due to far-field ice sheets is likely intermediate between -0.25 and 0.5 mm yr^{-1}. Three-dimensional earth modelling would be required to resolve this issue.

5.5 Paleo-shorelines

Large areas of the continental shelf north of Vancouver Island were exposed during the Late Pleistocene and early Holocene (Hetherington *et al.*, 2003, 2004; Hetherington and Barrie, 2004), though there are fewer studies to determine whether or not this also happened in southwestern British Columbia. In southwestern Vancouver Island, sea level dropped to 45-50 m below present in the late Pleistoscene (R. Enkin, pers comms, 2007). If the continental shelf was exposed during the Fraser Glaciation, it would serve as a route for the peopling of the Americas (*i.e.* Dixon, 2003; Hetherington *et al.*, 2003).

Figure 5.23 shows the position of sea level relative to present. The relative sea level is compared to the topography of ETOPO5 (NOAA, 1988). At 16.0 cal kyr BP, ice sheets covered most of southwestern British Columbia. Because of depression caused by the ice sheets, the continental shelf did not become exposed during the glacial maximum. By 14.5 cal kyr BP, much of the west coast of

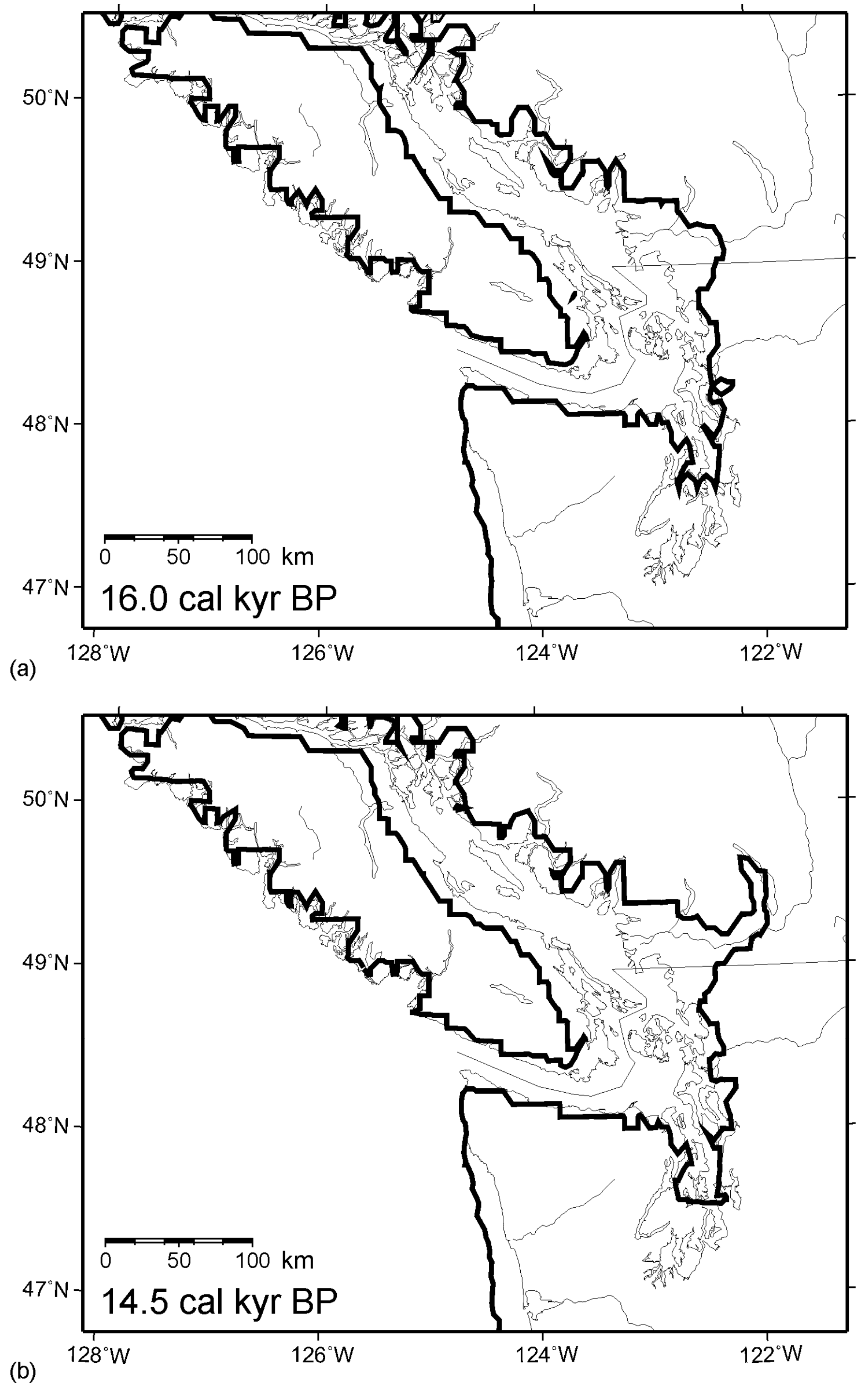

Figure 5.23. Predicted paleo-shoreline locations using the southwestern Cordilleran ice sheet model and an Earth model with a lithosphere thickness of 60 km, asthenosphere thickness of 300 km, and asthenosphere viscosity of $2.5\text{x}10^{19}$ Pa s. Dark line indicates shoreline position. (a) 16.0 cal kyr BP, (b) 14.5 cal kyr BP, (c) 13.5 cal kyr BP and (d) 11.5 cal kyr BP.

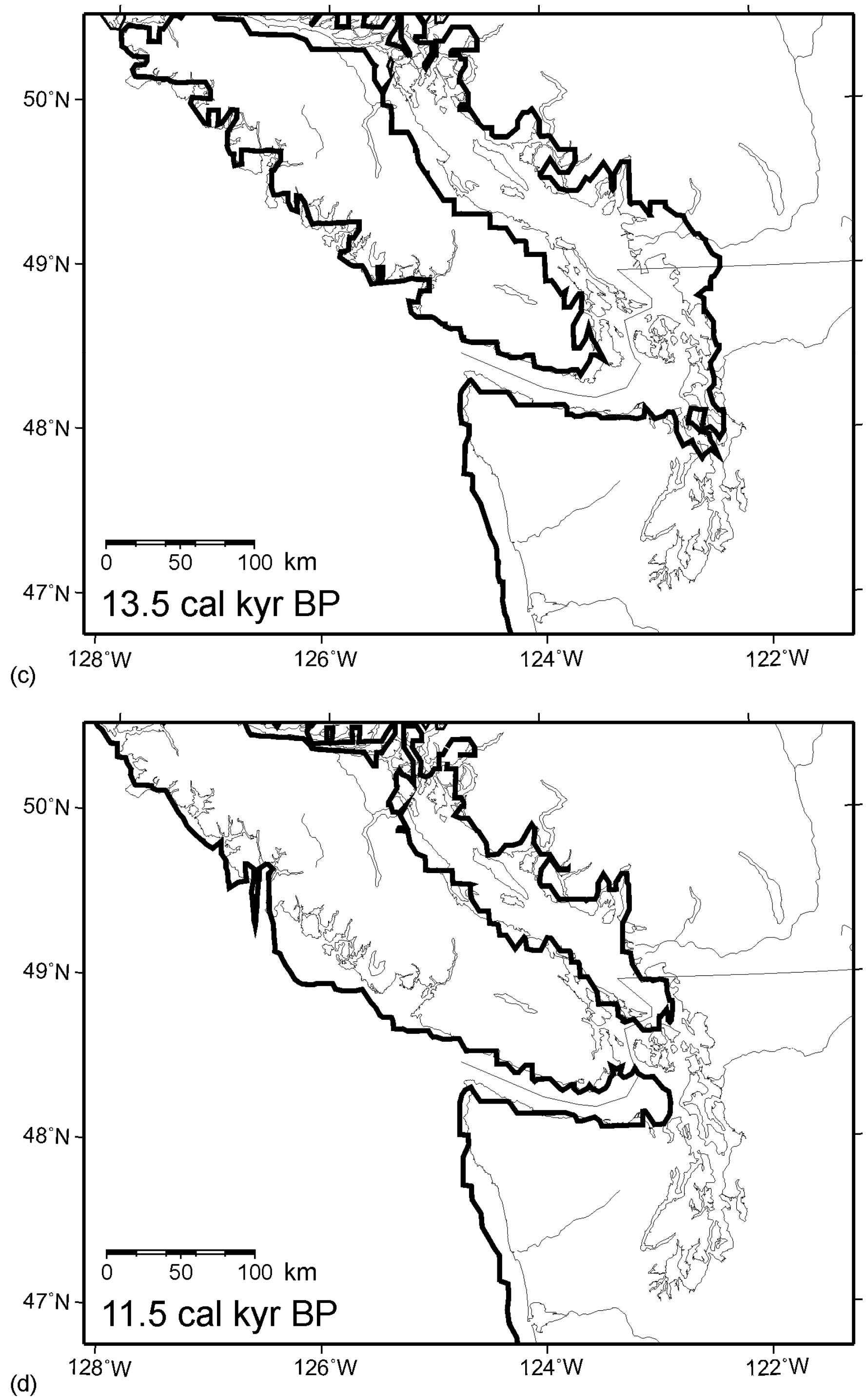

Figure 5.23. Predicted paleo-shoreline locations (continued).

Vancouver Island and the Juan de Fuca Strait were deglaciated. At this time, the coast was still near present. By 13.5 cal kyr BP the entire Strait of Georgia was deglaciated. Sea level in the Strait of Georgia was higher than present, causing the Strait to be much more extensive than present. Western Vancouver Island shoreline was still near present, indicating that the shelf was still depressed. By 11.5 cal kyr BP, large areas of the continental shelf were exposed on western Vancouver Island. This indicates that glacio-isostatic adjustment was almost complete by this time and the shelf was exposed due to low eustatic sea level.

People migrated to the Americas by about 12.5 kyr BP (14.3-14.8 cal kyr BP), indicated by cultural deposits found in Monte Verde, Chile (Dillehay *et al.*, 1982). Ice free conditions existed in central coastal areas of British Columbia as early as 13 790 ± 150 yr BP (16.2-16.7 cal kyr BP, TO-3738), which lends support to the hypothesis of a west coast migration route for people to the Americas (Hetherington *et al.*, 2003). However, from modelling of sea level on the west coast of Vancouver Island, relative sea level was high enough that the entire shelf remained submerged during the Fraser maximum. Therefore, the coastal route became available only after coastal areas became deglaciated. The oldest reliable date from coastal Vancouver Island is a wood fragment, which has an age of 15.1-15.5 cal kyr BP (Blake, 1983; Table 3.2 in Chapter 3). This date is likely a local maximum, and the entire west coast probably did not become deglaciated until after 15.0 cal kyr BP. A mountain goat bone dates to 14.1-14.4 cal kyr, indicating that ice retreated far enough away from the coast to allow animals to populate western Vancouver Island (Al-Suwadi et al., 2006). Though nunataks near the coast may have supported life during throughout the Fraser glaciation (Hebda *et al.*, 1997), they probably remained inaccessible to migrating people during the Fraser maximum. The west coast migration route likely remained unavailable while the Cordilleran ice sheet reached the Pacific Ocean, an interval that lasted between 15-19 cal kyr BP. Since the younger date only allows a few hundred years for people to reach the Monte Verde site, it is more likely that people migrated before the Fraser maximum if the coastal route is the way that people first entered the Americas.

5.6 Summary

A new ice model that fits geological, radiocarbon, and relative sea-level observations in southwestern British Columbia is presented here. The modelling found that there is no unique asthenospheric mantle viscosity to explain the relative sea-level data. The mantle viscosity that best fits the observations depends on the asthenospheric thickness. The optimal viscosity values are between $3x10^{18}$ and $4x10^{19}$ Pa s over a range of thickness from 180-380 km. This viscosity is 1-2 orders of magnitude lower than the asthenosphere in the VM2 model (Peltier, 1998). A thicker asthenosphere (>240 km) with a larger viscosity provides a better fit to the Victoria sea-level curve, though the central and northern Strait of Georgia fit well regardless of asthenosphere thickness. The response is almost completely insensitive to the mantle viscosity below the asthenosphere.

Several issues remain unresolved. The effect of far-field ice sheets is unknown at this point, due to the vastly different earth structure of southwestern British Columbia compared to continental North America, though it is expected to be small. The observed sea-level change during the early Holocene is not fit regardless of ice sheet or earth model. This is likely related to a combination of changes in earth structure north of the Cascadia subduction zone and slower deglaciation of central British Columbia. Current vertical motion due to glacio-isostatic adjustment is less than 1 mm yr^{-1}, though this value may be different due to the aforementioned problems.

Modelling of paleo-shorelines indicates that the continental shelf off Vancouver Island remained submerged during the Fraser Maximum. The shoreline remained near present until after 13.5 cal kyr BP. By 11.5 cal kyr BP, large areas of the shelf became exposed as glacio-isostatic adjustment completed. The implication of this is that any coastal migration route for the peopling of the Americas was cut off during the Fraser maximum when the ice sheets reached the Pacific Ocean.

Chapter 6 - Conclusions

6.1 Victoria relative sea level

A new relative sea level curve was developed for Victoria, British Columbia for postglacial times. The constraints were taken from several cores from isolation basins collected in 2000 and 2001, as well as from previously published data over the past 45 years. The samples range in age from 3500 to 15 000 cal yr BP. The data provide tight constraints on relative sea level in Victoria at elevations greater than -4 m. Below -4 m, there are only loose constraints on relative sea level due to a lack of data.

Relative sea level in Victoria rapidly dropped from a highstand position to below present levels during late glacial times before rising to near present levels in the Holocene. Shortly after the Victoria area was deglaciated at about 14 300 cal kyr BP, sea level stood at a 75-80 m highstand position. Sea level fell rapidly to 0 m at about 13 200 cal yr BP. The lowstand position was between -11 and -40 m, though analysis of crustal response favours the maximum case. Sea level slowly rose after reaching the lowstand position, and by 4000 to 6000 cal yr BP, sea level was within a few metres of present.

Relative sea-level in Victoria differs somewhat from that observed in the central and northern Strait of Georgia. The highstand position in Victoria is 75-100 m lower than in the central and northern Strait of Georgia, probably due to the closer proximity to the edge of the Cordillera ice sheet and earlier deglaciation. Sea level fell below present levels sooner than further north, by up to 1000 to 2000 years.

Relative sea level in the central and northern Strait of Georgia rose to within a couple of metres of present up to 2000 years before Victoria.

6.2 Modelling

The new relative sea-level curves from Victoria, the central Strait of Georgia and the northern Strait of Georgia provided tight constraints on postglacial crustal movements. The earth models had a 60 km elastic lithosphere, an asthenosphere of variable thickness and viscosity, and a transition zone and lower mantle with viscosity based on VM2 (Peltier, 1998). Predicted sea-level using the ice model of James *et al.* (2000) and Clague and James (2002) was unable to fit the good postglacial sea-level constraints from southwestern British Columbia.

A new ice model was developed to improve the fit of predicted sea level. Based on a review of constraints on ice sheet advance and retreat, changes were made to the ice sheet model. The ice sheet reached a maximum position sometime between 17 and 15.4 cal kyr BP. After 15.4 cal kyr BP, the ice sheet rapidly retreated, and by 13.9 cal kyr BP, the ice sheets no longer occupied the Strait of Georgia. The ice sheet model has a significant loss in volume between 13.9 and 12.9 cal kyr BP. From 12.9 to 11.5 cal kyr BP, there is a slight increase in ice volume, coinciding with ice sheet advances that happened at this time. By 10.7 cal kyr BP, the remnant portions of the ice sheet were at present levels.

The newly developed ice sheet model provides a response that fits late glacial sea level in southwestern British Columbia. For each choice of asthenosphere thickness, there is a viscosity value that fits the sea-level constraints. For asthenosphere thicknesses between 140-380 km, the optimal viscosity is between

$3x10^{18}$ and $4x10^{19}$ Pa s. The modelling showed that there is almost no sensitivity to the viscosity of the mantle below the asthenosphere. The modelling could not resolve the early Holocene sea-level rise observed in the central and northern Strait of Georgia. The predicted lowstand position for Victoria is closest to the maximum scenario.

The modelling results allow for the calculation of uplift rates and paleo-shorelines. The predicted present day uplift rates are less than 0.5 mm yr^{-1} and are smaller when the effects of farfield ice sheets are not taken into account. The predicted shorelines during glacial and postglacial times show that sea-level remained high throughout the Cordilleran ice sheet maximum, and that the continental shelves did not become exposed until after 13 cal kyr BP. The implication of this is that people would not be able to migrate down the Pacific coast while the Cordilleran ice sheet was at its maximum.

6.3 Recommendations for future work

Although the modelling was successful in predicting late glacial sea level in southwestern British Columbia, there are several outstanding issues to deal with. First, the modelling over-predicted the sea-level lowstand position in the central and northern Strait of Georgia. Although the modeled sea-level rise to present in the mid-Holocene for Victoria was close to observed time, the modelling could not predict the earlier rise to present levels observed central and northern Strait of Georgia. A farfield ice sheet model was not incorporated in the modelling, due to the different Earth structure outside the Cascadia subduction zone.

Several things could be done to improve future modelling studies. It is recommended that a three-dimensional earth model be incorporated into the analyses to provide a more accurate viscosity model within the Juan de Fuca subduction zone. If this three-dimensional model was extended eastward, a modern far-field ice sheet model such as ICE-5G (Peltier, 2004) could be incorporated. More relative sea level observations would improve the constraints on regional postglacial crustal response. Finally, additional constraints on ice sheet history, such as exposure dating, would provide better constraints on ice sheet history.

References

Alley, N.F., 1979. Middle Wisconsin stratigraphy and climatic reconstruction, southern Vancouver Island, British Columbia. Quaternary Research, 11, 213-237.

Alley, N.F. and Chatwin, S.C., 1979. Late Pleistocene history and geomorphology, southwestern Vancouver Island, British Columbia. Canadian Journal of Earth Sciences, 16, 1645-1657.

Alley, N.F. and Hicock, S.R., 1986. The stratigrapy, palynology, and climatic significance of pre-middle Wisconsin Pleistocene sediments, southern Vancouver Island, southern Vancouver Island, British Columbia. Canadian Journal of Earth Sciences, 23, 369-382.

Al-Suwaidi, M., Ward, B.C., Wilson, M.C., Hebda, R.J., Nagorsen, D.W., Marshall, D., Ghaleb, B., Wigen, R.J. and Enkin, R.J., 2006. Geoarchaeology: An International Journal, 21, 307-332.

Anderson, F.E., 1968. Seaward terminus of the Vashon continental glacier in the Strait of Juan de Fuca. Marine Geology, 6, 419-438.

Anundsen, K., Abella, S., Leopold, E., Stuiver, M. and Turner., 1994. Late-glacial and early Holocene sea-level fluctuations in the central Puget Lowland, Washington, inferred from lake sediments. Quaternary Research, 42, 149-161.

Armstrong, J.E., 1975. Quaternary geology, stratigraphic studies and revaluation of terrain inventory maps, Fraser Lowland, British Coumbia (92 G/1, 2, and parts of 92 G/3, 6, 7 and H/4). *In* Report of activities, part A. Geological Survey of Canada, Paper 75-1, pp. 377-380

Armstrong, J.E., 1981. Post-Vashon Wisconsin glaciation, Fraser Lowland, British Columbia. Geological Survey of Canada, Bulletin 322, 34 p.

Armstrong, J.E. and Clague, J.J., 1977. Two major Wisconsin lithostratigraphic units in southwest British Columbia. Canadian Journal of Earth Sciences, 14, 1471-1480.

Armstrong, J.E., Crandell, D.R., Easterbrook, D.J. and Noble, D.J., 1965. Late Pleistocene stratigraphy and chronology in southwestern British Columbia and northwestern Washington. Geological Society of America Bulletin, 76, 321-330.

Bard, E., 1988. Correction of accelerator mass spectrometry ^{14}C ages measured in planktonic foraminifera: paleooceanographic implications. Paleoceanography, 3, 635-645.

Barnosky, C.W., 1984. Late Pleistocene and early Holocene envirnomental history of southwestern Washington State, U.S.A. Canadian Journal of Earth Sciences, 21, 619-629.

Barrie, J.V. and Conway, K.W., 2000. A preliminary interpretation of surficial marine geology of central and northern Strait of Georgia, British Columbia. Current Research 2000-A21, Geological Survey of Canada, Natural Resources Canada, 7p.

Barrie, J.V. and Conway, K.W., 2002. Contrasting glacial sedimentation processes and sea-level changes in two adjacent basins on the Pacific margin of Canada. *In* Glacier-Influenced Sedimentation on High-Latitude Continental Margins, *Edited by* J.A. Dowdeswell and C. Ó Cofaigh. Geological Society, London, Special Publication, 203, 181-194.

Bassett, S.E., Milne, G.A., Mitrovica, J.X. and Clark, P.U., 2005. Ice sheet and solid earth influences on far-field sea-level histories. Science, 309, 925-928.

Bindoff, N.L., Willebrand, J., Artale, V., Cazenave, A., Gregory, J.M., Gulev, S., Hanawa, K., Le Quéré, C., Levitus, S., Nojiri, Y., Shum, C.K., Talley, L.D. and Unnikrishnan, A.K., 2007. Observations: oceanic climate change and sea level. *In* Climate Change 2007: The Physical Science Basis. Contribution of Working Group 1 to the Fourth Assessment Report of the Intergovernmental Panel on Climate Change, *Edited by* S. Solomon, D. Qin, M.Manning, Z. Chen, M. Marquis, K.B. Averyt, M. Tignor and H.L. Miller. Cambridge University Press, Cambridge UK and New York USA, 385-420

Blaise, B., Clague, J.J. and Mathewes, R.W., 1990. Time of maximum late Wisconsin glaciation, west coast of Canada. Quaternary Research, 34, 282-295.

Blais-Stevens, A., Bornhold, B.D., Kemp, A.E.S., Dean, J.M. and Vaan, A.A., 2001. Overview of late Quaternary stratigraphy in Saanich Inlet, British Columbia: results of Ocean Drilling Program Leg 169S. Marine Geology, 174, 3-26.

Blake, W., 1982. Geological Survey of Canada radiocarbon dates XXII. Geological Survey of Canada Paper 82-7, 22 p.

Blake, W., 1983. Geological Survey of Canada radiocarbon dates XXIII. Geological Survey of Canada Paper 83-7, 34 p.

Bobrowski, P.T. and Clague, J.J., 1992. Neotectonic investigations on Vancouver Island (92B, F). British Columbia Geological Survey Branch, Geological Fieldwork 1991, Paper 1992-1, 325-329.

Booth, D.B., 1987. Timing and processes of deglaciation along the southern margin of the Cordilleran ice sheet. *In* The Geology of North America, vol K-3, North America and Adjacent Oceans During the Last Deglaciation, *Edited by* W.F. Ruddiman and H.E. Wright, pp. 71-90.

Booth, D.B., Troost, K.G., Clague, J.J. and Waitt, R.B., 2003. The Cordilleran Ice Sheet. *In* Developments in Quaternary Science 1, The Quaternary Period in the United States. *Edited by* A.R. Gillespie, S.C. Porter, and B.F. Atwater. pp. 17-43.

Bretz, J.H., 1920. The Juan de Fuca Lobe of the Cordilleran ice sheet. Journal of Geology, 28, 333-339.

Broecker, W.S. and Kulp, J.L., 1957. Lamont natural radiocarbon measurements IV. Science, 126, 1324-1334.

Broecker, W.S., Kulp, J.L. and Tucek, C.S., 1956. Lamont natural radiocarbon measurements III. Science, 124, 154-165.

Buckley, J.D., Trautman, M.A. and Willis, E.H., 1968. Isotopes' radiocarbon measurements VI. Radiocarbon, 10, 246-294.

Buckley, J.D. and Willis, E.H., 1970. Isotopes' radiocarbon measurements VIII. Radiocarbon, 12, 87-129.

Cathles, L.M., 1975. The Viscosity of the Earth's Mantle. Princeton University Press, Princeton, New Jersey, 386 p.

Cassidy, J.F. and Waldhauser, F., 2003. Evidence for both crustal and mantle earthquakes in the subducting Juan de Fuca Plate. Geophysical Research Letters, 30, 1095, 4 p.

Clague, J.J., 1976. Quadra Sand and its relation to the late Wisconsin glaciation of southwest British Columbia. Canadian Journal of Earth Sciences, 13, 803-815.

Clague, J.J., 1980. Late Quaternary geology and geochronology of British Columbia, part 1: radiocarbon dates. Geological Survey of Canada, Energy Mines and Resources Canada, Paper 80-13, 28 p.

Clague, J.J., 1981. Late Quaternary geology and geochronology of British Columbia, part 2: summary and discussion of radiocarbon-dated Quaternary history. Geological Survey of Canada, Energy Mines and Resources Canada, Paper 80-35, 41 p.

Clague, J.J., 1989. Late Quaternary sea level change and crustal deformation, southwestern British Columbia. *In* Current Research, Part E, Geological Survey of Canada, Paper 89-1E, 233-236.

Clague, J.J., 1991. Quaternary glaciation and sedimentation, Chapter 12. *In* Geology of the Cordilleran Orogen in Canada, *Edited by* H. Gabrielse and C.J. Yorath. Geological Survey of Canada, no. 4, pp. 419-434.

Clague, J.J., 1994. Quaternary stratigraphy and history of south-coastal British Columbia. *In* Geology and geological hazards of the Vancouver Region, southwestern British Columbia. *Edited by* J.W.H. Monger. Geological Survey of Canada, Bulletin 481, pp. 181-192.

Clague, J.J. and James, T.S., 2002. History and isostatic effects of the last ice sheet in southern British Columbia. Quaternary Science Reviews, 21, 71-87.

Clague, JJ., Armstrong, J.E. and Mathews, W.H., 1980. Advance of the late Wisconsin Cordilleran Ice Sheet in southern British Columbia since 22,000 Yr B.P. Quaternary Research, 13, 322-326.

Clague, J., Harper, J.R., Hebda, R.J. and Howes, D.E., 1982. Late Quaternary sea levels and crustal movements, coastal British Columbia. Canadian Journal of Earth Sciences, 19, 597-618.

Clague, J.J., Saunders, I.R. and Roberts, M.C., 1988. Ice-free conditions in southwestern British Columbia at 16 000 years BP. Canadian Journal of Earth Sciences, 25, 938-941.

Clague, J.J., Mathewes, R.W., Guilbault, J.-P., Hutchinson, I. and Ricketts, B.D., 1997. Pre-Younger Dryas resurgence of the southwestern margin of the Cordilleran ice sheet, British Columbia, Canada. Boreas, 26, 261-277.

Clague, J.J., Froese, D., Hutchinson, I., James, T.S. and Simon, K.M., 2005. Early growth of the last Cordilleran ice sheet deduced from glacio-isostatic depression in southwest British Columbia, Canada. Quaternary Research, 63, 53-59.

Clowes, R.M., Zelt, C.A., Amor, J.R. and Ellis, R.M., 1995. Lithospheric structure in the southern Canadian Cordillera from a network of seismic refraction lines. Canadian Journal of Earth Sciences, 32, 1485-1513.

Clowes, R.M., Baird, D.J. and Dehler, S.A., 1997. Crustal structure of the Cascadia subduction zone, southwestern British Columbia, from potential field and seismic studies. Canadian Journal of Earth Sciences, 34, 317-335.

Dallimore, A., Enkin, R.J., Peinitz, R., Southon, J.R., Baker, J., Wright, C.A., Pedersen, T.F., Calvert, S.E. and Thomson, R.J., in press. Post-glacial evolution of a Pacific coastal fjord in British Columbia, Canada: interactions of sea-level change, crustal response and environmental fluctuations; results from MONA Core MD02-2494.

Denton, G.H. and Hughes, T.J., 1981. The Last Great Ice Sheets. John Wiley & Sons, Inc., New York, 484 p.

Dethier, D.P., Pessl Jr., F., Keuler, R.F., Balzarini, M.A. and Pevear, D.R., 1995. Late Wisconsinian glaciomarine deposition and isostatic rebound, northern Puget Lowland, Washington. GSA Bulletin, 107, 1288-1303.

Dillehay, T.D., Pino, M., Davis, M.E., Valastro, S., Varela, A.G. and Casamiquela, R., 1982. Monte Verde: radiocarbon dates from an early-man site in south-central Chile. Journal of Field Archaeology, 9, 547-550.

Dixon, R., 2003. The coast road. Nature, 422, 10-12.

Dorn, T.F., Fairhall, A.W., Schell, W.R. and Takashima, Y., 1962. Radiocarbon dating at the University of Washington I. Radiocarbon, 4, 1-12.

Dyke, A.S., 1996. Preliminary paleogeographic maps of glaciated North America. Geological Survey of Canada, Open File 3296.

Dyke, A.S., 2004. An outline of North American deglaciation with emphasis on central and northern Canada. *In* Quaternary Glaciations, Extent and Chronology Part II: North America, *Edited by* J. Ehlers and P.L. Gibbard, Elsevier, New York, 373-424.

Dyke, A.S., Andrews, J.T., Clark, P.U., England, J.H., Miller, G.H., Shaw, J. and Veillette, J.J., 2002. The Laurentide and Innuitian ice sheets during the Last Glacial Maximum. Quaternary Science Reviews, 21, 9-31.

Dyck, W., Fyles, J.G. and Blake, W. Jr., 1965. Geological Survey of Canada radiocarbon dates IV. Radiocarbon, 7, 24-46.

Dyck, W., Lowdon, J.A., Fyles, J.G. and Blake, W. Jr., 1966. Geological Survey of Canada radiocarbon dates V, 8, 96-127.

Dziewonski, A.M. and Anderson, D.L., 1981. Preliminary reference Earth model. Physics of the Earth and Planetary Interiors, 25, 297-356.

Easterbrook, D.J., 1963. Late Pleistocene glacial events and relative sea-level changes in the northern Puget Lowland, Washington. Geological Society of America Bulletin, 74, 1465-1484.

Easterbrook, D.J., 1969. Pleistocene chronology of the Puget Lowland and San Juan Islands, Washington. Geological Society of America Bulletin, 80, 2273-2286.

Easterbrook, D.J., 1986. Stratigraphy and chronology of Quaternary deposits of the Puget Lowland and Olympic Mountains of Washington and the Cascade Mountains of Wasthington and Oregon. Quaternary Science Reviews, 5, 145-159.

Easterbrook, D.J., 1992. Advance and retreat of Cordilleran ice sheets in Washington, U.S.A. Géographie Physique et Quaternaire, 46, 51-68.

Easterbrook, D.J., 2003. Comment on the paper "Determination of ^{36}Cl production rates from the well-dated deglaciation surfaces of Whidbey and Fidalgo Islands, Washington" by T.W. Swanson and M.C. Caffee. Quaternary Research, 59, 132-134.

Fairbanks, R.G., 1989. A 17,000-year glacio-eustatic sea level record: influence of glacial melting rates on the Younger Dryas even and deep-ocean circulation. Nature, 342, 637-642.

Fairhall, A.W., Schell, W.R. and Young, J.A., 1966. Radiocarbon dating at the University of Washington III. Radiocarbon, 8, 498-506.

Fairhall, A.W., Young A.W. and Erickson, J.L., 1976. University of Washington dates IV. Radiocarbon, 18, 221-239.

Farrell, 1972. Deformation of the Earth by surface loads. Reviews of Geophysics and Space Physics, 10, 761-797.

Farrell, W.E. and Clark, J.A., 1976. On postglacial sea level. Geophysical Journal of the Royal Astronomical Society, 46, 647-667.

Flück, P., Hyndman, R.D. and Wang, K., 1997. Three-dimensional dislocation model for great earthquakes of the Cascadia subduction zone. Journal of Geophysical Research, 102, 20539-20550.

Flück, P., Hyndman, R.D. and Lowe, C., 2003. Effective elastic thickness T_e of the lithosphere in western Canada. Journal of Geophysical Research, 108, 2430, 13 p.

Friele, P.A. and Hutchinson, I., 1993. Holocene sea-level change on the central west coast of Vancouver Island, British Columbia. Canadian Journal of Earth Sciences, 30, 832-840.

Friele, P.A. and Clague, J.J., 2002. Readvance of glaciers in the British Columbia Coast Mountains at the end of the last glaciation. Quaternary International, 87, 45-58.

Fulton, R.J., 1967. Deglaciation studies in Kamloops region, an area of moderate relief, British Columbia. Geological Survey of Canada Bulletin, 154, 36 p.

Gabrielse, H. and Yorath, C.J., 1989. DNAG #4: The Cordilleran orogen in Canada. Geoscience Canada, 16, 67-83.

Godwin, H., 1962. Half-life of radiocarbon. Nature, 195, 984.

Gowan, E**.** and James, T., 2006. Glacio-isostatic adjustment modelling of improved postglacial sea-level constraints from Vancouver Island, British Columbia. EOS Transaction, AGU, 87, Fall Meeting Suplemental, Abstract G33B-0052.

Guilbault, J-P., Barrie, J.V., Conway, K., Lapointe, M. and Radi, T., 2003. Paleoenvironments of the Strait of Georgia, British Columbia during the last deglaciation: microenvironments and microfloral evidence. Quaternary Science Reviews, 22, 839-857.

Guilderson, T.P., Reimer, P.J. and Brown, T.A., 2005. The boon and bane of radiocarbon dating. Science, 307, 362-364.

Haskell, N.A., 1935. The motion of a viscous fluid under a surface load. Physics, 6, 265-269.

Haugerud, R.A., Harding, D.J., Johnson, S.Y, Harless, J.L., Weaver, C.S. and Sherrod, B.L., 2003. High-resolution Lidar topography of the Puget Lowland, Washington – a bonanza for earth science. GSA Today, 13(6), 4-10.

Hebda, R.J., 1983. Late-glacial and postglacial vegetation history at Bear Cove Bog, northeast Island, British Columbia. Canadian Journal of Botany, 61, 3172-3192.

Hebda, R., 1988. Buffalo George update. The Midden, 20, 2.

Hebda, R.J., Howes, D. and Maxwell, B., 1997. Chapter 15, Brooks Peninsula as an ice age refugium. *In* Brooks Peninsula an ice age refugium on Vancouver Island, *Edited by* R.J. Hebda and J.C. Haggarty. BC Parks Ministry of Environment, Lands and Parks, Occasional Paper no. 5, 7 p.

Hedenström, A. and Possnert, G., 2001. Reservoir ages in Baltic Sea sediment – a case study of an isolation sequence from the Litorina Sea stage. Quaternary Science Reviews, 20, 1779-1785.

Herzer, R.H. and Bornhold, B.D., 1982. Glaciation and post-glacial history of the continental shelf off southwestern Vancouver Island, British Columbia. Marine Geology, 48, 285-319.

Hetherington, R. and Barrie, J.V., 2004. Interaction between local tectonics and glacial unloading on the Pacific margin of Canada. Quaternary International, 120, 65-77.

Hetherington, R., Barrie, J.V., Reid, R.G.B., MacLeod, R., Smith, D.J., James, T.S. and Kung, R., 2003. Late Pleistocene coastal paleogeography of the Queen Charlotte Islands, British Columbia, Canada, and its implications for terrestrial biogeography and early postglacial human occupation. Canadian Journal of Earth Sciences, 40, 1755-1766.

Hetherington, R., Barrie, J.V., Reid, R.G.B., MacLeod, R. and Smith, D.J., 2004. Paleogeography, glacially induced crustal displacement, and Late Quaternary coastlines on the continental shelf of British Columbia, Canada. Quaternary Science Reviews, 23, 295-318.

Heusser, C.J., 1973. Environmental sequence following the Fraser advance of the Juan De Fuca Lobe, Washington. Quaternary Research, 3, 284-306.

Hewitt, A.T. and Mosher, D.C., 2001. Late Quaternary stratigraphy and seafloor geology of eastern Juan de Fuca Strait, British Columbia and Washington. Marine Geology, 177, 295-316.

Hicock, S.R. and Armstrong, J.E., 1981. Coquitlam Drift: a pre-Vashon Fraser glacial formation in the Fraser Lowland, British Columbia. Canadian Journal of Earth Sciences, 18, 1443-1451.

Hicock, S.R. and Armstrong, J.E., 1983. Four Pleistocene formations in southwest British Coumbia: their implications for patterns of sedimentation of possible Sangamonian to early Wisconsin age. Canadian Journal of Earth Sciences, 20, 1232-1247.

Hicock, S.R., Hebda, R.J. and Armstrong, J.E., 1982. Lag of the Fraser glacial maximum in the Pacific Northwest: pollen and macrofossil evidence from western Fraser Lowland, British Columbia. Canadian Journal of Earth Sciences, 19, 2288-2296.

Howes, D.E., 1981a. Terrain inventory and geological hazards: northern Vancouver Island. Province of British Columbia Ministry of Environment, Assessment and Planning Division, APD Bulletin 5, 105 p.

Howes, D.E., 1981b. Late Quaternary sediments and geomorphic history of north-central Vancouver Island. Canadian Journal of Earth Sciences, 18, 1-12.

Howes, D.E. and Naismith, H.W., 1983. Quaternary geology of southern Vancouver Island. Geological Association of Canada, May 11-13, 1983, Field Trip Guidebook, Trip 11, 25p.

Hu, Y., Wang, K., He, J., Klotz, J. and Khazaradze, G., 2004. Three-dimensional viscoelastic finite element model for postseismic deformation of the great 1960 Chile earthquake. Journal of Geophysical Research, 109, B12403.

Hughen, K.A., Baillie, M.G.L., Bard, E., Bayliss., A., Beck., J.W., Bertrand, C.J.H., Blackwell, P.G., Buck, C.E., Burr, G.S., Cutler, K.B., Damon, P.E., Edwards, R.L., Fairbanks, R.G., Friedrich, M., Guilderson, T.P., Kromer, B., McCormac, F.G., Manning, S.W., Bronk Ramsey, C., Reimer, P.J., Reimer, R.W., Remmele, S., Southon, J.R., Stuiver, M., Talamo, S., Taylor, F.W., van der Plicht, J. and Weyhenmeyer, C.E., 2004. Marine04 Marine radiocarbon age calibration, 26 - 0 ka BP. Radiocarbon, 46, 1059-1086.

Hutchinson, I., 1992. Holocene sea level change in the Pacific Northwest: a catalogue of radiocarbon dates and an atlas of regional sea-level curves. Occasional Paper No. 1, Institute of Quaternary Research, Simon Fraser University, Burnaby, B.C., 100 p.

Hutchinson, I. and Friele, P.A., 1993. Holocene sea-level change on the central west coast of Vancouver Island, British Columbia. Canadian Journal of Earth Sciences, 30, 832-840.

Hutchinson, I., James, T.S., Clague, J.J., Barrie, J.V. and Conway, K.W., 2004a. Reconstruction of late Quaternary sea-level change in southwestern British Columbia from sediments in isolation basins. Boreas, 33, 183-194.

Hutchinson, I., James, T.S., Reimer, P.J., Bornhold, B.D. and Clague, J.J., 2004b. Marine and limnic radiocarbon reservoir corrections for studies of late-and postglacial environments in Georgia Basin and Puget Lowland British Columbia, Canada and Washington,USA. Quaternary Research, 61, 193-203.

Hyndman, R.D., Currie, C.A. and Mazzotti, S.P., 2005. Subduction zone backarcs, mobile belts, and orogenic heat. GSA Today, 15(2), 4-10.

Ives, P.C., Levin, B., Robinson, R.D. and Rubin, M., 1964. U.S. Geological Survey radiocarbon dates VII. Radiocarbon, 6, 37-76.

James, 1991. Post-glacial deformation. Unpublished Ph.D. dissertation, Princeton University, 190 p.

James, T.S., Clague, J.J., Wang, K. and Hutchinson, I., 2000. Postglacial rebound at the northern Cascadia subduction zone. Quaternary Science Reviews, 19, 1527-1541.

James, T.S., Hutchinson, I. and Clague, J.J., 2002. Improved relative sea-level histories for Victoria and Vancouver, British Columbia, from isolation-basin coring. Geological Survey of Canada, Current Research 2002-A16, Natural Resources Canada, 7 p.

James, T.S., Hutchinson, I., Barrie, J.V., Conway, K.C. and Mathews, D., 2005. Relative sea-level change in the northern Strait of Georgia, British Columbia. Géographie Physique et Quaternaire, 59, 113-127.

Karato, S.-i. and Wu, P., 1993. Rheology of the upper mantle: a synthesis. Science, 260, 771-778.

Kao, H., Shan, S.-J., Dragert, H., Rogers, G., Cassidy, J.F. and Ramachandran, K., 2005. A wide depth distribution of seismic tremors along the northern Cascadia margin. Nature, 436, 841-844.

Kelsey, H.M., Sherrod, B., Johnson, S.Y. and Dadisman, S.V., 2004. Land-level changes from a late Holocene earthquake in the northern Puget Lowland, Washington. Geology, 32, 469-472.

Kienast, S.S. and McKay, J.L., 2001. Sea surface temperatures in the subarctic northeast Pacific reflect millennial-scale climate oscillations during the last 16 kyrs. Geophysical Research Letters, 28, 1563-1566.

Kovanen, D.J. and Easterbrook, D.J., 2001. Late Pleistocene, post-Vashon, alpine glaciation of the Nooksack drainage, North Cascades, Washington. Geological Society of America Bulletin, 113, 274-288.

Kovanen, D.J. and Easterbrook, D.J., 2002a. Paleodeviations of radiocarbon marine reservoir values for the northeast Pacific. Geology, 30, 243-246.

Kovanen, D.J. and Easterbrook, D.J., 2002b. Timing and extent of Allerød and Younger Dryas age (ca. 12,500-10,000 ^{14}C yr B.P.) oscillations of the Cordilleran Ice Sheet in the Fraser Lowland, western North America. Quaternary Research, 57, 208-224.

Kovanen, D.J. and Slaymaker, O., 2004. Relict shorelines and ice flow patterns of the northern Puget Lowland from LIDAR data and digital terrain modelling. Geografiska Annaler, 86 A, 385-400.

Lewis, T.J., Bentkowski, W.H., Davis, E.E. and Hyndman, R.D., 1988. Subduction of the Juan de Fuca plate: thermal consequences. Journal of Geophysical Research, 93, 15207-15225.

Leopold, E.B., Nickmann, R., Hedges, J.I. and Ertel, J.R., 1982. Pollen and lignin records of late Quaternary vegetation, Lake Washington. Science, 218, 1305-1307.

Libby, W.F., 1946. Atmospheric helium three and radiocarbon from cosmic radiation. Physical Review, 69, 671-672.

Linden, R.H. and Schurer, P.J., 1988. Sediment characteristics and sea-level history of Royal Roads Anchorage, Victoria, British Columbia. Canadian Journal of Earth Sciences, 25, 1800-1810.

Lowdon, J.A. and Blake, W. Jr., 1970. Geological Survey of Canada radiocarbon dates IX. Radiocarbon, 12, 46-86.

Lowdon, J.A., Robertson, I.M. and Blake, W. Jr., 1971. Geological Survey of Canada radiocarbon dates XI, 13, 255-324.

Mackie, Q., 1987. Marly bison turns up in pond. The Midden, 19, 2.

Mathews, W.H., Fyles, J.G. and Nasmith, H.W., 1970. Postglacial crustal movements in southwestern British Columbia and adjacent Washington state. Canadian Journal of Earth Sciences, 7, 690-702.

Mazzotti, S., Dragert, H., Henton, J., Schmidt, M., Hyndman, R., James, T., Lu, Y. and Craymer, M., 2003. Current tectonics of northern Cascadia from a decade of GPS measurements. Journal of Geophysical Research, 108, 2554.

McCammon, J.W., 1977. Surficial geology and sand and gravel deposits of Sunshine Coast, Powell River, and Campbell River areas. Province of British Columbia Ministry of Mines and Petroleum Resources, Bulletin 65, 36 p.

McConnell, R.K., 1965. Isostatic adjustment in a layered Earth. Journal of Geophysical Research, 70, 5171-5188

McCrory, P.A., Blair, J.L., Oppenheimer, D.H. and Walter, S.R., 2004. Depth to the Juan de Fuca slab beneath the Cascadia subduction Margin – a 3-D model for sorting earthquakes. U.S. Geological Survey Data Series 91 <url: http://pubs.usgs.gov/ds/91>

McKay, J.L., Pedersen, T.F. and Kienast, S.S., 2004. Organic carbon accumulation over the last 16 kyr off Vancouver Island, Canada: evidence for increased marine productivity during the deglacial. Quaternary Science Reviews, 23, 261-281.

McNeely, R. and Jorgensen, P.K., 1992. Geological Survey of Canada radiocarbon dates XXX. Geological Survey of Canada Paper 90-7, 84 p.

McNeely, R. and Jorgensen, P.K., 1993. Geological Survey of Canada radiocarbon dates XXXI. Geological Survey of Canada Paper 91-7, 85 p.

Mitrovica, J.X. and Milne, G.A., 2003. On post-glacial sea level: I. general theory. Geophysics Journal International, 154, 253-267.

Mitrovica, J.X. and Peltier, W.R., 1991. On postglacial geoid subsidence over the equatorial oceans. Journal of Geophysical Research, 96, 20053-20071.

Monahan, P.A., Levson, V.M., Henderson, P. and Klohn-Crippen, A.S., 2000. Relative liquefaction and amplification of ground motion hazard maps of Greater Victoria (TRIM 92B.043, 044, 053, 054. Geoscience Map 2000-3. British Coumbia Ministry of Energy and Mines, Energy and Minerals Division, Geological Survey Branch. 25 p.

Mosher, D.C. and Hewitt., 2004. Late Quaternary deglaciation and sea-level history of eastern Juan de Fuca Strait, Cascadia. Quaternary International, 121, 23-39.

Niskanen, E., 1943. On the deformation of the Earth's crust under the weight of a glacial ice-load and related phenomena. Annales Academiae Scientiarum Fennicae AIII. Geologica-Geographica, 7, 59 p.

NOAA, 1988. Data Announcement 88-MGG-02, Digital relief of the Surface of the Earth. NOAA, National Geophysical Data Center, Boulder, Colorado.

Osborn, G., Menounos, B., Koch, J., Clague, J.J. and Vallis, V., 2007. Multi-proxy record of Holocene glacial history of the Spearhead and Fitzsimmons ranges, southern Coast Mountains, British Columbia. Quaternary Science Reviews, 26, 479-493.

Pazdur, A., Pazdur, M.F., Goslar, T., Wicik, B. and Arnold, M., 1994. Radiocarbon chronology of late glacial and Holocene sedimentation and water-level changes in the area of the Gościąż Lake basin. Radiocarbon, 36, 187-202.

Pellatt, M.G., Mathewes, R.W. and Clague, J.J., 2002. Implications of a late-glacial pollen record for the glacial and climatic history of the Fraser Lowland, British Columbia. Palaeogeography, Palaeoclimatology, Palaeoecology, 180, 147-157.

Peltier, 1974. The impulse response of a Maxwell Earth. Reviews of Geophysics and Space Physics, 12, 649-669.

Peltier, 1985. The LAGEOS constraint on deep mantle viscosity: results from a new normal mode method for the inversion of viscoelastic relaxation spectra. Journal of Geophysical Research, 90, 9411-9421.

Peltier, W.R., 1998. Postglacial variations in the level of the sea: implications for climate dynamics and solid-earth geophysics. Reviews of Geophysics, 36, 603-689.

Peltier, W.R., 2004. Global glacial isostasy and the surface of the ice-age Earth: the ICE-5G (VM2) model and GRACE. Annual Reviews of Earth and Planetary Science, 32, 111-149.

Peltier, W.R., 2005. On the hemispheric origins of meltwater pulse 1a. Quaternary Science Reviews, 24, 1655-1671.

Petersen, K.L., Mehringer, P.J. and Gustafson, C.E., 1983. Late-glacial vegetation and climate at the Manis mastodon site, Olympic Peninsula, Washington. Quaternary Research, 20, 215-231.

Peterson, C.D., Scheidegger, K.F. and Schrader, H.J., 1984. Holocene depositional evolution of a small active-margin estuary of the northwestern United States. Marine Geology, 59, 51-83.

Porter, S.C. and Carson, R.J., 1971. Problems of interpreting radiocarbon dates from dead-ice terrain, with an example from the Puget Lowland of Washington. Quaternary Research, 1, 410-414.

Porter, S.C. and Swanson, T.W., 1998. Radiocarbon age constraints on rates of advance and retreat of the Puget Lobe of the Cordilleran ice sheet during the last glaciation. Quaternary Research, 50, 205-213.

Ranalli, 1995. Rheology of the Earth, second edition. Chapman & Hall, London, UK, 413 p.

Reimer, P. J., Baillie, M. G. L., Bard, E., Bayliss, A., Beck, J. W., Bertrand, C. J. H., Blackwell, P. G., Buck, C. E., Burr, G. S., Cutler, K. B., Damon, P. E., Edwards, R. L., Fairbanks, R. G., Friedrich, M., Guilderson, T. P., Hogg, A. G., Hughen, K. A., Kromer, B., McCormac, F. G., Manning, S. W., Ramsey, C. B., Reimer, R. W., Remmele, S., Southon, J. R., Stuiver, M., Talamo, S., Taylor, F. W., van der Plicht, J. and Weyhenmeyer, C. E. 2004. IntCal04 Terrestrial radiocarbon age calibration, 26 - 0 ka BP. Radiocarbon, 46, 1029-1058.

Riddihough, R., 1984. Recent movements of the Juan de Fuca plate system. Journal of Geophysical Research, 89, 6980-6994.

Robinson, S.W., 1977. US Geological Survey, Menlo Park, California, radiocarbon measurements I. Radiocarbon, 19, 460-464.

Rubin, M. and Alexander, C., 1958. U.S. Geological Survey radiocarbon dates IV. Science, 127, 1476-1487.

Southon, J.R., Nelson, D.E. and Vogel, J.S., 1990. A record of past ocean-atmosphere radiocarbon differences from the northeast Pacific. Paleoceanography, 5, 197-206.

Stuiver, M. and Polach, H.A., 1977. Discussion: Reporting of ^{14}C data. Radiocarbon, 19, 355-363.

Stuiver, M. and Reimer, P.J., 1993. Extended ^{14}C data base and revised Calib 3.0 ^{14}C age calibration program. Radiocarbon, 35, 215-230.

Stuiver, M. and Suess, H.E., 1966. On the relationship between radiocarbon dates and true sample ages. Radiocarbon, 8, 534-540.

Stumpf, A.J., Broster, B.E. and Levson, V.M., 2000. Multiphase flow of the late Wisconsinan Cordlleran ice sheet in western Canada. Geological Society of America Bulletin, 112, 1850-1863.

Swanson, T.W. and Caffee, M.L., 2001. Determination of ^{36}Cl production rates derived from the well-dated deglaciation surfaces of Whidbey and Fidalgo Islands, Washington. Quaternary Research, 56, 366-382.

Thackray, G.D., 2001. Extensive early and middle Wisconsin glaciation on the western Olympic Peninsula, Washington, and the variability of Pacific moisture delivery to the northwestern United States. Quaternary Research, 55, 257-270.

Thorson, R.M., 1980. Ice-sheet glaciation of the Puget Lowland, Washington, during the Vashon Stade (Late Pleistocene). Quaternary Research, 13, 303-321.

Thorson, R.M., 1989. Glacio-isostatic response of the Puget Sound area, Washington. Geological Society of America Bulletin, 101, 1163-1174.

Trautman, M.A. and Willis, E.H., 1966. Isotopes, Inc. radiocarbon measurements V. Radiocarbon, 8, 161-203.

Turcotte, D.L. and Schubert, G., 2002. Geodynamics, second edition. Cambridge University Press, Cambridge, 456 p.

Tushingham, A.M. and Peltier, W.R., 1991. Ice-3G: a new global model of late Pleistocene deglaciation based upon geophyscial predictions of post-glacial relative sea level change. Journal of Geophysical Research, 96, 4497-4523.

Valentine, K.W.G., 1971. Soils of the Tofino-Ucluelet lowland of British Columbia. British Columbia Soil Survey, Report 11, 29 p.

Wada, I., K. Wang, J. He, and R. D. Hyndman, in press. Weakening of the subduction interface and its effects on surface heat flow, slab dehydration, and mantle wedge serpentinization. Journal of Geophysical Research

Walker, I.R. and Pellatt, M.G., 2003. Climate change in coastal British Columbia – a paleoenvironmental perspective. Canadian Water Resources Journal, 28, 531-566.

Wang, K., 2007. Elastic and viscoelastic models of crustal deformation in subduction earthquake cycles. *in* The seismogenic zone of subduction thrust faults, *Edited by* T.H. Dixon and J.C. Moore. Columbia University Press, pp. 540-575.

Wang, H. and Wu, P., 2006. Effects of lateral variations in lithospheric thickness and mantle viscosity on glacially induced relative sea levels and long wavelength gravity field in a spherical, self-gravitating Maxwell Earth. Earth and Planetary Science Letters, 249, 368-383.

Wang, K., Wells, R., Mazzotti, S., Hyndman, R.D. and Sagiya, T., 2003. A revised dislocation model of interseismic deformation of the Cascadia subduction zone. Journal of Geophysical Research, 108, 2026, 13 p.

Ward, B.C. and Thomson, B., 2004. Late Pleistocene stratigraphy and chronology of lower Chehalis River valley, southwestern British Columbia: evidence for a restricted Coquitlam Stade. Canadian Journal of Earth Sciences, 41, 881-895.

Wilson, J.T., Falconer, G., Mathews, W.H. and Prest, V.K., 1958. Glacial map of Canada. Geological Association of Canada, Toronto, Ontario.

Wu, P., Wang, H. and Schotman, H., 2005. Postglacial induced surface motions, sea-levels and geoid rates on a spherical, self-gravitating laterally heterogeneous earth. Journal of Geodynamics, 39, 127-142.